THE UNIVERSITY OF MICHIGAN

COLLEGE OF ENGINEERING
Department of Nuclear Engineering

Technical Report

CONTINUOUS CROSS-MODULATION OF MICROWAVES IN A HELIUM PLASMA

Kenneth D. Ware

ORA Project 07599

sponsored by:

Advanced Research Projects Agency
Project DEFENDER
ARPA Order No. 675

under contract with:

U.S. ARMY RESEARCH OFFICE-DURHAM
CONTRACT NO. DA-31-124-ARO(D)-403
DURHAM, NORTH CAROLINA

administered through:

OFFICE OF RESEARCH ADMINISTRATION ANN ARBOR

February 1968

This report was also a dissertation submitted in partial fulfillment of the requirements for the degree of Doctor of Philosophy in The University of Michigan, 1968.

ACKNOWLEDGMENTS

I am grateful for the willing support and direct assistance of several people. To Professor David R. Bach, project director, I am deeply indebted for his patience and guidance throughout the extent of this investigation. To Professors Ziya Akcasu (who suggested this study) and Richard K. Osborn, I wish to express sincere gratitude for directing my theoretical analysis. To Professor William N. Lawrence I am very thankful for many late hour sessions of technical assistance and personal counsel. I also acknowledge Professors John S. King and Andrejs Olte for their helpful suggestions during the early stages of the experiment, in particular, for their understanding of other research in this field, and for their critical evaluation of the results.

I wish to thank Professor Edward A. Martin for his guidance in the area of gaseous discharges and Mr. Ronald R. Rickwald for uncovering some of the properties of the glow discharge used in this investigation. Experimental assistance from students Mr. Douglas Kreifels and Mr. Thomas Leonard is gratefully acknowledged. Several discussions with Dr. Edmund K. Miller proved valuable to the project, and for his time and suggestions I am grateful.

In addition to the friendships of the persons above, my thanks go to Drs. Ralph R. Rudder, Leonard H. Wald, Carl M. Penney, and James F. Lafferty, and Mr. Erol Oktay. Discussion of problems with these friends was very helpful to my progress.

I would especially like to thank Professor William Kerr, Chairman of the Nuclear Engineering Department, for his personal encouragement and the availability of departmental facilities and services. His continued interest in keeping the paths to thesis progress clear of unscientific obstacles is gratefully acknowledged.

The love and understanding of my wife, Judy, have been invaluable throughout this study. For her encouragement, as well as our parents', I will always be thankful.

In preparation of the manuscript my thanks go to Miss Julie Calver and to the typing, technical illustration, photography, and reproduction staffs of the Office of Research Administration.

I appreciate the Ford Motor Company Technical Computer Center for giving me valuable time with their GE-235 computer during the course of this project. The major portion of this work was supported by the Advanced Research Projects Agency (Project DEFENDER) and monitored by the U. S. Army Research Office-Durham under Contract No. DA-31-124-ARO(D)-403.

TABLE OF CONTENTS

TABLE OF CONTENTS (Concluded)

LIST OF ILLUSTRATIONS

LIST OF ILLUSTRATIONS (Concluded)

ABSTRACT

The purpose of this study was to investigate continuous cross-modulation of microwaves in a steady state plasma. Earlier explorations of the technique in the ionosphere demonstrated its usefulness in plasma diagnostics, however, the measurements indicated that the phenomenon was not completely understood. The theoretical analysis is extended in this study to include effects arising from the dc conductivity, electron-ion collisions, and electron density variations, as well as those due to electron temperature variations which were considered in the previous work. Due to the heating effect of a modulated disturbing microwave, all of these plasma properties are disturbed and can cause variations in a second sensing microwave. The analysis describes the relative importance of the properties in continuous cross-modulation.

One of the most favorable features of cross-modulation is that only a relative measurement of the transferred modulation depth as a function of modulation frequency is required. This suggests that the technique might be useful for geometrically unwieldy plasmas since the analysis of standard microwave absorption experiments become very difficult due to the complex scattering pattern resulting from plasma inhomogeneity. The microwave scattering patterns are most complicated when the free space wavelength is comparable to the plasma dimensions, but they only contribute to the normalization of the cross-modulation coefficient in a cross-modulation experiment.

Measurements were made in a large volume (4 cu ft) helium glow discharge with 10 cm microwaves. In this case, cross-modulation depended primarily on electron density variations. Using independent measurements of electron temperature and density, the transferred modulation depth led to a value for the probability of collision for electron momentum transfer, P_m(18.7 ± 2.1 cm^{-1} $Torr^{-1}$ at 0°C), and to a value for the electron-ion recombination coefficient, α_o($3.6 \pm 2.2 \times 10^{-8}$ cm^3 sec^{-1}). These quantities are in good agreement with other published values.

I. INTRODUCTION

This experimental study was designed to measure the continuous cross-modulation between two microwaves interacting in a steady state helium plasma. The transfer of modulation is possible because of the nonlinear character of the interaction of microwaves with a plasma. A variable amplitude "disturbing" microwave can transfer energy to the plasma and cause time variations in the macroscopic properties of the plasma. In particular, the disturbing microwave can produce slow variations in the plasma conductivity, which will cause variations in the amplitude of a second "sensing" microwave interacting with the plasma.

The first report of cross-modulation was presented by Tellegen[1] in 1933 for radio waves in the ionosphere. He reported that Luxembourg radio programs, originally transmitted from Luxembourg on a carrier wave of 250 K Hz, were detected on a 650 K Hz carrier wave. This latter signal was transmitted from Beromunster, Germany to Einhoven, Holland via ionospheric reflection. Luxembourg was located nearly midway between the other two sites. After a year of speculation on the source of the interaction, Bailey and Martyn[2] presented a theory based on the nonlinear absorption of the two carrier waves in the ionosphere to explain the phenomenon. Their analysis demonstrated the relationship between the amplitude of the transferred modulation and the electron temperature relaxation time constant. Huxley and Ratcliffe,[3] in a survey article on cross-modulation, reported measurements made with two radio waves in the ionosphere which determined the electron-neutral collision frequency

using the relative transferred modulation dependence on frequency. They noticed that the transferred modulation depth consistently decreased faster with modulation frequency than the theory predicted.

The first extensive application of cross-modulation to laboratory studies of plasmas was reported by Goldstein et al.,[4] beginning in 1953. They measured the transmission of a sensing microwave passed through a plasma disturbed by a pulsed microwave signal. In these experiments, the afterglow plasmas were enclosed within the waveguide structure. They reported measurements of the electron-neutral and electron-ion collision cross-sections and the electron thermal conductivity.

For the studies cited above, the authors considered only the effects resulting from changes in the electron temperature, due to the continuously modulated or pulsed disturbing microwave. However, for some experimental conditions, such as in a dc discharge, the disturbing electric field can cause changes in the electron density through changes in the electron temperature. The magnitude of the electron density fluctuation depends on the electron density loss rate, as well as the electron temperature relaxation rate, compared to the modulation frequency. Therefore, the electron density variations exhibit a double frequency correlation with the modulation and the electron temperature variations exhibit primarily a single frequency correlation.

The relative importance of these variations in cross-modulation will also depend on the plasma conductivity for the sensing microwave. If the collision frequency for electrons is much less than the carrier microwave frequency, the imaginary part of the conductivity will be proportional to the electron density

and nearly independent of the electron temperature. However, for this condition, the real part of the conductivity depends strongly on both the electron density and the electron collision frequency which is a function of the electron temperature. When the sensing microwave interacts with the plasma primarily through the imaginary part of the conductivity, cross-modulation will depend strongly on the electron density variation. Furthermore, there are experimental conditions in which the change of the real part of the conductivity with temperature is zero, and then the complex conductivity is sensitive only to the variation in the electron density.[4]

Our experiment was dominated by electron density variations. We measured the continuous cross-modulation coefficient between two microwaves interacting with a steady state large volume (4 cu ft) helium glow discharge as a function of the modulation frequency. The measured frequency dependence of the relative cross-modulation depth was fitted numerically to the theoretical transfer function. This yielded an averaged electron-ion recombination rate and electron temperature relaxation rate. These measurements, and Langmuir probe measurements of the electron temperature and density, led to values for the electron-ion recombination coefficient and the electron-neutral cross-section. To the best of our knowledge, the electron recombination rate had not been observed before in cross-modulation measurements.

In Chapter II a theory for the continuous cross-modulation of microwaves is presented. Electron temperature and density balance equations obtained from the Boltzmann equation were taken as a suitable description of the plasma. These equations related the variations of the macroscopic properties of the

plasma to the effects of the disturbing high frequency electric field. Our analysis was complicated by the need to consider gradients in the density, the effect of the dc electric field, and the electron-ion collision rate. The balance equations, along with Maxwell's wave equation, were solved to determine the sensing microwave signal seen by an antenna located outside the plasma.

In Chapter III the experimental apparatus is described. Chapter IV contains a description of the experimental techniques and resulting data with cross-modulation and probe measurements in the large volume helium glow discharge. The results are presented and discussed in Chapter V.

II. THEORY OF CONTINUOUS CROSS-MODULATION

The task in this chapter is to describe analytically the continuous cross-modulation between two microwave signals interacting with a steady state helium glow discharge. In particular, we solve for the time varying output voltage of an antenna receiving the "sensing" microwave. The amplitude modulation of the sensing microwave results from its interaction with a plasma having slowly varying macroscopic properties. The variations in the plasma are due to non-linear heating by an amplitude modulated "disturbing" microwave.

The problem is nonlinear in space and time, and the general solution is not easily found even for the simplest of real experimental conditions. We begin the search for a useful solution, which can be approximated experimentally, by considering small signal interactions. This approximation serves several simplifying purposes. First, it allows us to separate the analysis into two meaningful problems: the effect of an amplitude modulated disturbing microwave on the macroscopic plasma properties and the effect of the disturbed plasma on a small sensing microwave signal. That is, we can neglect self-modulation of the microwaves and effects due to the coupling between the high frequency components of the two microwave signals. Also, this small signal assumption allows us to treat the leading high frequency components of the electric field in the plasma as those corresponding to the applied frequencies. However, we do not assume that the amplitude of the microwave electric field vectors are constant over the plasma volume. Furthermore, we can assume that

the variations in the plasma properties due to the disturbing microwave are small compared to the steady state values.

In Section A we solve for the small, time varying detector voltage output of an antenna receiving the sensing microwave signal. Using Maxwell's wave equation, we relate this response to the variations in the electron temperature and density through the complex conductivity of the plasma. Guided by the results of Sections B, C, and D, we consider linear balance equations relating the small variations in the electron temperature and density to the heating effect of the amplitude modulated disturbing microwave. We solve these coupled equations to obtain the functional dependence of the time varying detector voltage on the modulation frequency.

In Section B, we derive balance equations for the time rate of change of the electron temperature and density due to the presence of the disturbing microwave electric field and a dc electric field. For this analysis we use the conventional approach of solving the Boltzmann equation for the plasma state by expanding the electron distribution function $f^e(\underline{x},\underline{v},t)$ using spherical harmonics. We use the P_1-approximation by considering only the first two terms of the expansion. We solve for the slow variations in the plasma properties by averaging over the period of the high frequency disturbing electric field, $2\pi/\omega_D$.

In Sections C and D, we consider reduced forms for the electron temperature and density balance equations, respectively, pertaining to our experimental conditions. The nonlinear equations are solved by expanding the averaged variables about their steady state values for the first order linear

variations in the plasma properties. Careful consideration is given to describing the restoring rates of the variations in the electron temperature and density, as well as the coupling rates between the properties. As will be shown, it is these rates compared to the rate of energy input, the modulation frequency, which determine the relative magnitude of the cross-modulation coefficient of the sensing microwave detector voltage output.

In Section E, we discuss qualitatively a facet of our experimental result, that is, the dominance of the electron density variations. We present possible explanations for this observed response. However, these arguments are not necessary for quantitative interpretation of our results, but do hopefully shed light on understanding the response.

Our analysis contains all the response to continuous cross-modulation considered by previous authors with the additional effects due to dc conductivity, electron-ion collisions, and variations in the electron density. The response due to these latter effects is quite important to the interpretation of our experiment.

A. SENSING MICROWAVE RESPONSE TO TIME VARYING CONDUCTIVITY

We consider here the sensing microwave, given by $\underline{E}(\underline{x}_t)e^{-i\omega_s t}$ as a fixed input signal at the transmitting antenna located at $\underline{x}_t$, interacting with a plasma which can be characterized by the complex conductivity σ. In order to calculate the output field evaluated at the receiving antenna, we need to solve Maxwell's wave equation which can be written, in the absence of space charge effects, as[5]

$$(\nabla^2 + k^2)\underline{E} = 0 \tag{2.1}$$

where

$$k^2 = \frac{\omega_s^2}{c^2}\left(1 - i\frac{4\pi\sigma}{\omega_s}\right) \tag{2.2}$$

We want to consider a plasma with properties which are varying slowly about some steady state value. Describing these variations by $\delta k^2(\underline{x},t)$ about the value $k_o^2(\underline{x})$, we let $\delta\underline{E}(\underline{x},t)$ be the desired change in the field about the value $\underline{E}_o(\underline{x})$. Then assuming that $\underline{E}_o(\underline{x})$ is a known solution of Eq. (2.1) with $k_o^2(\underline{x})$, we can find $\delta\underline{E}(\underline{x},t)$ by solving

$$(\nabla^2 + k_o^2)\,\delta\underline{E}(\underline{x},t) = -\delta k^2(\underline{x},t)\,\underline{E}_o(\underline{x}) \tag{2.3}$$

Solving Eq. (2.3) and evaluating the field at the receiving antenna located at $\underline{x}_r$, we obtain

$$\delta\underline{E}(\underline{x}_r,t) = \int d^3x'\, \underline{E}_o(\underline{x}')\, G_o(\underline{x}';\underline{x}_r)\, \delta k^2(\underline{x}',t) \tag{2.4}$$

where $\underline{x}'$ corresponds to points in the plasma and the Green's function is defined by[6]

$$\left(\nabla^2 + k_o^2\right) G_o(\underline{x}'; \underline{x}_r) = \delta(\underline{x}' - \underline{x}_r) \tag{2.5}$$

where the right hand side is a Dirac delta function.

We now consider the measurable quantity. Since there is no mixing of the polarizations, the vector signs are of no significance and may be dropped. When the complex electric field $[E_o(\underline{x}_r) + \delta E(\underline{x}_r,t)]e^{-i\omega_s t}$, is detected and measured with standard microwave equipment (e.g., a diode and integrating circuit with $\omega_m \ll 1/RC \ll \omega_s$, where ω_m is the rate of variations of δk^2) the resulting voltage is of the form

$$V(t) = V_o \left| 1 + \frac{\delta E}{E_o} \right|^{\epsilon} \tag{2.6}$$

where ϵ is the "power law" of the detecting circuit. The vertical bars represent the absolute value of the complex quantity. V_o is proportional to $|E_o(\underline{x}_r)|^{\epsilon}$. Since the second term of Eq. (2.6) is small, we expand V(t) as

$$V(t) = V_o \left(1 + \epsilon \mathcal{R}_e \left(\frac{\delta E}{E_o} \right) + \frac{\epsilon}{2} \left| \frac{\delta E}{E_o} \right|^2 + \cdots \right) \tag{2.7}$$

In terms of the normalized perturbation, $\delta e = \delta E/E_o$, only the real part is required for the first order variation in the detector voltage.

We write the normalized variation in the detector voltage, $\delta v(t) = \delta V(t)/V_o$, in terms of the variation in the conductivity, using Eq. (2.2), as

$$\delta v(t) = \epsilon \, \mathrm{Re}\left[\frac{-i4\pi\omega_s}{c^2 E_0(\underline{x}_1)} \int d\underline{x}' \, E_s(\underline{x}') G_0(\underline{x}'; \underline{x}_1) \delta\sigma(\underline{x}', t)\right] \tag{2.8}$$

The high frequency complex conductivity of the plasma for the sensing microwave is given by[7] (see Appendix A)

$$\sigma(\underline{x}, t) = \frac{n^e e^2}{m\omega_s^2}(\nu_{en} + \nu_{ei}) - i\frac{n^e e^2}{m\omega_s} \tag{2.9}$$

where we have assumed that $\omega_s^2 \gg \nu^2$. The effective collision frequency for electron-neutral atom collisions is

$$\nu_{en} = \frac{4}{3} N q_{en} \sqrt{\frac{8\theta^e}{\pi m}} \tag{2.10}$$

where q_{en} is the total cross-section and for electron-ion collisions is

$$\nu_{ei} = \frac{4}{3} n^i \frac{(Zc^2)^2 \pi}{2(\theta^e)^2} \sqrt{\frac{8\theta^e}{\pi m}} \ln\left(\frac{3\theta_c^e}{2e^3}\sqrt{\frac{\theta_c^e}{\pi n^i}}\right) \tag{2.11}$$

where N and n^i are the density of scattering centers and the remaining variables are properties of the electrons. (We write the temperature as $\theta^e = kT^e$ throughout this report.) The complex conductivity is essentially a function of only

the electron temperature and density. We Taylor expand $\sigma(\underline{x},t)$ about its steady state value. Keeping only the first order terms, we take

$$\delta\sigma(\underline{x},t) = \left(\frac{\partial\sigma}{\partial\theta^e}\right)_o \delta\theta^e + \left(\frac{\partial\sigma}{\partial n^e}\right)_o \delta n^e \tag{2.12}$$

in terms of the variations in the electron temperature and density. We have in mind letting $\theta^e(\underline{x},t) = \theta^e_o(\underline{x}) + \delta\theta^e(\underline{x},t)$ and $n^e(\underline{x},t) = n^e_o(\underline{x}) + \delta n^e(\underline{x},t)$. Further, treating the normalized variations in the electron temperature and density as slowly varying functions of space, we expand them about the point $\underline{x}_p$ and neglect the gradients of $\delta\theta^e/\theta^e_o$ and $\delta n^e/n^e_o$. We shall discuss some of the implications of this operation and the identification of $\underline{x}_p$ in Chapter V. We can now write Eq. (2.8) as

$$\delta\sigma(t) = a\frac{\delta\theta^e}{\theta^e} + b\frac{\delta n}{n_o} \tag{2.13}$$

where

$$a \equiv \mathcal{R}\left[-\frac{i4\pi\omega_s\epsilon}{c^2 E_o(\underline{x}_1)}\int d^3x' E_o(\underline{x}')G_s(\underline{x}';\underline{x}_1)\theta^e_o(\underline{x}')\left(\frac{\partial\sigma}{\partial\theta}\right)_o\right] \tag{2.14}$$

and

$$b \equiv \mathcal{R}\left[-\frac{i4\pi\omega_s\epsilon}{c^2 E_o(\underline{x}_1)}\int d^3x' E_o(\underline{x}')G_s(\underline{x}';\underline{x}_1) n^e_o(\underline{x}')\left(\frac{\partial\sigma}{\partial n^e}\right)_o\right] \tag{2.15}$$

To continue, we need to know the time variations of the electron temperature and density about their steady state values. We consider the effect of an amplitude modulated electric field, with a leading term in the plasma given by

$$\underline{E}(x,t) = \underline{E}_o(x)\left(1 + \delta_o \cos \omega_m t\right) e^{-i\omega_D t} + c.c. \tag{2.16}$$

on the electron temperature and density of an independently sustained plasma. The modulation frequency ω_m is much less than the carrier frequency ω_D, and the modulation depth δ_o is less than unity. This electric field produces slow variations in the plasma properties of electron temperature and density. As we shall show in the following sections, they are, to first order, solutions of the linear equations

$$\frac{1}{\theta_o^e}\frac{\partial \delta\theta^e}{\partial t} + \omega_m \frac{\delta\theta^e}{\theta_o^e} + \omega_c \frac{\delta n^e}{n_o^e} = P_1 \tag{2.17}$$

and

$$\frac{1}{n_o^e}\frac{\partial \delta n^e}{\partial t} + \omega_b \frac{\delta n^e}{n_o^e} = \omega_d \frac{\delta\theta^e}{\theta_o^e} \tag{2.18}$$

where

$$P_1 = \frac{2e^2 E_p^2}{3m\omega_p^2 c^2}(\text{[illegible]})\,\delta_0\left[\cos\omega_m t + \text{[illegible]}\right] \tag{2.19}$$

The frequencies ω_a, ω_b, ω_c, and ω_d in Eqs. (2.17) and (2.18) will be discussed in detail in Sections C and D of this chapter. As was discussed before Eq. (2.13), these frequencies, as well as P_1, are to be evaluated at the particular point in the plasma denoted by $\underline{x}_p$.

We now solve the coupled set of equations, Eqs. (2.13), (2.17), and (2.18), for the time variation in the detector output voltage. We will neglect the harmonic term in the source P_1, since it varies like $\delta_0/4$ compared to the first term. We obtain

$$\delta v(t) = \delta(\omega_m)\cos(\omega_m t - \phi) \tag{2.20}$$

where

$$\delta(\omega_m) \equiv \frac{2e^2 E_p^2 \delta_0\, \alpha(\text{[illegible]})}{3m\omega_p^2 c^2}\left|\frac{i\omega_m + \omega_a + \frac{b}{a}\text{[illegible]}}{(i\omega_m + \omega_a)(i\omega_m + \omega_b) + \omega_c\omega_d}\right| \tag{2.21}$$

and ϕ is the phase corresponding to the complex function in the last factor.

In our experiment, we measured the cross-modulation coefficient $\delta(\omega_m)$ as a function of the modulation frequency ω_m. To evaluate Eq. (2.21) we define

$$\omega_1 = \frac{\omega_a + \omega_b}{2} + \frac{1}{2}\sqrt{(\omega_a - \omega_b)^2 - 4\omega_c\,\omega_d} \tag{2.22}$$

$$\omega_2 = \frac{\omega_a + \omega_b}{2} - \frac{1}{2}\sqrt{(\omega_a - \omega_b)^2 - 4\omega_c\,\omega_d} \tag{2.23}$$

and

$$\omega_3 = \omega_b + \frac{b}{a}\,\omega_d \tag{2.24}$$

Using the relations discussed in the following sections for the four frequencies (subscripts a, b, c, and d), we found that ω_1 and ω_2 are real for our experimental conditions. Hence, we consider only the case in which the normalized cross-modulation coefficient is of the form

$$\frac{\delta(\omega_m)}{\delta(0)} = \sqrt{\frac{(1 + (\omega_m/\omega_3)^2)}{(1 + (\omega_m/\omega_1)^2)(1 + (\omega_m/\omega_2)^2)}} \tag{2.25}$$

We wish to point out an important feature pertaining to the real variables (a) and (b), defined in Eqs. (2.14) and (2.15). From Eq. (2.13), the relative values of (a) and (b) determine the importance of the variations in the electron temperature and density, respectively, to the cross-modulation coefficient.

Some authors have neglected the effect due to the density variation as a primary response. From Eq. (2.18), this is equivalent to taking ω_d as zero, since $\omega_d \delta\theta^e$ is the source term for the density variation. For this case $\delta(\omega_m)$, from Eq. (2.21), reduces to

$$\frac{\delta(\omega_m)}{\delta(0)} = \frac{1}{\sqrt{1 + (\omega_m/\omega_1)^2}} \qquad (2.26)$$

This is the form considered by Huxley and Ratcliffe[3] for continuous cross-modulation of radio waves in the ionosphere and equivalent to the form considered by Goldstein et al.,[4] for the pulsed cross-modulation of microwaves in an afterglow plasma. (Langberg and Siegel[8] allowed electron density variation due to a disturbing microwave, however their report deals primarily with radiation emission.) In the two cases cited, neglecting the electron density variation appears justified. However, there are experimental conditions, such as ours as we shall discuss in Section E of this chapter and in Chapter V, in which $(\omega_d b/a)$ dominates ω_3. Therefore, we use Eq. (2.25) rather than the simplified Eq. (2.26) to interpret our experimental results, to allow for density variation arising from temperature variation.

We now have the form of the continuous cross-modulation coefficient with which we analyze our measurements. The remaining theoretical task is to derive the linear electron temperature and density balance equations, Eqs. (2.17) and (2.18), in order to describe the functions ω_a, ω_b, ω_c, and ω_d. This problem is considered in the next three sections of this chapter.

B. FORMULATION OF ELECTRON DENSITY AND TEMPERATURE EQUATIONS

In this section, we are interested in developing suitable equations for describing the slow variations in the electron density and temperature due to the presence of an amplitude modulated high frequency electric field. The slightly ionized plasma is sustained by a dc electric field. Let the singlet electron velocity distribution function be defined by $f^e(\underline{x},\underline{v},t)$, such that $f^e d^3x d^3v$ is the number of electrons in the six dimensional element of volume $d^3x d^3v$ about $\underline{x}$ and $\underline{v}$ at time t. It follows that the electron density is given by

$$n^e(\underline{x},t) = \int d^3v\, f^e(\underline{x},\underline{v},t) \tag{2.27}$$

and the electron temperature is defined by

$$n^e(\underline{x},t)\,\theta^e(\underline{x},t) = \int d^3v\, \frac{1}{3} m v^2 f^e(\underline{x},\underline{v},t) \tag{2.28}$$

We take as a description of the variations of the singlet electron distribution function in the presence of an electric field the Boltzmann equation[9]

$$\frac{\partial f^e}{\partial t} + \underline{v}\cdot\underline{\nabla}_x f^e - \frac{e}{m}\underline{E}\cdot\underline{\nabla}_v f^e = \mathcal{J} \tag{2.29}$$

where $\underline{\nabla}_v$ and $\underline{\nabla}_x$ are gradient operators in velocity space and configuration space, respectively. The magnetic field effects are explicitly neglected.

The term on the right hand side represents the net gains per unit time in the distribution function due to collisions. That is,

$$\mathcal{J} \equiv \sum_{B} \left(\frac{\partial f^e}{\partial t} \right)^{B}_{\text{COLLISIONS}} \tag{2.30}$$

where the summation is for collisions with particles of all kind B.

We begin by expanding f^e using spherical harmonics. Keeping only the first two terms of the expansion (P_1-approximation), we have

$$f^e(\underline{x}, \underline{v}, t) = \frac{f_0(\underline{x}, v, t)}{4\pi} + \frac{3}{4\pi v^2} \underline{v} \cdot \underline{J}(\underline{x}, v, t) \tag{2.31}$$

Substituting Eq. (2.31) into Eq. (2.29) and integrating over the solid angle $d\Omega$, where $\underline{\Omega} = \underline{v}/v$, we obtain

$$\frac{\partial f_0}{\partial t} + \nabla_x \cdot \underline{J} - \frac{e}{m v^2} \frac{\partial}{\partial v} (v \underline{E} \cdot \underline{J}) = \int \mathcal{J} d\Omega \tag{2.32}$$

Multiplying Eq. (2.29) by $\underline{\Omega}$ and then integrating we obtain

$$\frac{\partial \underline{J}}{\partial t} + \frac{v^2}{3} \nabla_x f_0 - \frac{ev}{3m} \underline{E} \frac{\partial}{\partial v} f_0 = \int \underline{\Omega} \mathcal{J} d\Omega \tag{2.33}$$

The collision integrals on the right hand sides of Eqs. (2.32) and (2.33) have been discussed in great detail for this expansion by several authors. Some of the earlier work was done by Lorentz,[10] Morse et al.,[11] Chapman and Cowling,[12] and, more recently by, Dreicer,[13] Desloge,[14] and Bowe.[15] Although the functional dependences of these terms are quite important to our analytical solution, we shall make no effort to improve on the previous authors' results. Under the approximation of $m \ll M$ the collision integrals can be shown to be

$$\int d\Omega\, \mathcal{J} = S(f_o) + \frac{1}{M v^2} \frac{\partial}{\partial v}\left[g_m v^2 \left(m v f_o + \theta^n \frac{\partial f_o}{\partial v} \right) \right] \qquad (2.34)$$

and

$$\int \underline{\Omega}\, d\Omega\, \mathcal{J} = -\left(g_m + g_1 \right) \underline{J} \qquad (2.35)$$

where θ^n is the temperature, (kT^n), of the neutral atoms and ions. The collision rate for momentum transfer g_m is defined in terms of the differential cross sections for electron-neutral atom and electron-ion elastic scattering collisions, dq_{en} and dq_{ei}, respectively, by[16]

$$g_m = v \int (1 - \cos\theta_{cm}) \left(N dq_{en} + n^i dq_{ei} \right) \qquad (2.36)$$

where N and n^i are the density of scattering centers, and Θ_{cm} is the angle through which the electron is scattered in the CMCS. Electron-electron collisions are explicitly neglected, however they are implicitly considered to be responsible for keeping the electrons in equilibrium with themselves. In Eq. (2.35), g_1 is the total collision rate for inelastic collisions suffered by the electrons. Note that $g = g_m + g_1$ is in general a function of $\underline{x}$ and t, as well as v, due to its dependence on $n^i(\underline{x},t) \simeq n^e(\underline{x},t)$. The term in Eq. (2.34) identified as $S(f_o)$ represents collectively the dependence on inelastic collisions, including ionization and recombination collisions, where it is sufficient at this point to note that it is simply a linear functional of f_o, after making the assumption that the inelastic collisions are isotropic in velocity space.

We now substitute Eq. (2.35) into Eq. (2.33) in order to solve for $\underline{J}(\underline{x},v,t)$ in terms of the distribution function $f_o(\underline{x},v,t)$. We obtain

$$\underline{J}(\underline{x},v,t) = \int_0^\infty du\, \underline{L}(\underline{x},v,t-u) \exp\left[-\int_0^u g(\underline{x},v,t-u')\,du'\right] \tag{2.37}$$

where

$$\underline{L} = \frac{ev}{3m}\underline{E}\frac{\partial f_o}{\partial v} - \frac{v^2}{3}\underline{\nabla}_x f_o \tag{2.38}$$

Substituting this result into Eq. (2.32) yields

$$\frac{\partial f_o}{\partial t} - \int d\Omega \mathcal{J} = -\underline{\nabla}_x \cdot \int_0^\infty du\, \underline{\underline{L}}(t-u) \exp\left[-\int_0^u g(t-u')\,du'\right]$$

$$+ \frac{e}{mv^2}\frac{\partial}{\partial v}\left\{v \int_0^\infty du\, \underline{\underline{E}}(t)\cdot\underline{\underline{L}}(t-u) \exp\left[-\int_0^u g(t-u')\,du'\right]\right\} \tag{2.39}$$

Recall that we are interested mainly in the electron density and temperature as they are defined in Eqs. (2.27) and (2.28). In the P_1-approximation used here they become

$$n^e(\underline{x},t) = \int_0^\infty dv\, v^2 f_o(\underline{x},v,t) \tag{2.40}$$

and

$$n^e(\underline{x},t)\,\theta^e(\underline{x},t) = \int_0^\infty dv\, \frac{mv^4}{3} f_o(\underline{x},v,t) \tag{2.41}$$

Therefore, to obtain an electron density balance equation from Eq. (2.39), we multiply through by v^2 and integrate over the electron speed. The result of this operation is

$$\frac{\partial n^e}{\partial t} - \int_0^\infty dv\, v^2 S(f_o) =$$

$$- \underline{\nabla}_x \cdot \int_0^\infty dv\, v^2 \int_0^\infty du\, \underline{\underline{L}}(t-u) \exp\left[-\int_0^u g(t-u')\,du'\right] \tag{2.42}$$

The terms from Eq. (2.39) due to elastic scattering integrate to zero, which is to be expected from consideration of the conservation of particles. The last term in Eq. (2.39) also becomes a perfect differential, and therefore is identically zero for the functions considered here.

To obtain an electron temperature balance equation we multiply Eq. (2.39) by $mv^4/3$ and integrate over the speed v. We obtain

$$n^e \frac{\partial \theta^e}{\partial t} + \int_0^\infty dv\, v^2 \left(\theta^e - \tfrac{1}{3} m v^2\right) S(f_0) +$$

$$+ \frac{2m}{3M} \int_0^\infty dv\, v^2 g_m \left(mv f_0 + \theta^n \frac{\partial f_0}{\partial v}\right) =$$

$$- \int_0^\infty dv\, v^2 \left(\tfrac{1}{3} m v^2 - \theta^e\right) \int_0^\infty du\, \nabla_x \cdot \underline{L}(t-u) \exp\left[-\int_0^u g(t-u')\, du'\right] +$$

$$- \frac{2e}{3} \int_0^\infty dv\, v^2 \int_0^\infty du\, \underline{E}(t) \cdot \underline{L}(t-u) \exp\left[-\int_0^u g(t-u')\, du'\right] \qquad (2.43)$$

where we have substituted the term $\theta^e \partial n^e/\partial t$ from Eq. (2.42).

We now take the leading components of the electric field in the plasma as

$$\underline{E}(\underline{x}, t) = \underline{E}_0(\underline{x}) \left(1 + \delta_0 \cos \omega_m t\right) \cos \omega_D t + \underline{E}_{dc}(\underline{x}) \qquad (2.44)$$

which represents a modulated signal with a modulation frequency ω_m and depth δ_0, plus a dc electric field. Note that there are two distinct time scales, one associated with variations on the order of ω_D and one associated with the

much slower variations on the order of ω_m. As mentioned earlier, we are interested explicitly in the slow variations of the electron density and temperature. Therefore, consider the slow variations in n^e and θ^e by averaging Eqs. (2.42) and (2.43) with respect to t over the period of the high frequency electric field. During the extent of this time integration, $(t - \pi/\omega_D)$ to $(t + \pi/\omega_D)$, we neglect the changes in slowly varying functions of $\cos \omega_m t$ and $f_o(t)$. With this reasoning we find that the only surviving contribution of the high frequency electric field is the first term of

$$\left\langle \underline{E}(t) \cdot \underline{E}(t-u) \right\rangle \approx \frac{E_D^2}{2} \gamma(t) \cos \omega_D u + E_{dc}^2 \tag{2.45}$$

where

$$\gamma(t) = \left(1 + \frac{\delta_o^2}{2}\right) + 2\delta_o \left(\cos \omega_m t + \frac{\delta_o}{4} \cos 2\omega_m t\right) \tag{2.46}$$

in the last term of Eq. (2.43). We now perform the indicated integration over the time variable u, after noting that $f_o(t - u)$ and $g(t - u')$ can be approximated by $f_o(t)$ and $g(t)$. This approximation is justified by the fact that the function $\exp(-gu)$ will make the entire integrand very small for u greater than the collision period $1/g$, which is much smaller than the period of variations of interest in f_o or any macroscopic average property such as $n^i(t)$.

The balance equation for slow variations in the electron density is

$$\frac{\partial n^e}{\partial t} - \int_0^\infty dv\, v^2\, S(f_0) =$$

$$-\underline{\nabla}_x \cdot \underline{E}_{dc} \frac{e}{m} \int_0^\infty dv\, \frac{v^3}{3g} \frac{\partial f_0}{\partial v} + \underline{\nabla}_x \cdot \int_0^\infty dv\, \frac{v^4}{3g} \underline{\nabla}_x f_0 \qquad (2.47)$$

and in the electron temperature is

$$n^e \frac{\partial \theta^e}{\partial t} + \int_0^\infty dv\, v^2 \left(\theta^e - \tfrac{1}{3} m v^2\right) S(f_0) +$$

$$+ \frac{2m}{3M} \int_0^\infty dv\, v^3 g_m \left(m v f_0 + \theta^n \frac{\partial f_0}{\partial v}\right) =$$

$$- \frac{2e^2}{9m} \left\{ \frac{E_0^2 \gamma'(t)}{2} \int_0^\infty dv\, \frac{v^3 g}{g^2 + \omega_0^2} \frac{\partial f_0}{\partial v} + E_{dc}^2 \int_0^\infty dv\, \frac{v^3}{g} \frac{\partial f_0}{\partial v} \right\} +$$

$$- \int_0^\infty dv\, v^2 \left(\tfrac{1}{3} m v^2 - \theta^e\right) \underline{\nabla}_x \cdot \left\{ \frac{e \underline{E}_{dc}}{3m} \frac{v}{g} \frac{\partial f_0}{\partial v} - \frac{v^2}{3g} \underline{\nabla}_x f_0 \right\}$$

$$+ \frac{2e}{9} \underline{E}_{dc} \cdot \int_0^\infty dv\, \frac{v^4}{g} \underline{\nabla}_x f_0 \qquad (2.48)$$

We now make an approximation by assuming that the several averages, defined in the two balance equations above, over the electron speed are adequately described by taking $f_o(v)$ as the Maxwellian distribution function

$$f_0(\underline{x}, v, t) = 4\pi n^e(\underline{x}, t) \left(\frac{m}{2\pi \theta^e(\underline{x}, t)}\right)^{3/2} \exp\left[-\frac{m v^2}{2\theta^e(\underline{x}, t)}\right] \qquad (2.49)$$

The assumption of Eq. (2.49) has been discussed by Cahn[17] and Margenau[18] to be a good approximation, even in the presence of electric fields, when taking averages over the electron speed.

In order to evaluate the collision rate $g_m(v)$, we take as the differential cross-sections for the electron-neutral atom and ion collisions, for a helium gas, respectively

$$dq_{en} = q_{en} \frac{d\Omega_{cm}}{4\pi} \tag{2.50}$$

and

$$dq_{ei} = \frac{(ze^2)^2}{4m^2v^4} \frac{d\Omega_{cm}}{\sin^4\frac{\Theta}{2}} , \quad \Theta \geq \Theta^\circ$$

$$= 0 , \quad \Theta < \Theta^\circ \tag{2.51}$$

The cut-off angle Θ° is taken as that scattering angle corresponding to a screened Coulomb potential of separation λ_d, where

$$1/\lambda_d = \frac{mv^2}{2ze^3} \left(\frac{\theta^e}{\pi n^e}\right)^{1/2} \tag{2.52}$$

Relating λ_d to the impact parameter of a two-body Coulomb collision we find, since Θ° is small,[19]

$$\Theta^\circ \approx \frac{4ze^3}{mv^2} \left(\frac{\pi n^e}{\theta^e}\right)^{1/2} \tag{2.53}$$

Substituting into Eq. (2.36) we obtain for the collision rate

$$g_m = N q_{en} v + \frac{\Gamma_{ei} n^i}{v^3} \tag{2.54}$$

where

$$\Gamma_{ei} \equiv 4\pi \left(\frac{Ze^2}{m}\right)^2 \ln\left(\frac{mv^3}{2Ze^3}\sqrt{\frac{\theta^e}{\pi n^e}}\right) \tag{2.55}$$

We evaluate Γ_{ei} at the average energy by letting $v = (3\theta^e/m)^{1/2}$ and will treat both q_{en} and Γ_{ei} as constants throughout the remainder of this analysis for a helium plasma. Also, we assume that g can be replaced by simply g_m, since g_1 is expected to be relatively small. Further, we neglect $\underline{\nabla}_x \theta^e$ and will discuss this approximation in Chapter IV when we consider the data in Fig. 4.7.

We can now write the electron density balance equation as

$$\frac{\partial n^e}{\partial t} - \int_0^\infty dv\, v^2 S(f_0) = \underline{\nabla}_x \cdot \left[\mathcal{D} \underline{\nabla}_x n^e + \frac{\mathcal{D} n^e}{\theta^e} e \underline{E}_{dc}\right] \tag{2.56}$$

where

$$\mathcal{D} \equiv \frac{32\,\theta^e}{9\pi m \nu_{en}} (1 - y^2 g(y)) \tag{2.57}$$

The effective collision frequencies ν_{en} and ν_{ei} are defined as

$$\nu_{en} = \frac{4}{3} N q_{en} \sqrt{\frac{8\theta^e}{\pi m}} \tag{2.58}$$

and

$$\nu_{ei} = \frac{4}{3} n^i \frac{e^4 \sqrt{2\pi}}{\theta^e \sqrt{m \theta^e}} \ln\left(\frac{3}{2e^3}\sqrt{\frac{(\theta_o^e)^3}{\pi n_o^e}}\right) \tag{2.59}$$

for singly ionized ions. The term g(y) is a tabulated auxiliary exponential integral function defined as (see Appendix B)

$$g(y) \equiv \int_0^\infty \frac{x\, e^{-yx}}{x^2 + 1}\, dx \quad , \quad (\mathrm{Re}\ y > 0) \tag{2.60}$$

for the case considered here, y is a real variable given by

$$y^2 \equiv \frac{2\nu_{ei}}{\nu_{en}} \tag{2.61}$$

When evaluating the high frequency conductivity term in Eq. (2.48), first term on the right hand side, we take the carrier frequency, ω_D, to be much greater than the collision rate, g, and therefore neglect g^2 compared to ω_D^2. With this additional assumption the electron temperature balance equation, Eq. (2.48), becomes

$$\frac{\partial \theta^e}{\partial t} + \frac{1}{n^e}\int_0^\infty dv\, v^2\left(\theta^e - \tfrac{1}{3}mv^2\right) S(f_0) + \frac{2m}{M}(\theta^e - \theta^n)(\nu_{en} + \nu_{ei})$$

$$= \frac{E_0^2 \gamma(t)}{3} \mathrm{Re}(\sigma_{ac})_n + \frac{2}{3} E_{dc}^2 (\sigma_{dc})_n + \frac{2e}{3n^e}\left(\underline{E}_{dc} \cdot \underline{\nabla}_x n^e\right) D +$$

$$- \frac{1}{n^e} \underline{\nabla}_x \cdot \left[\left(e \underline{E}_{dc} n^e + \theta^e \underline{\nabla}_x n^e\right) D \varrho_{dc}\right] \tag{2.62}$$

where the real part of the high frequency conductivity, normalized by n^e, is

$$\mathrm{Re}(\sigma_{ac})_n = \frac{e^2}{m\omega_D^2}(\nu_{en} + \nu_{ei}) \tag{2.63}$$

the dc conductivity is, normalized by n^e, (see Appendix A)

$$(\sigma_{dc})_n = \frac{32 e^2}{9\pi m \nu_{en}}\left(1 - y^2 g(y)\right) \tag{2.64}$$

and

$$\varrho_{dc} = \frac{\left[-\frac{1}{3} - y^2 g(y) - \frac{4}{3} y^3 \frac{\partial g(y)}{\partial y}\right]}{\left[1 - y^2 g(y)\right]} \tag{2.65}$$

In the following sections of this chapter, we expand $\theta^e(t)$ and $n^e(t)$ about their steady state values as $\theta_o^e + \delta\theta^e(t)$ and $n_o^e + \delta n^e(t)$. By neglecting

products of the small variables, we obtain linear equations for the electron temperature and density time variations and nonlinear equations for the steady state values. We take θ_o^e and n_o^e to be known solutions of the steady state equations and solve for the variations $\delta\theta^e(t)$ and $\delta n^e(t)$ in terms of them.

For the electron temperature balance equation, treated in the next section, we reduce Eq. (2.62) in order to obtain a useful solution. We noted that the measured steady state electron temperature and dc electric field (using Langmuir probes as discussed in Chapter IV) correlate very well by equating the volume loss rate, third term on the left hand side of Eq. (2.62) and the dc conductivity term. Hence, we neglect the variations in θ^e due to particle flow rates by dropping the last two terms of Eq. (2.62). Furthermore, we neglect the variance-like term resulting from the inelastic collisions, the second term on the left hand side of Eq. (2.62).

For the electron density balance equation, treated in Section D, we consider the effects due to electron-ion recombination and electron-neutral atom ionization collisions by taking

$$\int_0^\infty dv\, v^2 S(f_o) = \beta n^e - \alpha (n^e)^2 \tag{2.66}$$

where β is the ionization rate and α is the recombination coefficient. We assume that the coefficients are not explicit functions of n^e, although they may depend on θ^e. The entire right hand side of Eq. (2.56) is retained since for the steady state discharge used in this experiment the dominant contributions

to n_o^e, both in magnitude and spatial variation, come from the effects of diffusion and mobility. Note that the dc electric field considered here is the actual field in the plasma, which is to be measured if needed.

C. VARIATIONS IN THE ELECTRON TEMPERATURE

In the previous section we derived a fairly general electron temperature balance equation. A reduced form of the equation, which neglects all gradients in configuration space but retains the space dependence of all the variables, can be written as

$$\frac{\partial \theta^e(\underline{x},t)}{\partial t} + L(\underline{x},t) = G(\underline{x},t) + P(\underline{x},t) + P_i(\underline{x},t) \tag{2.67}$$

where

$$L = \frac{2m}{M}(\nu_{en} + \nu_{ei})(\theta^e - \theta^n) \tag{2.68}$$

$$G = \frac{64 e^2 E_{dc}^2}{27\pi m \nu_{en}}\left[1 - y^2 g(y)\right] \tag{2.69}$$

$$P = \frac{e^2 E_D^2}{3m\omega_D^2}(\nu_{en} + \nu_{ei})\left(1 + \frac{\delta_o^2}{2}\right) \tag{2.70}$$

and

$$P_1 = \frac{2e^2 E_0^2}{3 m \omega_0^2} (\nu_{en} + \nu_{ei}) \delta_0 \left(\cos \omega_m t + \frac{\delta_0}{4} \cos 2\omega_m t \right) \tag{2.71}$$

The terms in Eq. (2.67) are given the following physical interpretations: L is the electron temperature loss rate due to collisions with the neutral atoms and ions; G is the electron temperature gain rate due to the dc electric field; and $(P + P_1)$ is the gain rate to the electron temperature due to the amplitude modulated high frequency electric field.

We now linearize Eq. (2.67) for small variations in the electron temperature and density due to the slowly varying source term P_1. That is, we expand θ^e and n^e about their steady state value as $\theta^e = \theta_o^e + \delta\theta^e$ and $n^e = n_o^e + \delta n^e$, and neglect all products in the small quantities of P_1, $\delta\theta^e$, and δn^e. The equation for the time variations of $\delta\theta^e$ is

$$\frac{1}{\theta_o^e} \frac{\partial \delta\theta^e}{\partial t} + \omega_a \frac{\delta\theta^e}{\theta_o^e} + \omega_c \frac{\delta n^e}{n_o^e}$$

$$= \frac{2e^2 E_0^2}{3 m \omega_0^2 \theta_o^e} (\nu_{en} + \nu_{ei}) \delta_0 \left(\cos \omega_m t + \frac{\delta_0}{4} \cos 2\omega_m t \right) \tag{2.72}$$

where

$$\omega_a = \left[\frac{\partial L}{\partial \theta^e} - \frac{\partial G}{\partial \theta^e} - \frac{\partial P}{\partial \theta^e} \right]_{\theta^e = \theta_o^e} \tag{2.73}$$

and

$$\omega_c = \frac{n_o^e}{\theta_o^e}\left[\frac{\partial L}{\partial n^e} - \frac{\partial G}{\partial n^e} - \frac{\partial P}{\partial n^e}\right]_{n^e = n_o^e} \tag{2.74}$$

The coupling term in Eq. (2.72) proportional to ω_c results from the electron-ion collision frequency through its dependence on the ion density. We are assuming that the density of scattering centers for the electron-ion collision frequency can be taken as n^e instead of n^i at each point in the plasma. Furthermore, for the slow variations considered in this analysis, we have replaced $\delta n^i/n_o^i$ by $\delta n^e/n_o^e$ in Eq. (2.72). The steady state electron temperature is taken as the solution of the nonlinear equation

$$L(\theta_o^e, n_o^e) = G(\theta_o^e, n_o^e) + P(\theta_o^e, n_o^e) \tag{2.75}$$

or more explicitly

$$\theta_o^e = \theta_o^n + \frac{e^2 E_D^2 M}{6 m^2 \omega_D^2}\left(1 + \frac{\delta_o^2}{2}\right) + \frac{e^2 E_{dc}^2 M}{3 m^2 \nu_{en}^2}\left(\frac{64}{9\pi}\right)\left[\frac{1 - y^2 g(y)}{2 + y^2 g(y)}\right] \tag{2.76}$$

Note that the last term is a nonlinear function of θ_o^e through y and ν_{en}^2.

We will digress slightly to consider the plasma conditions discussed by previous authors on cross-modulation in the ionosphere[3] and afterglow[4] plasmas. In these examples, the dc heating, i.e., G, was not present or was taken to be independent of the electron temperature. Also, for these experiments,

the variations in n^e were neglected entirely. Under these conditions our electron balance Eq. (2.72) reduces to

$$\frac{1}{\theta_o^e}\frac{\partial \delta\theta^e}{\partial t} + \omega_a \frac{\delta\theta^e}{\theta_o^e} = \frac{2\epsilon^2 E_o^2}{3m\theta_o^e \omega_D^2}\delta_o(\nu_{en}+\nu_{ei})\left[\cos\omega_m t + \frac{\delta_o}{4}\cos 2\omega_m t\right] \tag{2.77}$$

and Eqs. (2.76) and (2.73) reduce to

$$\theta_o^e = \theta_o^n + \frac{e^2 E_o^2 M}{6m^2\omega_D^2}\left(1+\frac{\delta_o^2}{2}\right) \tag{2.78}$$

and

$$\omega_a = \left[\frac{\partial L}{\partial \epsilon^e} - \frac{\partial P}{\partial \theta^e}\right]_{\theta^e=\theta_o^e} \tag{2.79}$$

or simply

$$\omega_a = \frac{2m}{M}(\nu_{en}+\nu_{ei})_o \tag{2.80}$$

This expression for ω_a agrees with the decay rate for pulsed cross-modulation derived by Dougal and Goldstein[4] and by Bloch.[20] The latter author's results were for a general velocity dependence for the cross-section for electron momentum transfer, when $\omega_D^2 \gg \nu^2$ total.

We can readily solve Eq. (2.77) for the time dependent variation in the electron temperature. We obtain, after allowing the transients to decay,

$$\delta\theta^e = \frac{e^2 E_D^2}{3 m \omega_D^2} (\nu_{en} + \nu_{ei})_o \left\{ \frac{2\delta_o \cos(\omega_m t - \tan^{-1}\frac{\omega_m}{\omega_a})}{\sqrt{\omega_a^2 + \omega_m^2}} + \frac{\delta_o^2 \cos(2\omega_m t - \tan^{-1}\frac{2\omega_m}{\omega_a})}{\sqrt{\omega_a^2 + 4\omega_m^2}} \right\} \tag{2.81}$$

This result for the electron temperature will be identical to that of Huxley and Ratcliffe,[3] if we further neglect the effects due to the electron-ion collisions. This approximation appears reasonable in the ionosphere, as was considered by Huxley and Ratcliffe. However, in our plasma the effects of the electron-ion collisions, dc electric field, and the variations in the electron density are found to be important to interpreting the experimental results. Therefore, we will treat the entire effect on the electron temperature as given by Eq. (2.72), along with Eqs. (2.73) and (2.74).

The electron temperature of the steady state plasma considered in this experiment is larger than the neutral atom and ion temperature due to the dc electric field. For this case we can neglect the small effect due to the high frequency heating, P. We take θ_o^e as the solution of

$$L(\theta_o^e, n_o^e) = G(\theta_o^e, n_o^e) \tag{2.82}$$

and ω_a as

$$\omega_a = \left[\frac{\partial L}{\partial \theta^e} - \rho_\theta \frac{L}{\theta^e} \right]_{\theta^e = \theta_c^e} \tag{2.83}$$

where in writing Eq. (2.83) we have used Eq. (2.82) and defined the factor

$$\rho_\theta = \left[\frac{\theta^e}{G} \frac{\partial G}{\partial \theta^e} \right]_{\theta^e = \theta_o^e} = \frac{\left[-\frac{1}{2} + \frac{5}{2} y^2 g(y) + y^3 \frac{\partial g(y)}{\partial y} \right]}{\left[1 - y^2 g(y) \right]} \tag{2.84}$$

The values for ρ_θ are plotted in Appendix B, Fig. B.1, and vary from -0.5 to +1.5 as $y^2 = 2\nu_{ei}/\nu_{en}$ varies from 0 to ∞. After performing the indicated derivative in Eq. (2.83) we can express the break frequency as

$$\omega_a = \frac{2m}{M} \left\{ \nu_{en} \left[\left(\frac{3}{2} - \rho_\theta \right) - \left(\frac{1}{2} - \rho_\theta \right) \frac{\theta_o^n}{\theta_o^e} \right] \right.$$

$$\left. - \nu_{ei} \left[\left(\frac{1}{2} + \rho_\theta \right) - \left(\frac{3}{2} + \rho_\theta \right) \frac{\theta_o^n}{\theta_o^e} \right] \right\} \tag{2.85}$$

A detailed study of the break frequency in Eq. (2.85) shows that the dependence of the dc conductivity on the electron-ion collision frequency has an important effect on the value of ω_a. At the equilibrium value of $\theta_o^e = \theta_o^n$, Eq. (2.85) reduces to Eq. (2.80) and ω_a increases with the electron density through the electron-ion collision frequency. However, at electron temperatures greater than $3\theta_o^n/2$ the effect due to the electron-ion collision frequency

is eventually to decrease ω_a as the electron density increases. In fact, at quite modest electron densities the break frequency will pass through zero and take on negative values.* For example, at the electron temperature of 0.06 eV, in a helium plasma at a gas pressure of 0.378 Torr and $\theta_o^n = 0.025$ eV, we find that ω_a is zero at an electron density of about 6.2×10^{11} elec/cc. This condition corresponds to a fractional ionization, n_o^e/N, of only 4.5×10^{-5}.

Another interesting extreme condition for ω_a, in contrast to the thermodynamic equilibrium condition, is for high electron temperatures. When $\theta_o^e \gg \theta_o^n = \theta_o^i$, Eq. (2.85) becomes

$$\omega_a = \frac{2m}{M}\left[(2 + \delta\rho_\theta)\nu_{en} - \delta\rho_\theta \nu_{ei}\right] \tag{2.86}$$

We have written ρ_θ as $(-0.5 + \delta\rho_\theta)$ since at these higher electron temperatures and modest electron densities, $\delta\rho_\theta$ is very small. Neglecting the electron-ion contribution, the break frequency ω_a is about twice as large in Eq. (2.86) as for the equilibrium condition in Eq. (2.80).

---

*The condition of negative values for ω_a corresponds to the electron temperature runaway phenomenon in the presence of neutral atoms. This phenomenon results from energy being absorbed by the electron gas from the dc electric field at a rate exceeding the temperature loss rate. Since the electron-ion collision frequency varies inversely with the electron temperature this condition can be obtained when the loss rate is dominated by the electron-ion collisions. The phenomenon in a fully ionized gas is discussed by Dreicer[21] or for more references see Delcroix.[22]

To evaluate the coupling rate ω_c, we can also neglect the small effect due to the high frequency heating, P. We can then write it as

$$\omega_c = \frac{2m}{M}\left(1 - \frac{\theta_o^n}{\theta_o^e}\right)\left[\nu_{ei} + \frac{(\nu_{en} + \nu_{ei})}{2}\left(\rho_\theta + \frac{1}{2}\right)\right] \tag{2.87}$$

The ρ_θ is the same as given in Eq. (2.84), and recall that it varies from -0.5 to +1.5 as the ratio of the electron-ion to electron-neutral atom collision frequencies increases from zero. We see that ω_c is always a positive quantity and varies approximately like $(2m/M)\ \nu_{ei}$ for high electron temperatures and/or low electron densities. In the range of electron temperatures and densities of interest in this experiment (see Fig. 4.6), ω_c is found to be of the same order as the frequency ω_a.

D. VARIATIONS IN THE ELECTRON DENSITY

In Section B we derived an electron density balance equation, neglecting the gradients of the electron temperature, which can be written

$$\frac{\partial n^e}{\partial t} = \beta n^e - \alpha (n^e)^2 + S \tag{2.88}$$

where α is the volume recombination coefficient and βn^e is the volume source rate for electrons due to ionizations. The "leakage" term is given by

$$S = \underline{\nabla}_x \cdot D\, \underline{\nabla} n^e + \frac{1}{\theta^e}\, \underline{\nabla}_x \cdot n^e D e \underline{E}_{dc} \tag{2.89}$$

where

$$D = \frac{32\theta^e}{9\pi m \nu_{en}}\left[1 - y^2 g(y)\right] \tag{2.90}$$

D is the electron diffusion coefficient and eD/θ^e is the electron mobility. Note that $\underline{E}_{dc}$ is the actual steady state electric field in the plasma at any point due to the applied electrode voltage and space charge effects. Often, Poisson's equation is used to eliminate the radial space charge electric field and then the diffusion coefficient becomes the ambipolar diffusion coefficient.[22] This will not be necessary for our analysis.

We take the steady state electron density, n_o^e, to be the solution of

$$\alpha_o (n_o^e)^2 = \beta n_o^e + S_o \tag{2.91}$$

We then make the small variable expansion of n^e and θ^e, about n_o^e and θ_o^e, to obtain an equation for the slow variations in the electron density. We neglect the gradients of $\delta n^e/n_o^e$, as well as $\delta\theta^e/\theta_o^e$, and the products in the small variations δn^e and $\delta\theta^e$ to obtain

$$\frac{1}{n_o^e}\frac{\partial \delta n^e}{\partial t} + \omega_b \frac{\delta n^e}{n_o^e} = \omega_d \frac{\delta\theta^e}{\theta^e} \tag{2.92}$$

where

$$\omega_b = 2\alpha_o n_o^e - \beta_o - \left(\frac{\partial S}{\partial n^e}\right)_{n^e=n_o^e} \tag{2.93}$$

and

$$\omega_d = \frac{\theta_o^e}{n_o^e}\left[n^e \frac{\partial \beta}{\partial \theta^e} - (n^e)^2 \frac{\partial \alpha}{\partial \theta^e} + \frac{\partial S}{\partial \theta^e}\right]_{\theta^e=\theta_o^e} \tag{2.94}$$

We rewrite the break frequency ω_b by introducing the factor

$$\rho_n = \left[\frac{n^e}{S}\frac{\partial S}{\partial n^e}\right]_{n^e=n_o^e} = \frac{\left[1 - 2y^2 g(y) - \frac{y^3}{2}\frac{\partial g(y)}{\partial y}\right]}{\left[1 - y^2 g(y)\right]} \tag{2.95}$$

which in terms of the previously discussed factor ρ_θ is simply

$$\rho_n = -\frac{\rho_\theta}{2} + \frac{3}{4} \tag{2.96}$$

Subtracting $\rho_n S_o$ from Eq. (2.93), using Eq. (2.91), we obtain

$$\omega_b = \alpha_o n_o^e (2 - \rho_n) - \beta_o (1 - \rho_n) \tag{2.97}$$

As the ratio $y^2 = 2\nu_{ei}/\nu_{en}$ increases from 0, the factor ρ_n varies from 1 to 0. Therefore, the break frequency ω_b ranges from $\alpha_o n_o^e$, when ν_{ei} is small compared to ν_{en}, to $(2\alpha_o n_o^e - \beta_o)$ when ν_{ei} is the dominant collision frequency. The term $-\beta_o$ is generally quite small and can be neglected compared to $\alpha_o n_o^e$.

We can rewrite ω_d, by subtracting $\rho_\theta S_o$ and neglecting the gradient of ρ_θ, as

$$\omega_d = \alpha_o n_o^e \left(\rho_\theta - \frac{\theta_o^e}{\alpha_o}\left[\frac{\partial \alpha}{\partial \theta^e}\right]_o\right) + \frac{\nabla_x \cdot D_o \nabla_x n_o^e}{n_o^e}$$

$$- \beta_o \left(\rho_\theta - \frac{\theta_o^e}{\beta_o}\left[\frac{\partial \beta}{\partial \theta^e}\right]_o\right) \qquad (2.98)$$

If we let α have an electron temperature dependence of $(\theta^e)^{-3/2}$, then the coefficient of the recombination rate in Eq. (2.98) varies from 1 to 3, as $2\nu_{ei}/\nu_{en}$ increases from 0.[23] The diffusion term is negative in most of the regions of our plasma and, due to the large diameter of the plasma, is on the order of $\alpha_o n_o^e$ or less. The last term in Eq. (2.98) is dominated by the derivative term and is a positive contribution to ω_d. However, since β_o is quite small the entire term can be neglected, except when the other two terms nearly cancel each other. Clearly this brief discussion is not conclusive, but is presented as an indication that ω_d can be a small positive number, about $\alpha_o n_o^e$. It will be calculated later in Chapter V when we discuss the evaluation of the experimental response. However, the assumption that the frequencies ω_1 and ω_2 are real numbers, Eqs. (2.22) and (2.23), is supported by the above estimate and is found later to be consistent with the experimental results.

E. RELATIVE IMPORTANCE OF TEMPERATURE AND DENSITY VARIATIONS

The relative contributions to the detector output voltage of the electron temperature and density variations is predominantly determined by the values of (a) and (b) in Eq. (2.13). The results of this experiment indicate that the ratio (a/b) was less than 1/20, and hence that the detector response was primarily due to the variations in the electron density. Since this result may be surprising in contrast to the results and assumptions of other experiments with cross-modulation, we present a qualitative discussion of the parameters (a) and (b).

From Eqs. (2.14) and (2.15)

$$a = \mathcal{R}e\left\{ -\frac{i4\pi\omega_s \epsilon}{c^2 E_o(\underline{x}_r)} \int d^3x' E_o(\underline{x}') G_o(\underline{x}';\underline{x}_r)\, \theta_o^e(\underline{x}') \left[\frac{\partial \sigma}{\partial \theta^e}\right]_o \right\} \tag{2.99}$$

and

$$b = \mathcal{R}e\left\{ -\frac{i4\pi\omega_s \epsilon}{c^2 E_o(\underline{x}_r)} \int d^3x' E_o(\underline{x}') G_o(\underline{x}';\underline{x}_r)\, n_o^e(\underline{x}') \left[\frac{\partial \sigma}{\partial n^e}\right]_o \right\} \tag{2.100}$$

The ratio is written as

$$\frac{a}{b} = \frac{\mathcal{R}e\left\{ \frac{i}{E_o} \int d^3x' E_o G_o \theta_o^e \left[\frac{\partial \sigma_R}{\partial \theta^e}\right]_o \right\}}{\mathcal{R}e\left\{ \frac{i}{E_o} \int d^3x' E_o G_o n_o^e \left[\frac{\partial \sigma_R}{\partial n^e} - i\frac{\partial \sigma_I}{\partial n^e}\right]_o \right\}} \tag{2.101}$$

The complex conductivity in these equations is given explicitly by, Eq. (2.9), Eq. (A.9), or

$$\sigma = \frac{n^e e^2}{m\omega_s^2}\nu - i\frac{n^e e^2}{m\omega_s} \tag{2.102}$$

where $\nu = \nu_{en} + \nu_{ei}$. The imaginary part of $\sigma = \sigma_R - i\sigma_I$ is independent of θ^e as a result of the approximation of $\nu^2 \ll \omega_s^2$.

For the purpose of this discussion, we assume the logarithmic derivatives, such as

$$\frac{\partial \log \sigma_R}{\partial \log n^e} = \frac{n^e}{\sigma_R}\frac{\partial \sigma_R}{\partial n^e} \tag{2.103}$$

to be slowly varying functions of position as compared to the remaining factors in the integrands. This approximation enables us to treat quantities like Eq. (2.103) as constants and take them outside the integrals. To be more specific, we evaluate these slowly varying quantities at a certain point $\underline{x}_p$ in the plasma. Clearly, this approximation is equivalent to assuming that the sensing microwave interacts locally with the plasma at the point $\underline{x}_p$. Other authors have demonstrated that when the collision frequency is much less than the carrier frequency, the microwave begins to interact with the plasma quite strongly when ω_p^2/ω_s^2 is near unity.[24] The plasma frequency is defined by

$$\omega_p^2 = 4\pi \frac{n^e e^2}{m}$$

(2.104)

and we use this to help define the point $\underline{x}_p$. This condition for the interaction is particularly applicable for the reflected signal, which appeared to be the major contribution to cross-modulation in our experiment.

With this reasoning, we define

$$K_1 = \frac{i}{E_0(\underline{x}_r)} \int d^3x' E_0(\underline{x}') G_0(\underline{x}'; \underline{x}_r) \sigma_R(\underline{x}')$$

(2.105)

and

$$K_2 = \frac{i}{E_0(\underline{x}_r)} \int d^3x' E_0(\underline{x}') G_0(\underline{x}'; \underline{x}_r) \sigma_I(\underline{x}')$$

(2.106)

Equation (2.101) is now written as

$$\frac{a}{b} = \frac{\theta_0^e (\partial\sigma_R/\partial\theta^e)_0}{n_0^e (\partial\sigma_R/\partial n^e)_0} \left[1 + \frac{Re(K_2)\, \sigma_R (\partial\sigma_I/\partial n^e)_0}{Re(K_1)\, \sigma_I (\partial\sigma_R/\partial n^e)_0} \right]^{-1}$$

(2.107)

Evaluating the partial derivatives using Eq. (2.102), we obtain

$$\frac{a}{b} = \frac{(\frac{1}{2}\nu_{en} - \frac{3}{2}\nu_{ei})}{(\nu_{en} + 2\nu_{ei})}\left[1 + \frac{(\nu_{en} + \nu_{ei})\,Re(K_2)}{(\nu_{en}+2\nu_{ei})\,Re(K_1)}\right]^{-1} \tag{2.108}$$

Although the first factor in Eq. (2.108) vanishes when $\nu_{en} = 3\nu_{ei}$ (which is satisfied in a cylindrical region at about half of the plasma radius under the conditions of Fig. 4.6), the main reason for (a/b) to be small is perhaps due to the large denominator, second factor in the equation. It is difficult to evaluate the terms $Re(K_1)$ and $Re(K_2)$ appearing in Eq. (2.108) quantitatively to demonstrate this point because they involve the Green's function for the steady state sensing microwave. However, we can still gain some insight to the magnitude of the second factor by considering a plane wave reflected from a semi-infinite plasma. For this case, we find that the denominator (see Appendix C for some of the details of this calculation) can be written as

$$\left\{\left[1 - \frac{(1-\eta)}{\eta d^2}\right]\left[1 - \frac{\eta(2-\eta)(1-\eta) + \eta^3 d^2/4}{2(1-\eta)\left[\eta(1-\eta)^2 - (1-\eta)\eta^2 d^2/2 - \eta^3 d^2/4\right]}\right]\right\}^{-1} \tag{2.109}$$

where $\eta = (\omega_p^2/\omega_s^2) < 1$ and $d^2 = (\nu^2/\omega_s^2) \ll 1$. It can be shown that for low electron densities, i.e., $\eta \ll 1$, Eq. (2.109) reduces to approximately

$$\frac{2d^2}{3} \tag{2.110}$$

For higher electron densities, such that $(1 - \eta) \ll 1$, Eq. (2.109) reduces to approximately

$$2\eta(1-\eta)d^2 \tag{2.111}$$

Both of the limits in Eqs. (2.101) and (2.111) make the ratio (a/b) very small.

From the preceding discussion, we conclude that there are experimental conditions in which the variations in the electron density dominate the cross-modulation measurement. This has been found experimentally to be the case for our measurements.

III. EXPERIMENTAL APPARATUS

The experimental apparatus consisted of a vacuum station and discharge, microwave, and Langmuir probe circuits. A photographic view of the entire system is shown in Fig. 3.1.

A. VACUUM SYSTEM

The discharge volume was a bell jar, 18 in. in diam and 30 in. in height, supported by a 20 in. stainless steel base plate. A Kinney PV-400 vacuum station proved satisfactory for this experiment. To obtain a stable vacuum-discharge system it was necessary to cycle the discharge and pumping periods. This technique served to outgas the bell jar and "age" the cathode surface. After several weeks of this conditioning procedure, the vacuum was stable for discharge times over 12 hr with no apparent outgassing.

The pressure rise rate after the outgassing procedure was less than 10^{-5} Torr/hr or an equivalent leak rate of 3×10^{-7} Torr-liter/sec. At an operating pressure of .5 Torr and for a discharge time of 12 hr this was less than a .03% change in the pressure.

Helium (10 parts/million impurity) was used throughout this study as the discharge gas. The gas was admitted to the bell jar through an inlet port passing through the base plate (anode). The system pressure was recorded by a thermocouple gauge, which was also mounted on the base plate. The helium pressure response of the thermocouple gauge was calibrated using a Cenco McCleod gauge. The standard deviation for reproducing a given pressure was less than ±3%.

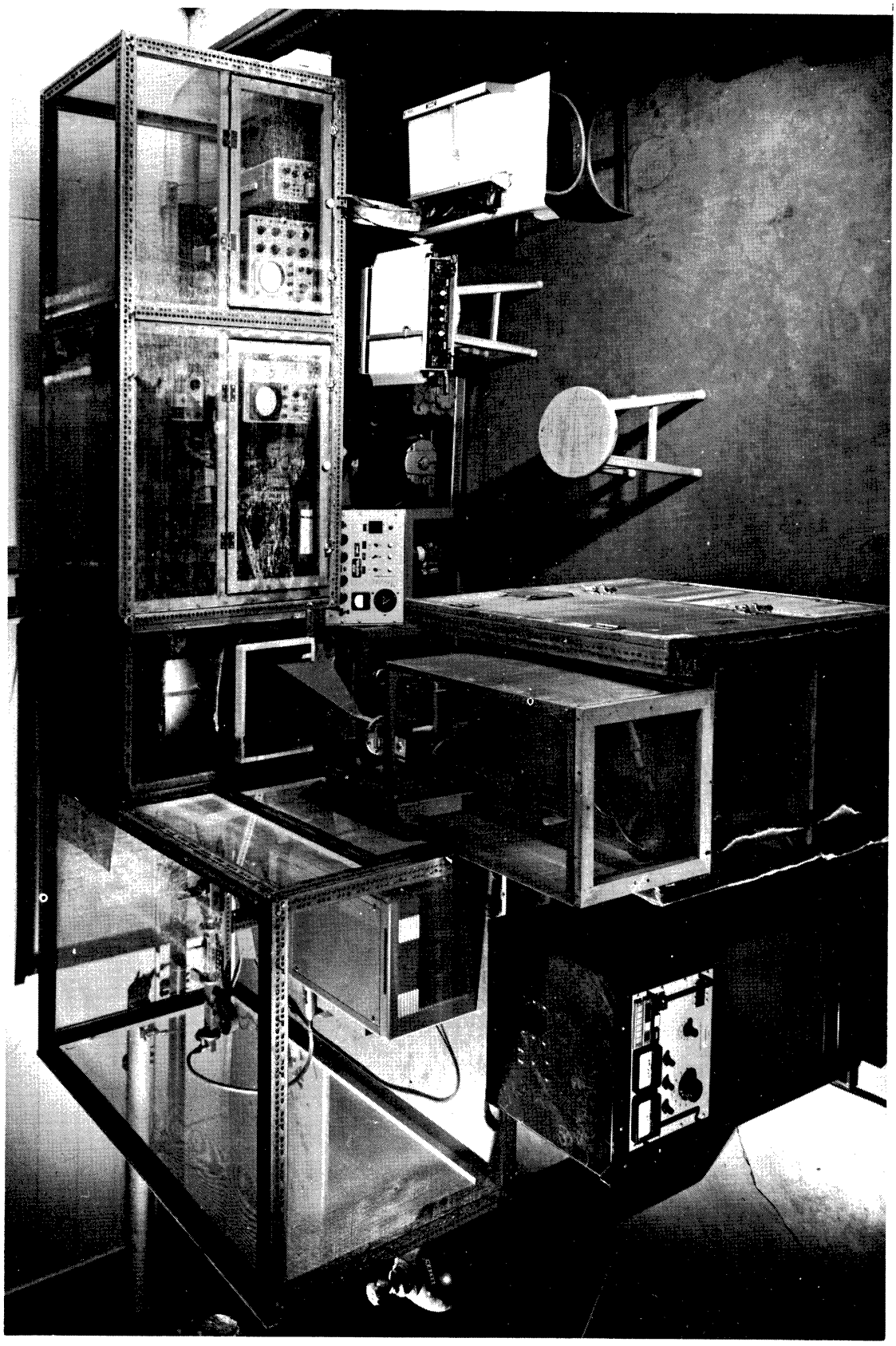

Fig. 3.1. Photographic view of the apparatus showing: the high voltage power supply; the movable disturbing microwave circuit; the sensing microwave circuit; the bell jar discharge with some of the microwave absorber removed; the pumping station; and the receiving and recording instrumentation on the right.

B. DISCHARGE SYSTEM

The high voltage discharge circuit is illustrated in Fig. 3.2. The power supply was a Universal Voltronic BAL 6-300-M, with maximum output power of 1200 w. This power supply had a rated 2% rms ripple which resulted in a comparable oscillation in the discharge and an additional 30 Hz low pass filter was necessary. This resulted in less than .02% rms ripple for a 20 kohm loading.

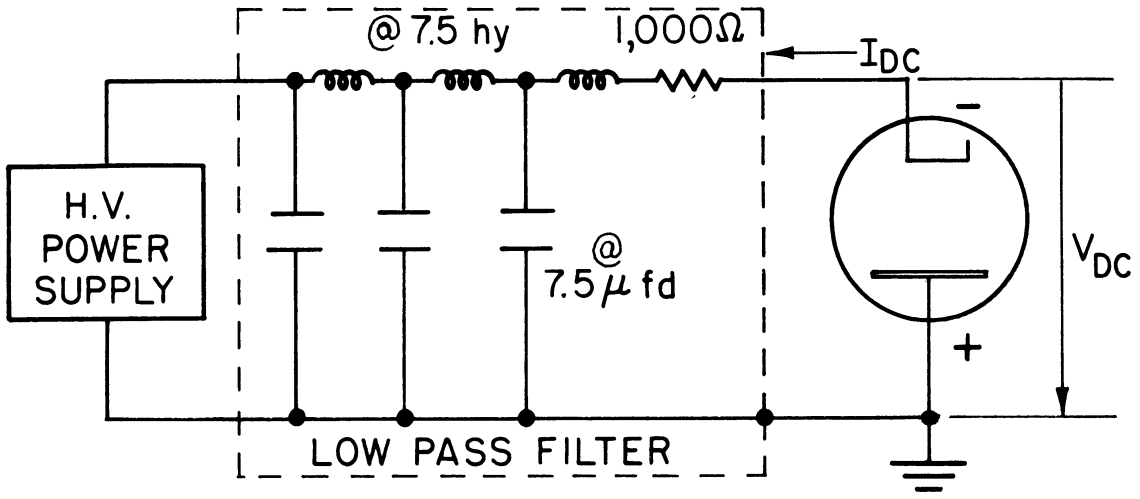

Fig. 3.2. High voltage discharge circuit.

The stainless steel base plate provided the grounded anode for the glow discharge. The high voltage cathode was made of a 12 in. aluminum disc placed 24 in. above the anode. The cathode was supported by a 1/2 in. copper rod which passed through the base plate at a radial point of 7 in. and was connected to the top of the cathode. The edge and top of the cathode disc, as well as the supporting rod, were insulated by teflon. The feed through supporting post was made of low density polyethylene, which insulated and sealed the electrode to the base plate (see Figs. 3.3 and 3.4).

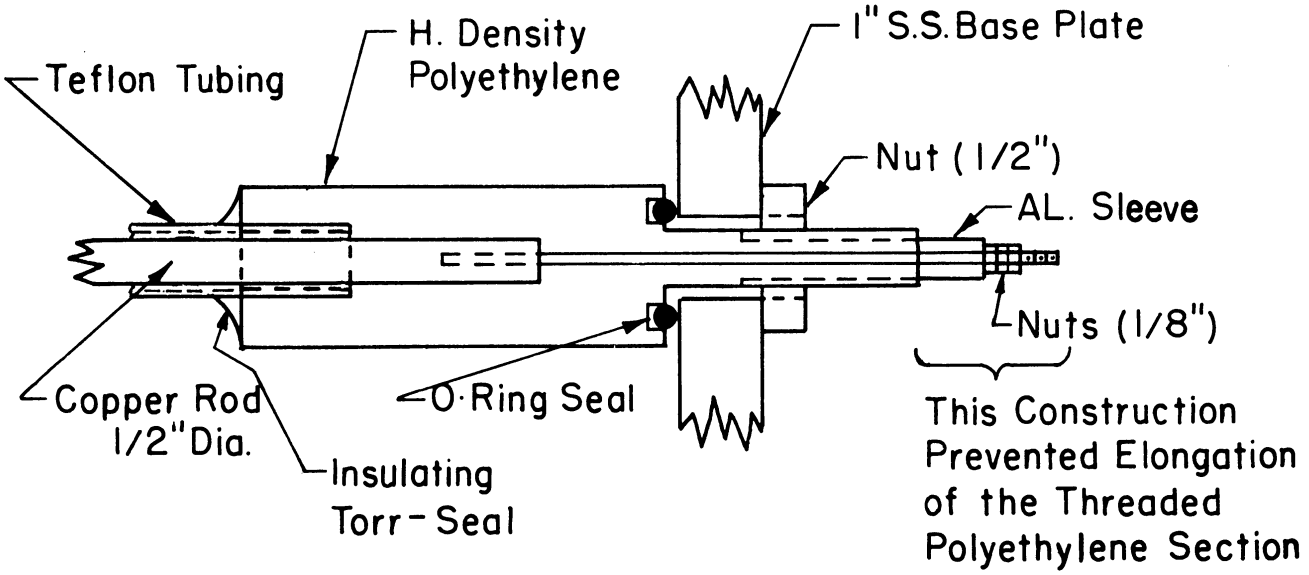

Fig. 3.3. Detail of the H.V. cathode supporting post and its vacuum seal construction.

Aluminum was selected as the cathode material since it reportedly had a relatively low sputtering rate.[25] Nevertheless, aluminum was evolved from the cathode and depositions of the powder were noted on the bell jar walls and supporting structure near the cathode.

C. LANGMUIR PROBE CIRCUIT

A very important diagnostic tool used in this experiment was the single element Langmuir probe. Properly used, this probe can yield quantitative information on the free electron density and temperature with reasonable spatial resolution.

Two different probes were used. The first was a 1 cm length of 10 mil tungsten wire and the second was a hairpin loop of 10 mil tungsten wire which had a total exposed length of 1.8 cm. Both probes were mounted on a 4 ft

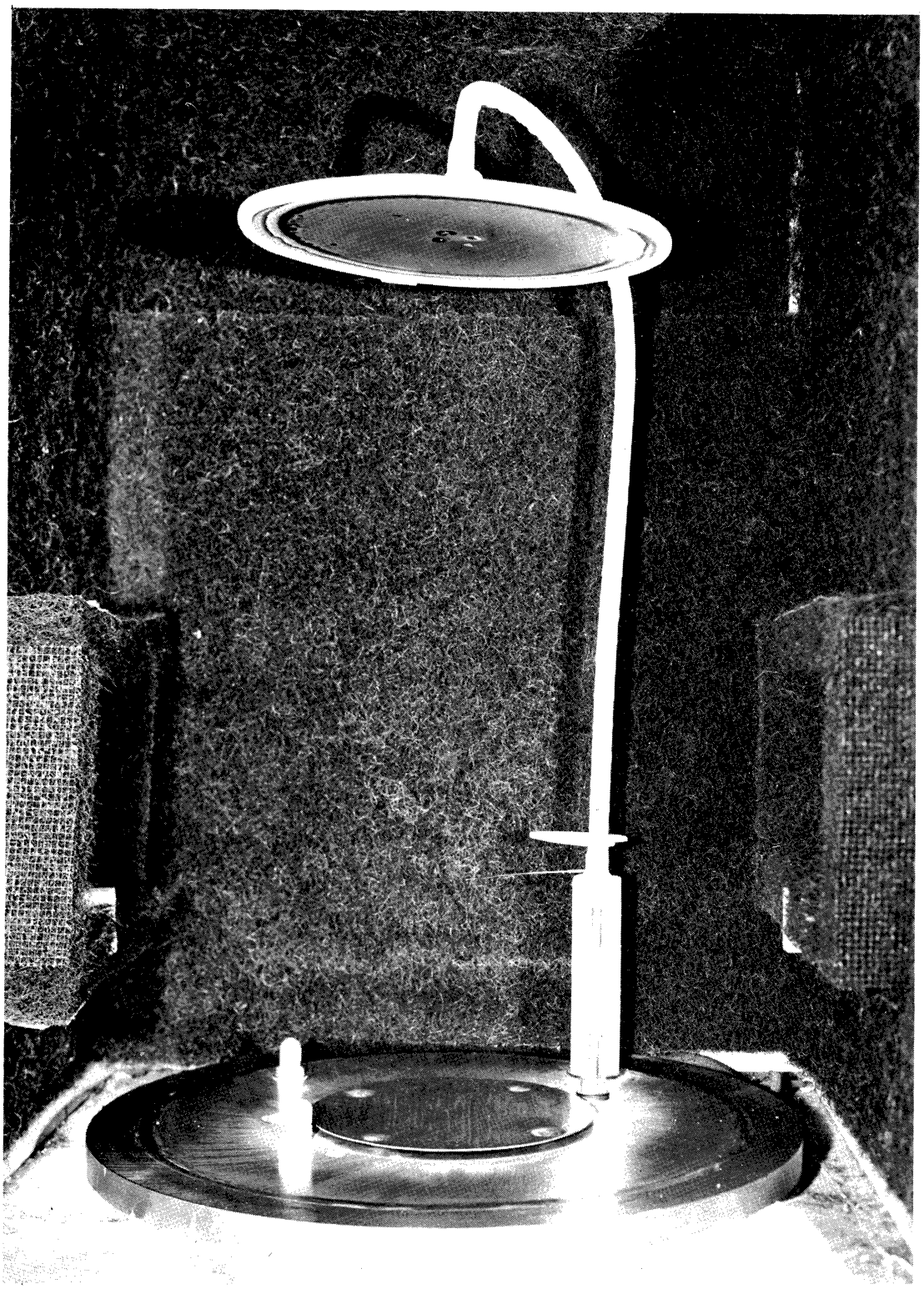

Fig. 3.4. Photographic view of electrode structure with bell jar removed. As shown, the entire discharge was enclosed within a microwave absorbing "box."

length of 3/8 in. diam pyrex tubing. This support was sealed to the base plate at a radius of 4-3/4 in. by a dual sealing rubber stopper. This seal allowed the probe to be placed at any vertical position and at representative radial positions. The probe leads were vacuum sealed by a Torr-Seal plug moulded around the leads at the bottom of the glass tubing (see Fig. 3.5).

The complete probe circuit is shown in Fig. 3.6 and consisted of four individual circuits. Circuit A provided a dc current of about 3 amperes to heat the hairpin probe to a dull red. This feature of the loop probe yielded a more stable probe surface condition. The single element probe used earlier showed a continuous change in its response (on a time scale of seconds) after heating by electron bombardment. This heating was provided by circuit B. When the continuously heated hairpin probe was used, only long time changes over several minutes were noticed in the probe responses and these could be "rezeroed" by flash heating the probe by electron bombardment. The primary probe circuit C provided a time varying voltage to the probe through a decaying RC circuit. The resulting probe voltage was recorded directly on the X-axis of a Mosely 2-D X-Y recorder. The probe current passed through a 1% precision 200 ohm resistor. This latter voltage was amplified with a gain from 2 to 10 and then the log of this voltage was recorded on the Y-axis of the recorder. This resulted in a semi-log trace of the current-voltage response of the probe in the plasma.

Because of the very low electron temperature, the circuit D was used to obtain a more sensitive measurement of the slope of the semi-log probe response. The circuit consisted of a transistor controlled square-wave current source.

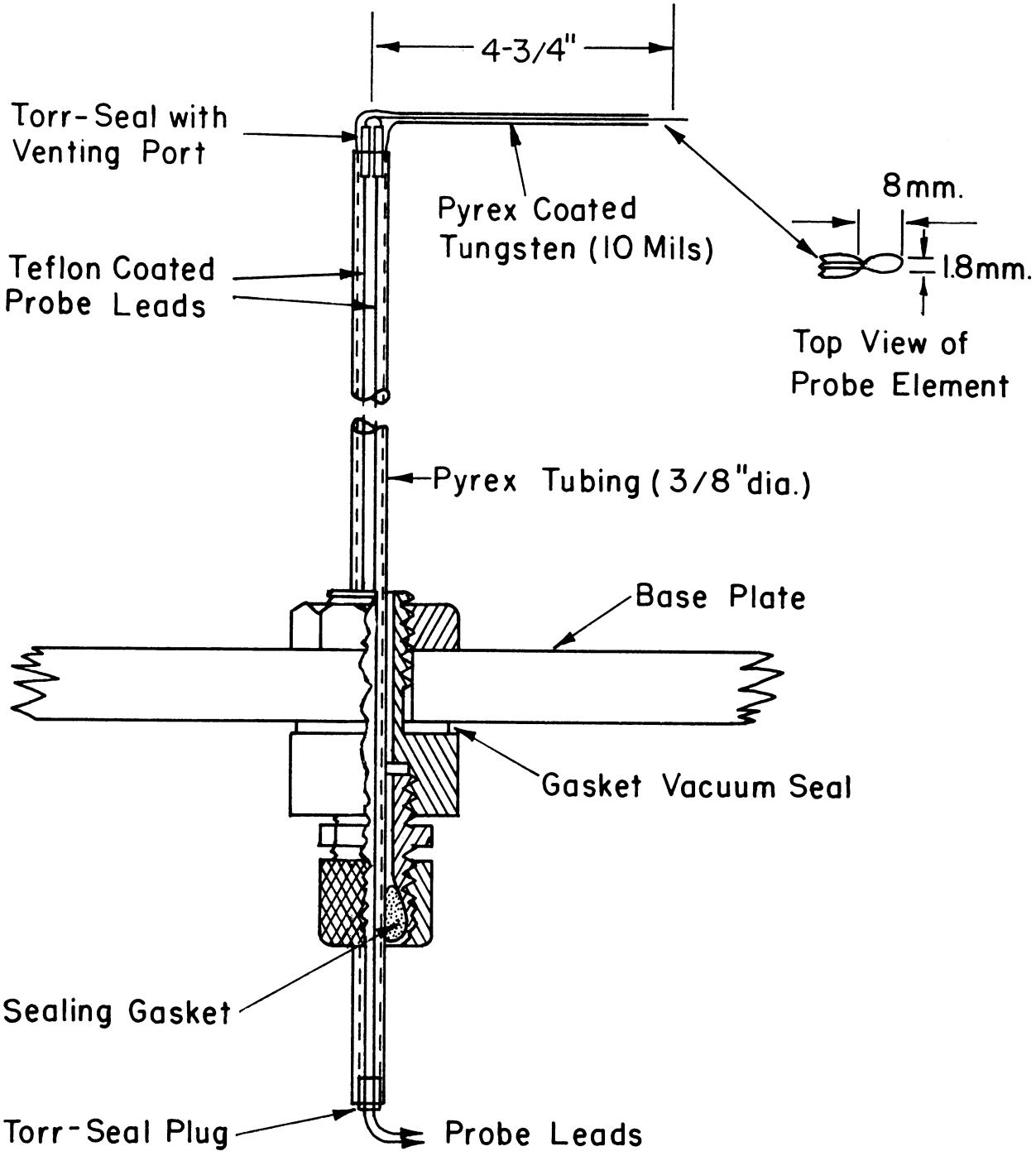

Fig. 3.5. Construction of the Langmuir hairpin probe and the movable probe vacuum seal.

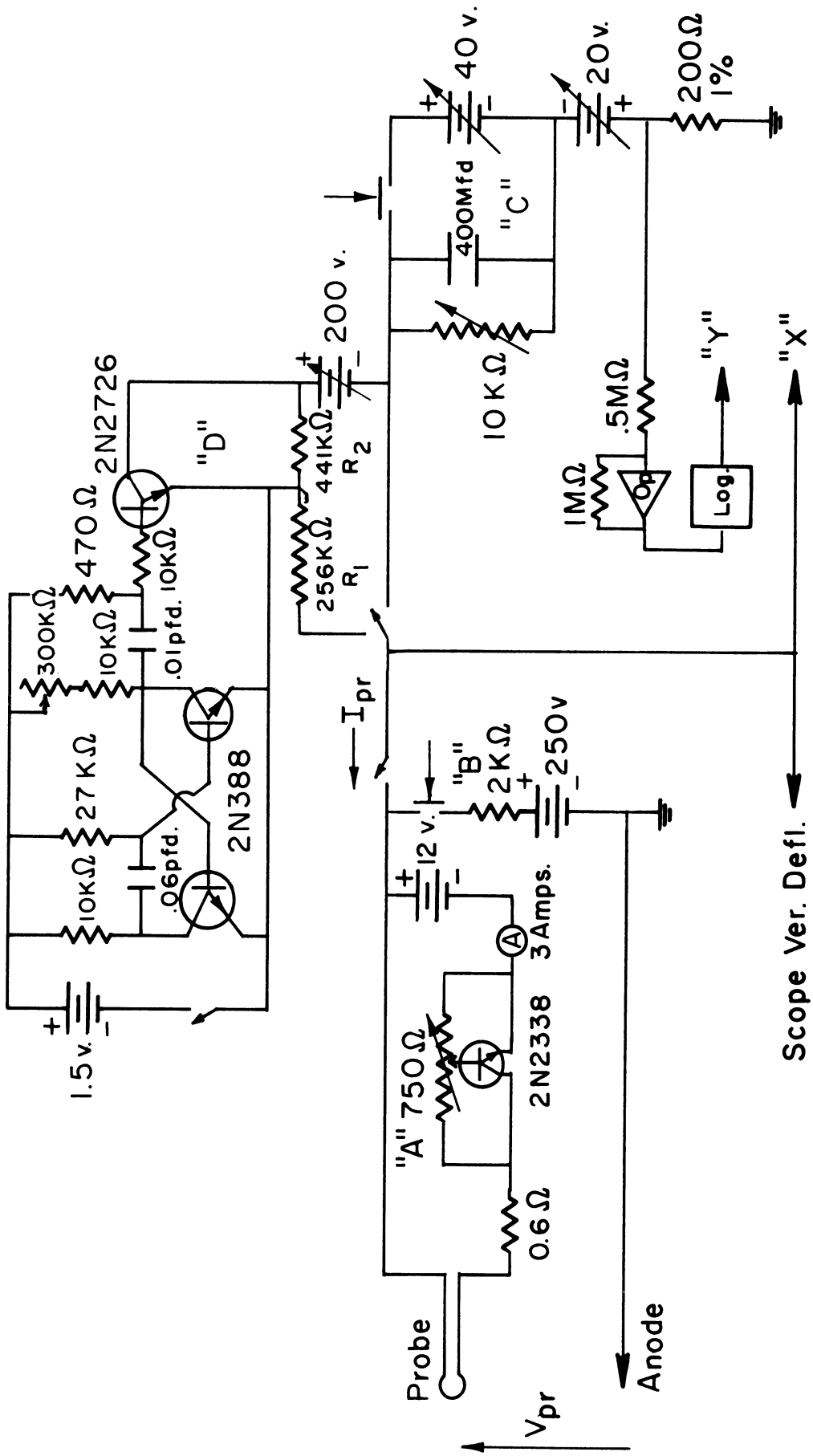

Fig. 3.6. Langmuir probe circuit.

The resistors R_1 and R_2 were chosen such that $(R_1 + R_2)/R_1 = 2.72$. Since the voltage change in the electron transition region was exponential (see Eq. (4.2)), this choice of current ratio led to a direct calibration of resulting change in probe voltage, ΔV_{pr}, in terms of the electron temperature in electron volts. The oscillating voltage was recorded directly on an oscilloscope.

D. MICROWAVE CIRCUITRY

The microwave equipment and related instrumentation were composed of two independent systems. The first system generated and transmitted the disturbing microwave signal to the plasma. This signal was produced by a 2K41 Sperry klystron powered by a FXR Z-815B power supply with a supplementary power supply to provide the grid current. The operating conditions were: beam voltage 1250 V, reflector voltage from 440 to 600 V, beam current 50 mA and grid current 15 mA. The signal frequency was 2.7 G Hz and klystron output power was approximately 0.6 w. The sinuscidal modulation was provided by a Hewlett-Packard signal generator model 200CD. The disturbing signal was transmitted to the plasma by S-band rectangular wave guides and horn, and partially collimated by B. F. Goodrich microwave absorber.

The sensing microwave was generated by a 2K42 Sperry klystron powered by a FXR Z-815B power supply. The operating conditions were: beam voltage 100 V, reflector voltage 550 V, beam current 40 mA, and grid current 0 mA. The signal frequency was 3.0 G Hz with klystron output power of 0.1 w. The transmitted and received sensing microwave signals were guided by H-band rectangular wave guides and horns. A schematic drawing of the microwave circuit is shown in Fig. 3.7.

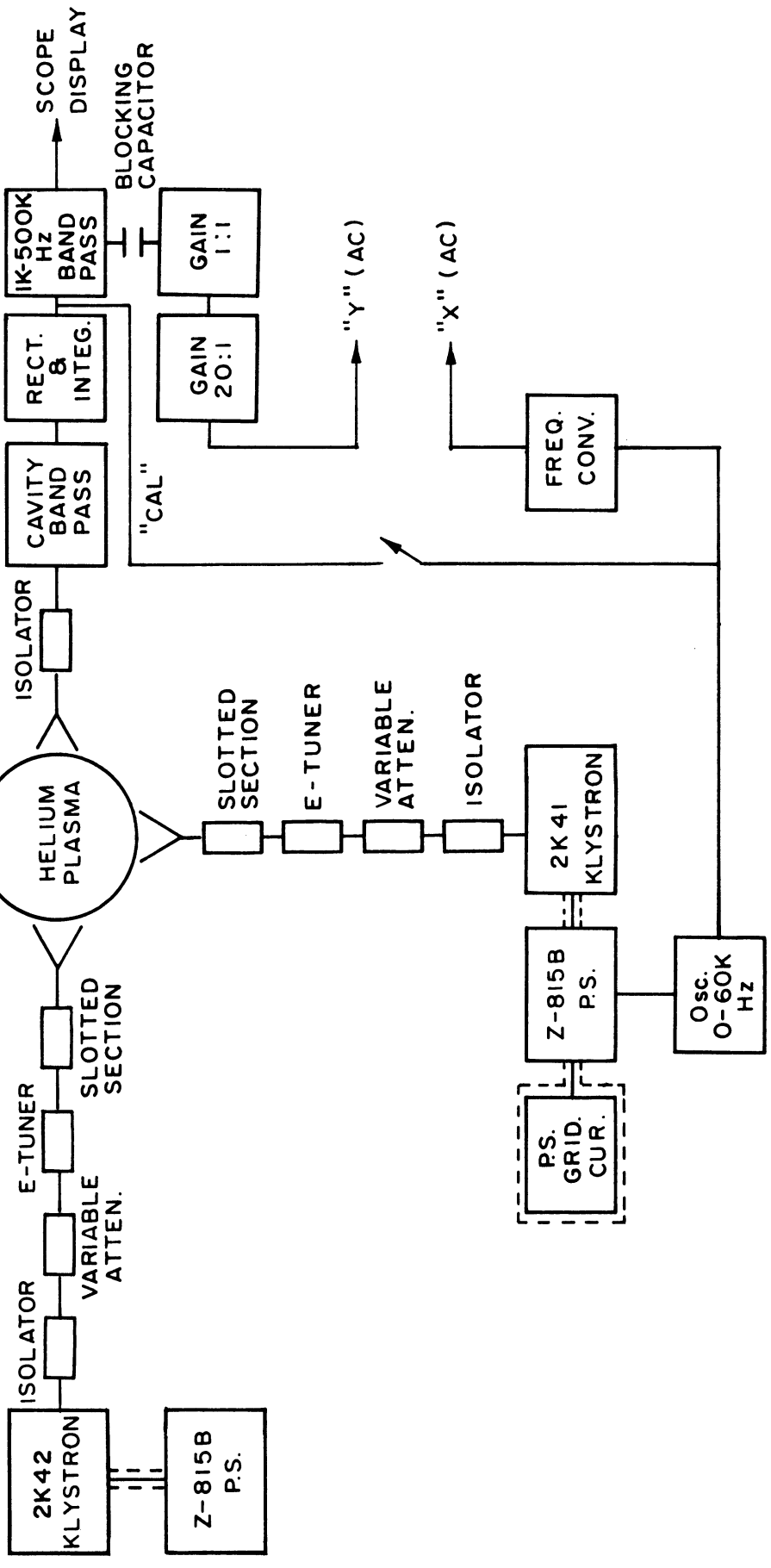

Fig. 3.7. Schematic of the microwave circuit.

The purpose of the receiving circuit, in the upper right of Fig. 3.7, was to detect and record the modulation depth of the audio modulation transferred to the sensing wave from the disturbing wave via the plasma. It was important not to detect any of the disturbing wave directly. The H-band receiving horn and wave guides damped the 2.7 G Hz signal relative to the 3.0 G Hz signal. Then the received signals were separated completely by the 20 M Hz band width cavity tuned to 3.0 G Hz. This signal was rectified by a 1N23B diode and integrated, so that 1/RC was much greater than the modulation frequency, ω_m, and much less than the carrier frequency, ω_s. The resulting signal was amplified and displayed on a Type 545A Tektronix oscilloscope with a 1A7 plug-in unit using a 1 K Hz to 500 K Hz band pass filter. The filter was necessary to help eliminate modulation of the sensing wave due to plasma disturbances which included 60 Hz variations from the cathode voltage source.

The modulation of the received sensing microwave was a maximum of about 0.1% and the entire signal was 30 db less than the original transmitted signal. Much of the signal loss was due to plasma reflection. The oscilloscope signal ac output was amplified by a factor greater than 20 and fed into the ac (full wave rectifier) vertical input of the X-Y recorder amplifier. The recording was completed by sweeping the horizontal response with a voltage related to the modulation frequency. The calibration curve in Fig. 3.8 was the response, from the circuit point marked "Cal" in Fig. 3.7 to the recorder, of the sinusoidal signal from the oscillator.

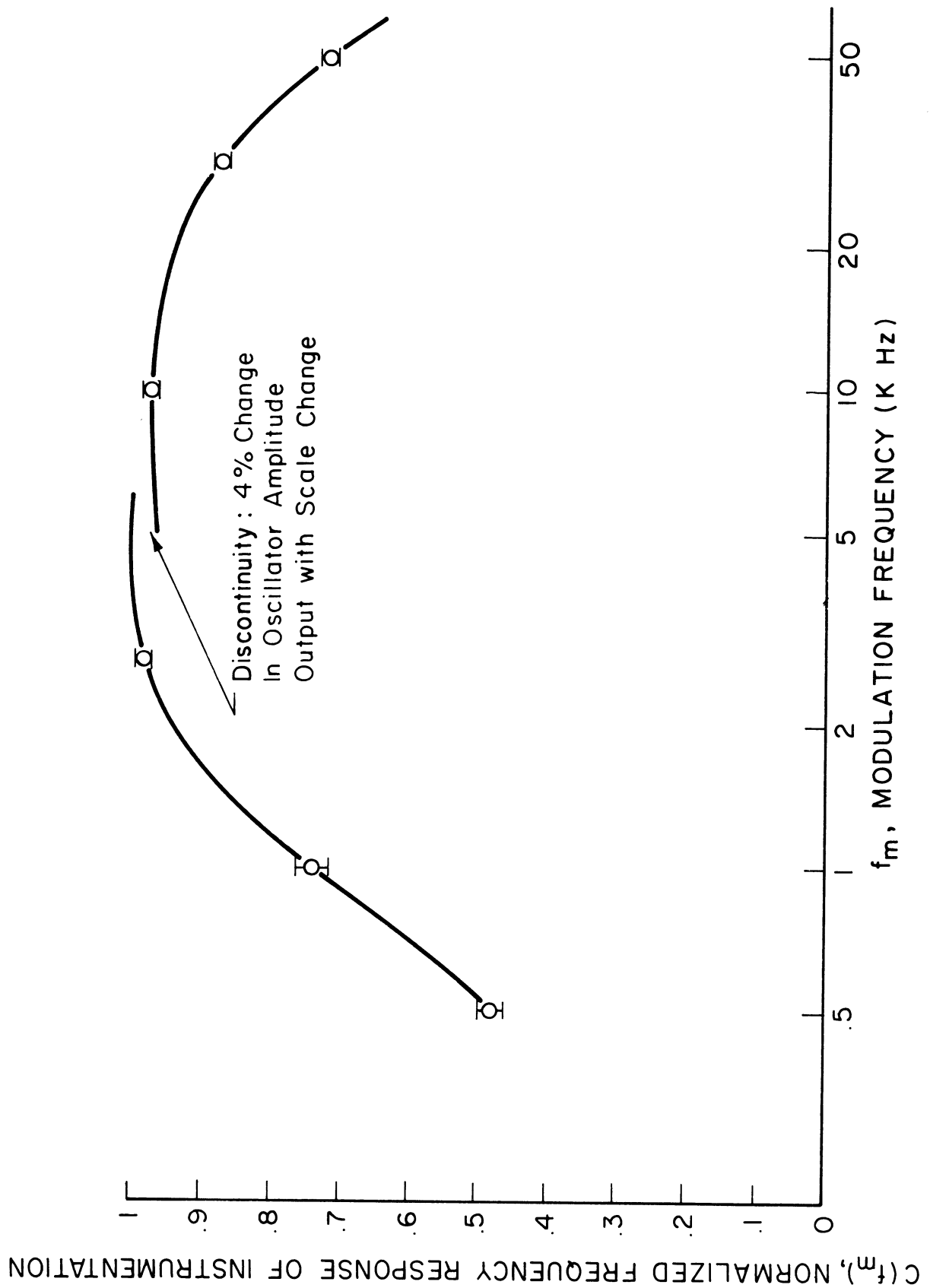

Fig. 3.8. Calibration curve or frequency response of the receiving instrumentation.

E. ELECTRONIC NOISE SUPPRESSION

Even though the discharge was basically a dc power system, very small 60 Hz ripples and other oscillations on the power supply voltage affected the measurements. Also, weak electric fields, such as local radio station signals, were troublesome. In this experiment, the disturbing microwave was an unwanted local electric field since any direct pickup in the receiving instrumentation of this field could affect the measurement.

As can be seen in Fig. 3.1, the entire system was enclosed in screen cages. There were actually six compartments constructed of slotted-sections of angle iron with complete screen covering. All the joints were soldered including the screen to angle iron contacts. The floor of each compartment was a copper sheet with a heavy copper braided wire leading to the building ground. The six compartments were: the power supply filter, movable disturbing microwave system, sensing microwave system, discharge region, and two receiving systems.

The 110 V, 60 Hz power leads entering each compartment passed through a power line filter, as shown in Fig. 3.9. These 10 ampere filters worked quite well for blocking the local radio station signals and high frequency transients due to other research projects within the building. Coaxial cable was used for most leads and many had an additional braided copper shield. All instruments were grounded by copper straps to the common ground plane.

Extra care was also taken with the microwave circuits. The klystrons were mounted in heavy Narda tube mounts. The mounts were enclosed in a copper

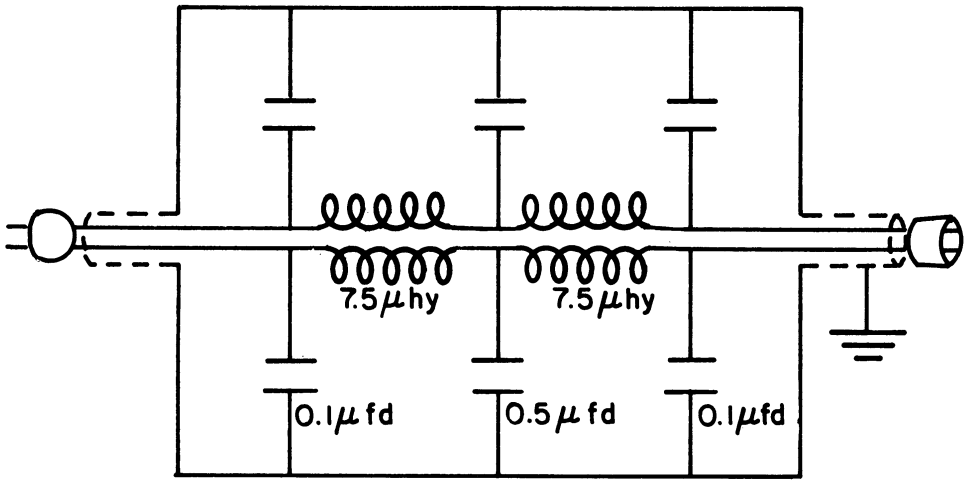

Fig. 3.9. Low pass filter for 110 V, 60 Hz power lines.

box and the power leads were all coaxial cables. In both microwave circuits 20 decibel isolators were used to prevent nonlinear mixing of the signals within the klystrons.

Mechanical vibrations were a noise source since any motion of the suspended cathode caused small variations in the plasma. Therefore, mechanical pumps had to be turned off during the measurements.

IV. EXPERIMENTAL TECHNIQUES AND DATA ANALYSIS

This chapter has two parts discussing the experimental measurements and analysis of the data with the helium discharge system. Section A concerns basic current-voltage-pressure and Langmuir probe measurements and Section B concerns the cross-modulation measurements.

A. HELIUM GLOW DISCHARGE

The glow discharge used as the plasma source in this experiment was unique due to the large volume and the length to diameter ratio of only 2:1. Glow discharges are generally classified as "normal" or "abnormal," depending on whether or not the entire cathode is used for electron emission. The discharge becomes abnormal when the ion bombardment covers the entire cathode. With geometries having a larger length to diameter ratio, the abnormal discharge consists of well defined transition layers near the cathode and a low field, nearly constant density, positive column to the anode.[25]

The glow discharge used in this experiment was abnormal as defined above. In fact, the normal discharge did not appear to be stable at any current for gas pressures less than 1 Torr. Because of the large diameter, diffusion losses were low and the discharge did not appear to have a positive column except at very low currents. The main volume of plasma was partially controlled by recombination losses and had some advantages over the positive column. It did not generate the noise which is found with moving striations in a typical positive column. The electron density was somewhat higher, over 10^{11} electrons/cu cm, and the electron temperature was lower, about .04 to .10 eV, than

usually obtained with abnormal glow discharge positive columns. A disadvantage was that the plasma properties were more sensitive to the cathode surface condition than were the positive column plasmas.

Figure 4.1 is a photograph of the glow discharge. The cathode was at the top of the discharge. The discharge was usually a fairly uniform blue-white and somewhat brighter in the inner half of the volume. Near the cathode was a narrow region of emerald green with a dark transition region to the cathode. It was this latter region, less than 1 in. thick, which supported the main voltage drop of the discharge. (This voltage drop accelerates the ions for bombarding the cathode and liberation of the electrons.) At lower discharge currents the lower region was dark and was supposedly the Faraday dark space.[25]

As mentioned earlier a newly evacuated bell jar and a clean cathode produced a discharge with unstable properties. In particular, the current-voltage-pressure relationship continued to change during the early stages of the discharge. It was found after several weeks of cycling the discharge and evacuating periods that the properties stabilized. The experimental approach to stability was accomplished by producing a plasma with the helium gas pressure and discharge current held constant and recording the discharge voltage. At first the voltage changed as much as a factor of two during a three hour period. After a few weeks the voltage would change only during the first hour and asymptotically approach a constant value. Eventually this voltage was stable within ±5% for discharge times exceeding 12 hr. The asymptotic voltage was also reproducible for different discharge runs to within ±10%.

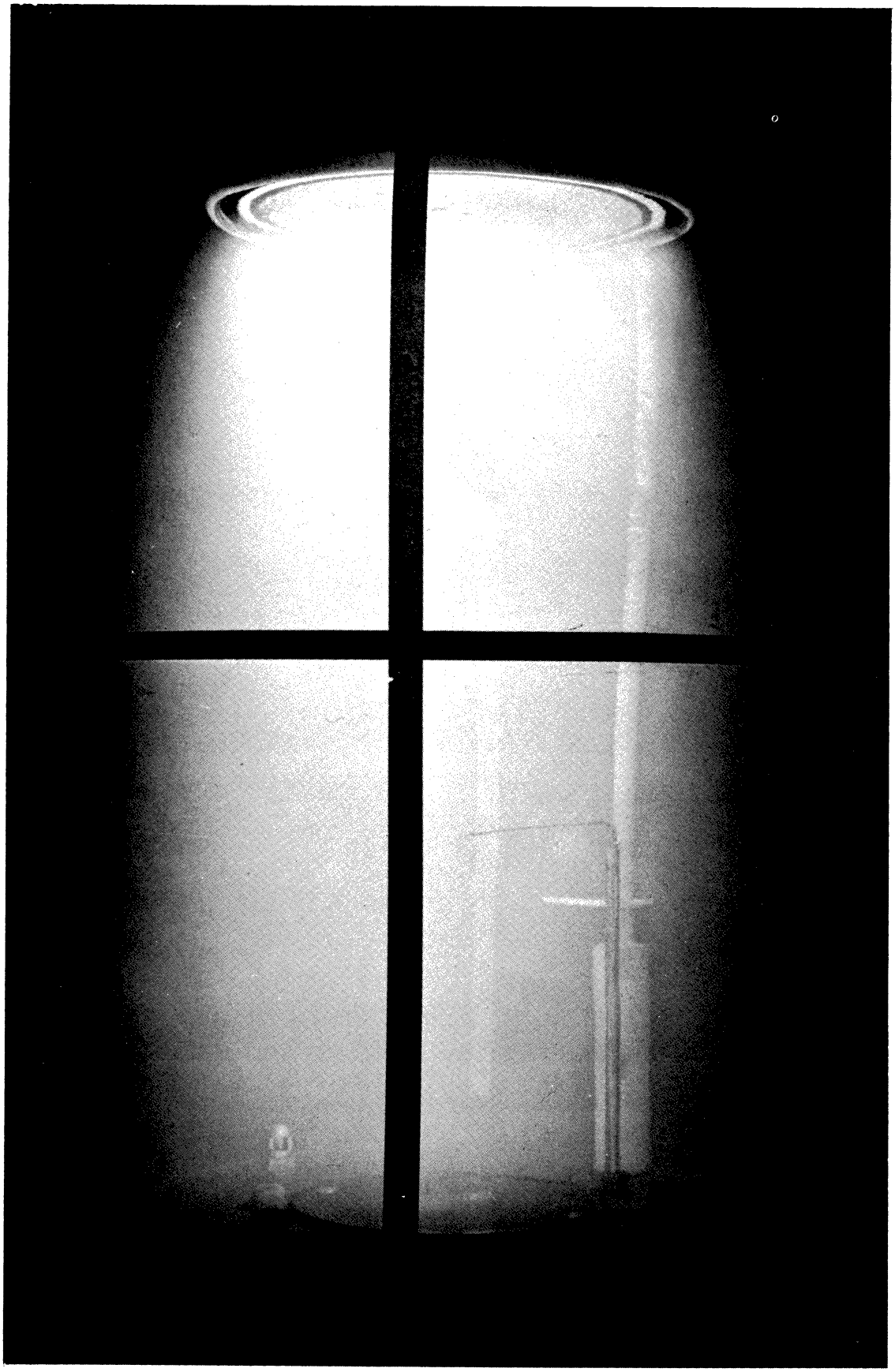

Fig. 4.1. Photographic view of the helium glow discharge.

Figure 4.2 is a plot of the asymptotic voltage drop across the helium glow discharge versus the discharge current over the pressure squared, (I/P^2). The solid curve matching the data is from the expression

$$V_{DC}(\text{VOLTS}) = 170 + 630\left[\frac{I_{DC}(\text{AMPERES})}{P_o^2(\text{TORR}^2)}\right]^{1/2} \tag{4.1}$$

During the conditioning period, Langmuir probe traces were recorded. A typical trace with the hairpin probe is shown in Fig. 4.3. The theory for the current-voltage properties of a conducting element in an ionized gas was first developed by Langmuir and Mott-Smith in 1924 and has been discussed by several authors.[26] The relationship needed in this experiment was for the probe current, I^e_{pr}, due to electron flow to the probe against a retarding field. It is given by

$$I^e_{pr} = -I^e_{sa} \exp\left[\frac{e(V_{pr} - V_{pl})}{\theta^e}\right] \tag{4.2}$$

where V_{pr} is the potential of the probe and V_{pl} is the plasma potential surrounding the probe, both with respect to the anode. I^e_{sa} is the saturation electron current given by

$$I^e_{sa} = -e n^e \sqrt{\frac{\theta^e}{2\pi m}} \tag{4.3}$$

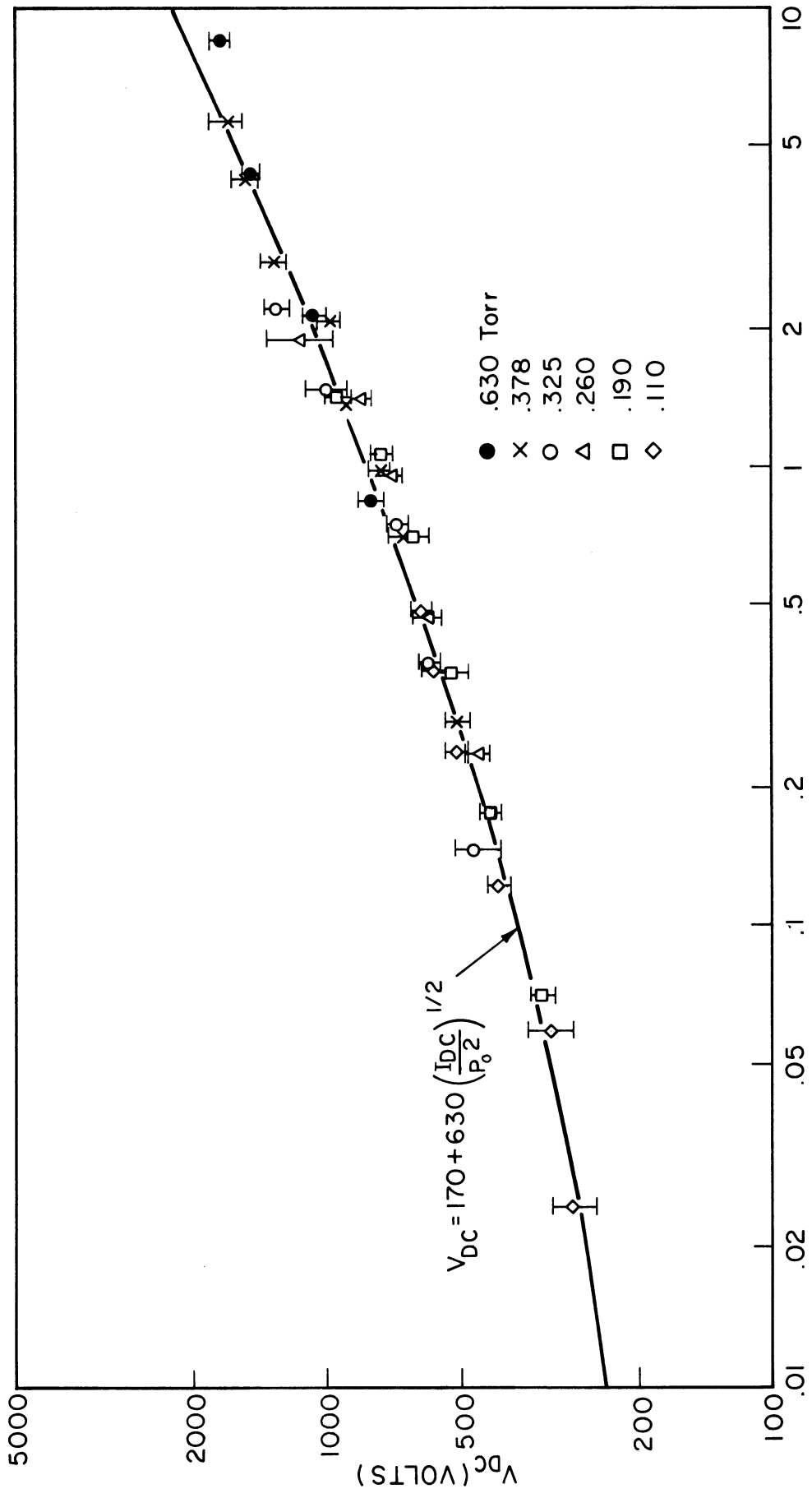

Fig. 4.2. Current-voltage-pressure dependence of the helium glow discharge with an aluminum cathode.

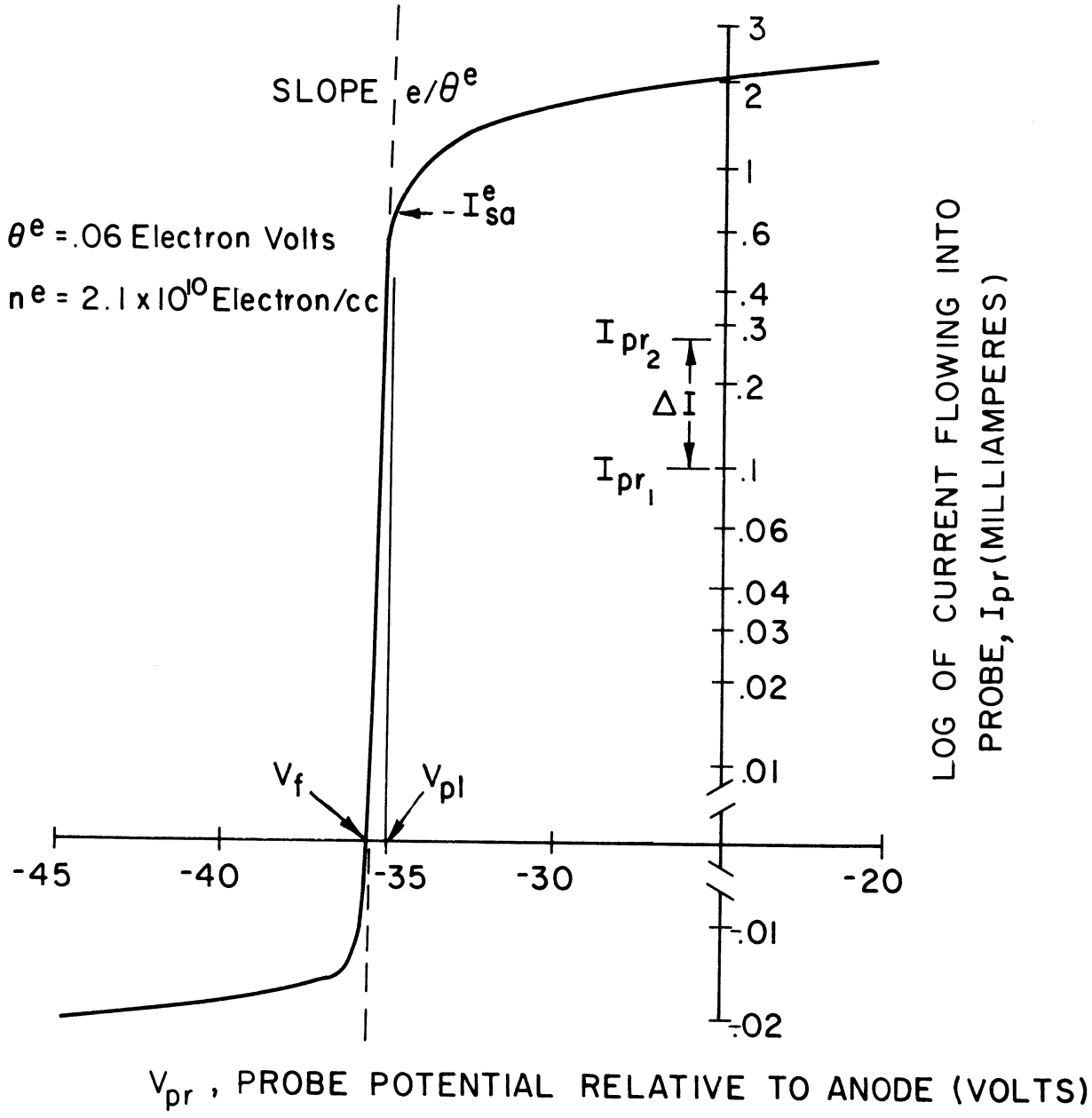

Fig. 4.3. Typical Langmuir probe trace.

where n^e is the local electron density, θ^e is the local electron temperature (KT^e), and m is the mass of an electron. A semi-log plot of I^e_{pr} vs. V_{pr} has a slope of e/θ^e, which yields the electron temperature. A measurement of I^e_{sa} yields the electron density.

Another parameter of interest was the probe floating potential, V_f. This open circuit voltage is maintained by the probe when the electron and ion flow to the probe are equal. V_f differs from V_{pl} due to the difference in the random speeds of the equally dense electrons and ions. Measurements of V_f, corrected for the electron temperature, vs. probe position can yield information on the dc electric field in the plasma.

Electron temperature measurements were also made using the oscillating square-wave current source discussed in IV-C. From Eq. (4.2)

$$\Delta V = V_{pr_2} - V_{pr_1} = \frac{\theta^e}{e} \ln \frac{I_{pr_2}}{I_{pr_1}} \qquad (4.4)$$

so that in the electron transition region the resulting oscillating probe voltage will be proportional to the electron temperature. With the choice of current ratio of 2.72, the voltage change is directly calibrated in terms of θ^e, in electron volts.[27]

Figures 4.4 and 4.5 are plots of the electron densities and temperatures measured by the Langmuir probe at the asymptotic current-voltage-pressure conditions. All these measurements were taken at the microwave cross-over point, i.e., 9-1/2 in. above the anode and on the center line of the discharge.

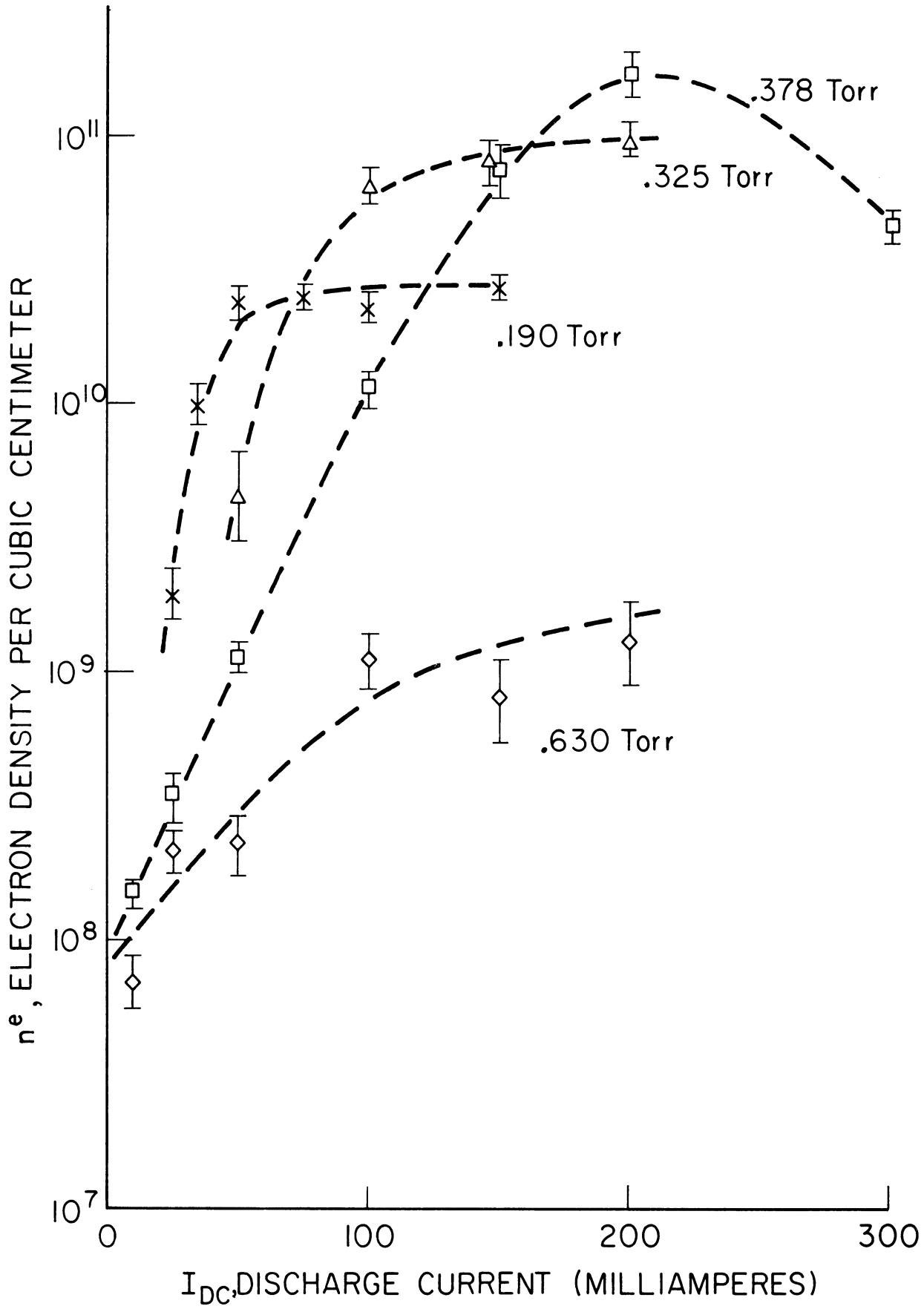

Fig. 4.4. Electron density variation with discharge current and helium gas pressure, on axis 9-1/2 in. above the anode.

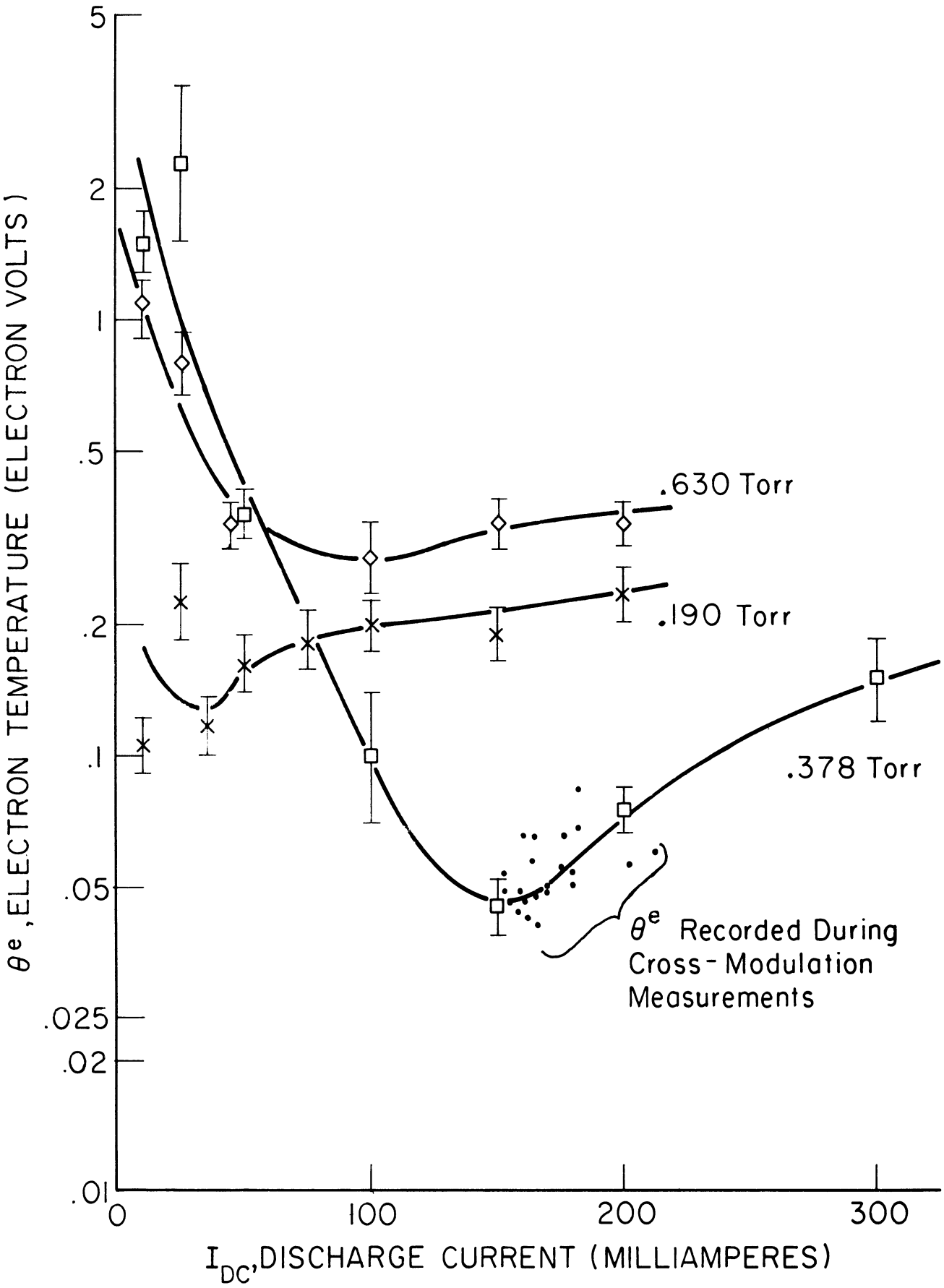

Fig. 4.5. Electron temperature variation with the discharge current and helium gas pressure, on axis 9-1/2 in. above the anode.

Note from Fig. 4.4 that a near maximum electron density is obtained here for a pressure of about .378 Torr and for currents between 150 to 250 mA. Nearly all cross-modulation measurements were made at these conditions. The electron density decreases for higher or lower discharge currents or pressures. Figure 4.5 shows that the high electron density region corresponds to the lowest electron temperature region. The uncertainties indicated on the figures include the reproducibility of the measurements as well as an indication of their absolute value. This latter uncertainty is based on locating the point I^e_{sa} and measuring the slope e/θ^e.

The radial distribution of the electron density and temperature are shown in Fig. 4.6. It can be seen that the density variation is close to a zero-order Bessel function. The rise in the electron temperature toward the bell jar wall is due in part to the relatively negative potential of the wall which repels the lower energy electrons. The electric field measured along the radial path was 0.038 V/in. directed outwardly.

In Fig. 4.7 the axial variation of the electron density and temperature are plotted. The axial plasma potential is shown in Fig. 4.8. Note that the minimum electron temperature, for the conditions indicated, occurred near the region of zero axial field. The electric field which heated the electrons in the lower region and contributed to the electron flow to the anode was 0.136 V/in. and directed toward the cathode. Because of the slow variation of θ^e with position, we have neglected the gradient of θ^e_o in the balance equations, Eqs. (2.56) and (2.62).

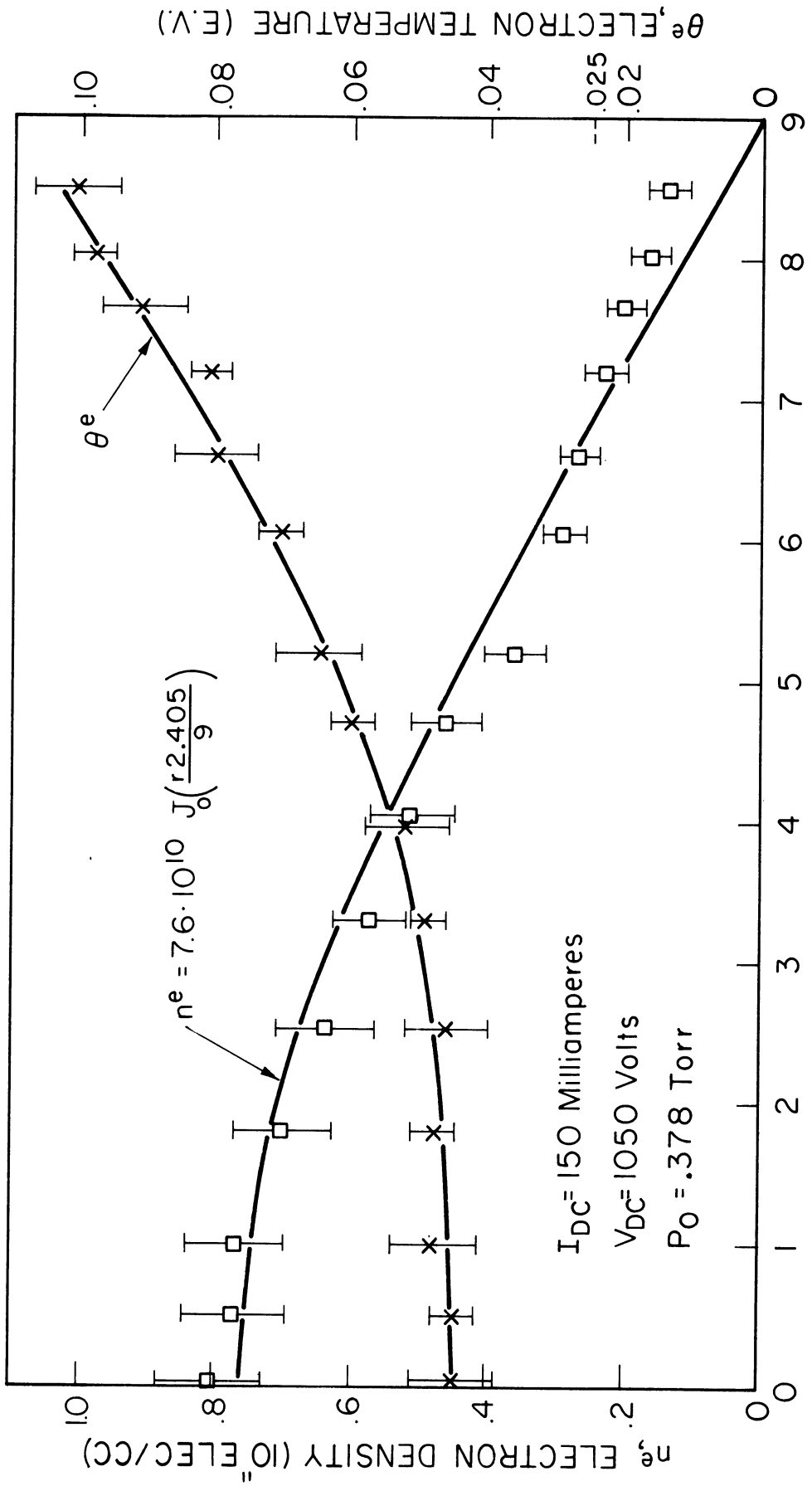

Fig. 4.6. Electron density and temperature radial variation, 9-1/2 in. above the anode.

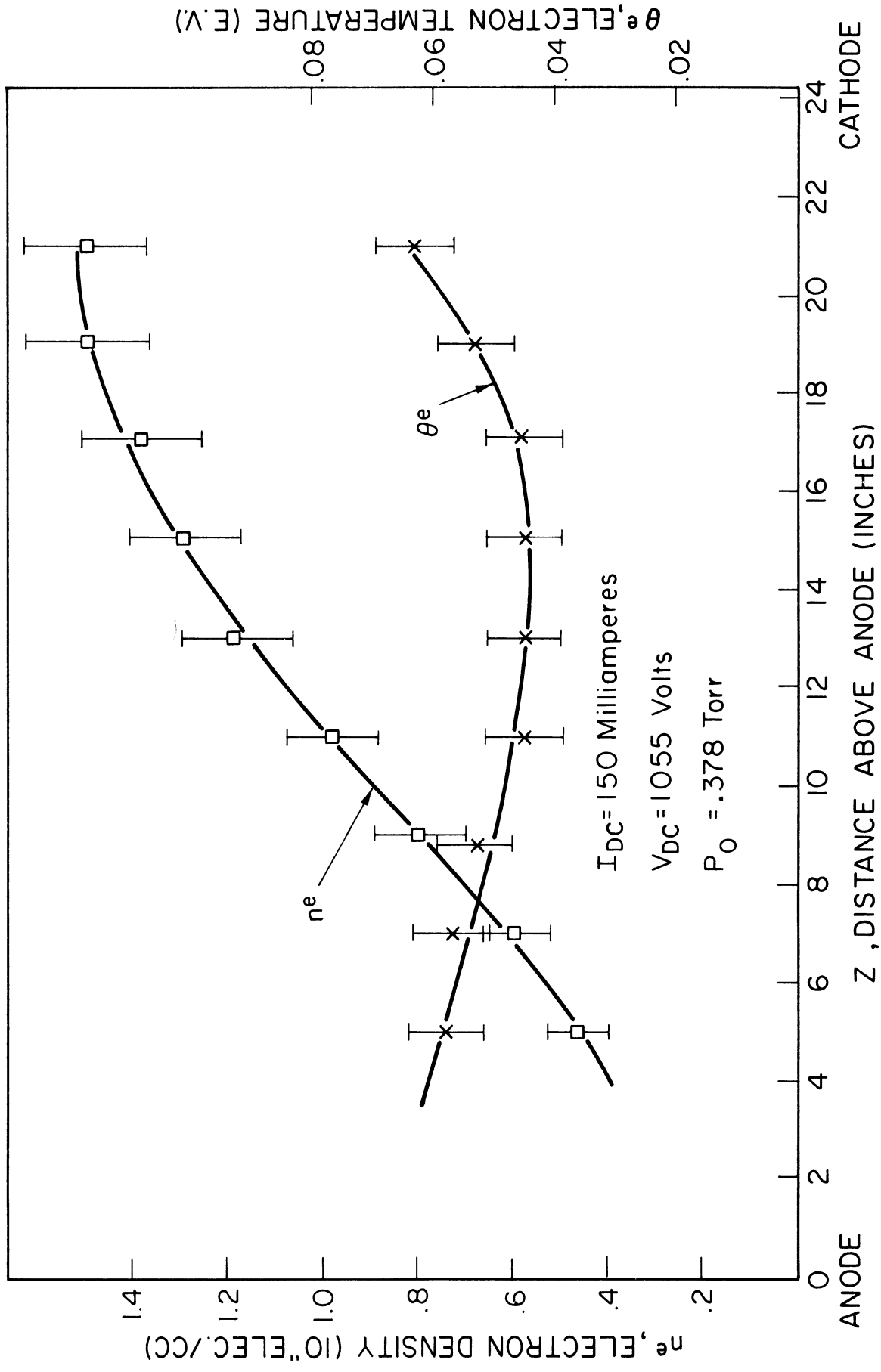

Fig. 4.7. Electron density and temperature axial variations.

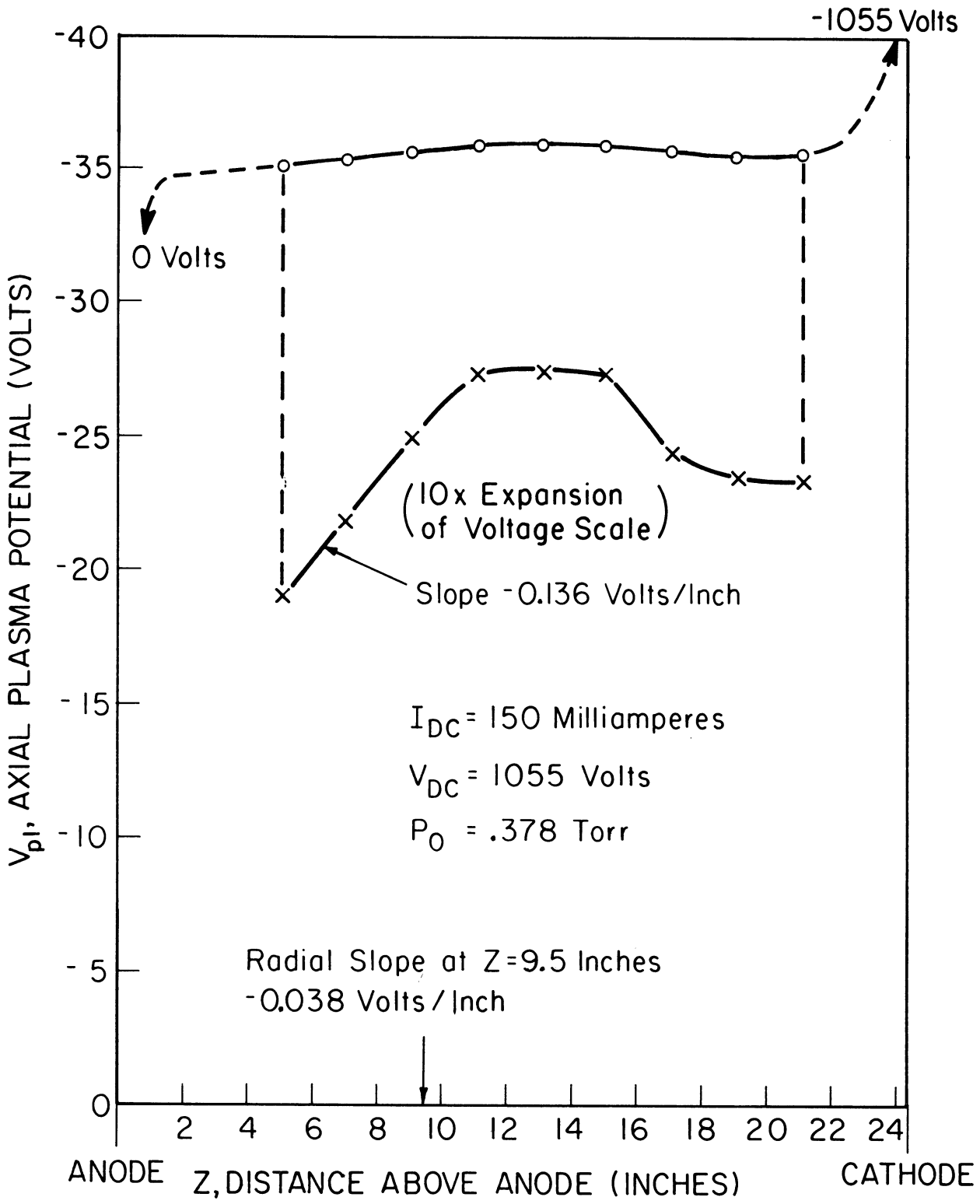

Fig. 4.8. Axial variation of the plasma potential.

B. CROSS-MODULATION RESPONSE

An analysis of the microwave absorption theory[24] indicated that the discharge conditions of .378 Torr and 150 ± 50 mA would probably yield a measurable cross-modulation between the carrier wave frequencies of 2.7 and 3.0 G Hz. A calculation of ω_1, the electron temperature restoring rate, indicated that $f_1 = \omega_1/2\pi$ would lie between 5 and 12 K Hz for these discharge parameters. Therefore, the helium gas pressure was held at .378 Torr and the modulation frequency set at 2 K Hz during the cross-modulation tuning procedure. At these conditions, and with the disturbing and sensing microwaves turned on, the discharge current was varied over the indicated range. The modulation on the sensing microwave was displayed on an oscilloscope. To facilitate the observation of the cross-modulation, the oscilloscope was phase locked with the modulation signal from the oscillator.

When cross-modulation was observed on the oscilloscope, the task was to stabilize the discharge at the current which yielded the maximum cross-modulation signal. Whenever the current was increased or decreased from a stable condition it required about 30 min to restabilize. This discharge current had to be continuously adjusted for the maximum cross-modulation signal as the stabilized condition was approached asymptotically. Also during the power adjustment period, the microwave wave guide equipment was tuned in the presence of the plasma to yield the maximum cross-modulation signal to noise ratio. This noise was caused by macroscopic oscillations in the plasma properties, mechanical vibrations in the microwave receiving instrumentation, and direct modulation on the sensing wave such as that due to the cooling fan

vibrations in the klystron. During the final stage of this tuning period, the X-Y recorder response to the ac modulation on the sensing microwave was used to obtain the maximum signal to noise ratio.

Once the entire system was tuned for maximum cross-modulation response, the modulation frequency was varied from 0.5 to 50 K Hz and the ac modulation was recorded over this frequency range. An example of this recording is shown in Fig. 4.9. Each horizontal traverse of the recorder required about 2 to 3 sec because of the low frequencies in the response. One or more traces were made over the two frequency ranges in order to average out the fluctuations in the traces, as well as to make sure that there were no changes in the response occurring during the single tracing. Often, the recording did not retrace and the data were disregarded. The discontinuity occurring between 2 and 2.5 K Hz in this example was caused by a short duration change in the discharge which apparently restabilized. These were accompanied by very tiny momentary arc spots on the cathode.

The response from Y = 0 to the Cross-Modulation Zero Line represents the various sources of modulation on the sensing microwave which were independent of the modulation frequency, f_m. At one time this level was several factors larger than shown in Fig. 4.9 due to the 60 Hz ripple on the dc power supply and other stray noise sources. The filter shown in Fig. 3.2 and the shielding explained in III-E partially corrected for the noise level. The C-M Zero Line represents the asymptotic cross-modulation high frequency response, as well as the level of the response with the disturbing microwave modulation turned off.

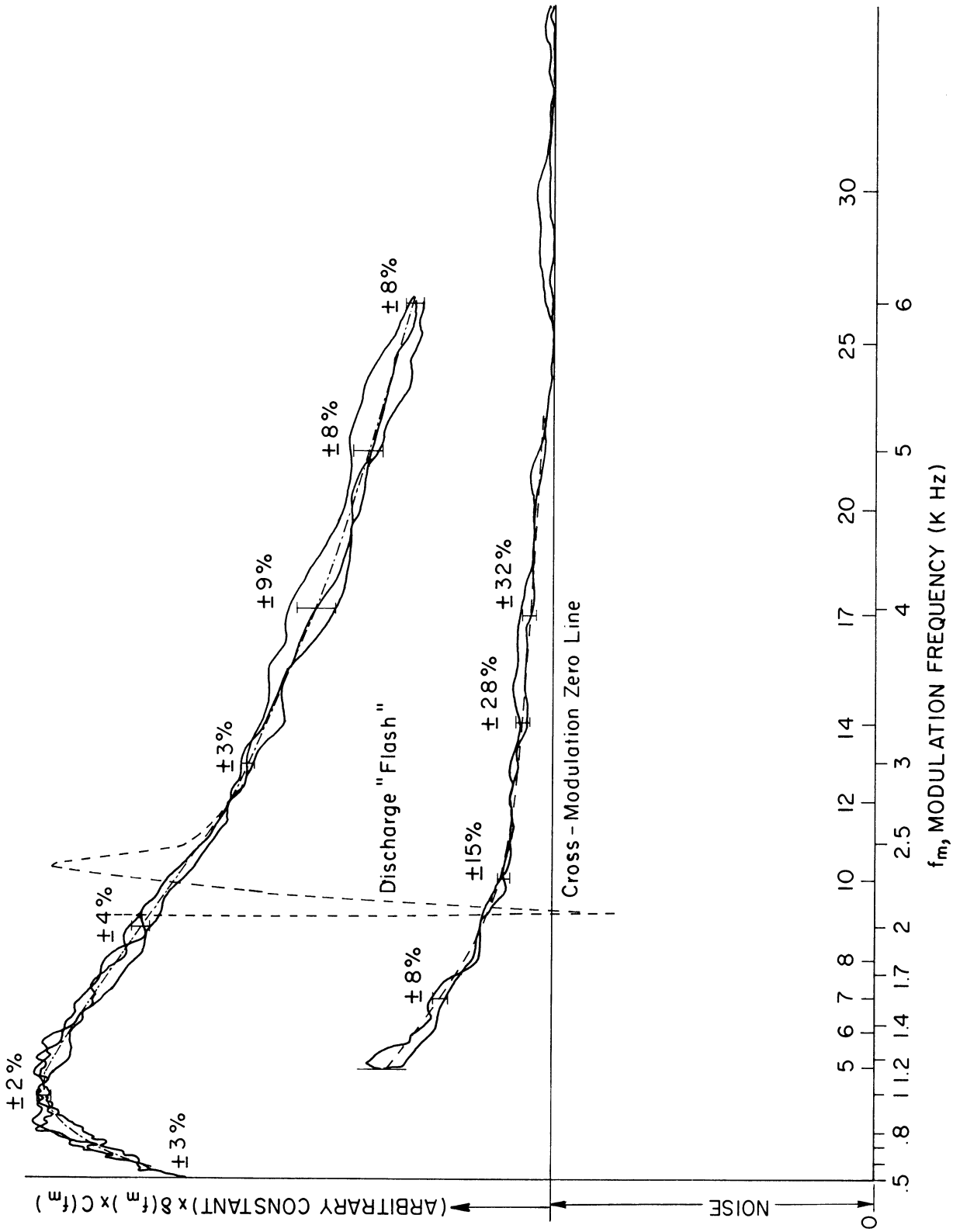

Fig. 4.9. Sample trace of the cross-modulation depth on the sensing microwave as recorded by the X-Y recorder.

The desired response was taken as the vertical displacement between the C-M Zero Line and an average smooth curve indicated by the broken line in Fig. 4.9. In this example the individual uncertainties of each data point range from ± 2% to ± 32%. These data had to be corrected for the frequency response of the instrumentation, $C(f_m)$. This correction function is shown in Fig. 3.8. Data were used for all the discrete frequencies indicated in Fig. 4.9 up to 17 K Hz. Each set of corrected data was fit, using the methods of least-squares (see Appendix D), by a computer to the relation

$$\delta(f_m) = \frac{\delta(0)\sqrt{1 + (f_m/f_3)^2}}{\sqrt{\left(1 + (f_m/f_1)^2\right)\left(1 + (f_m/f_2)^2\right)}} \tag{4.5}$$

This technique yielded the normalization $\delta(o)$ and the break frequencies f_1, f_2, and f_3. In all cases analyzed f_3 was much greater than f_1 and f_2.

In Fig. 4.10 the solid curve is the computer solution to $\delta(f_m)/\delta(o)$ for the average of the four individual sets of normalized data shown. The four sets were taken at a constant discharge condition over about a 1/2 hr period. The data with the error bars were from the recording in Fig. 4.9. For illustration, the two functions

$$\frac{1}{\sqrt{1 + (f_m/f_1)^2}} \tag{4.6}$$

and

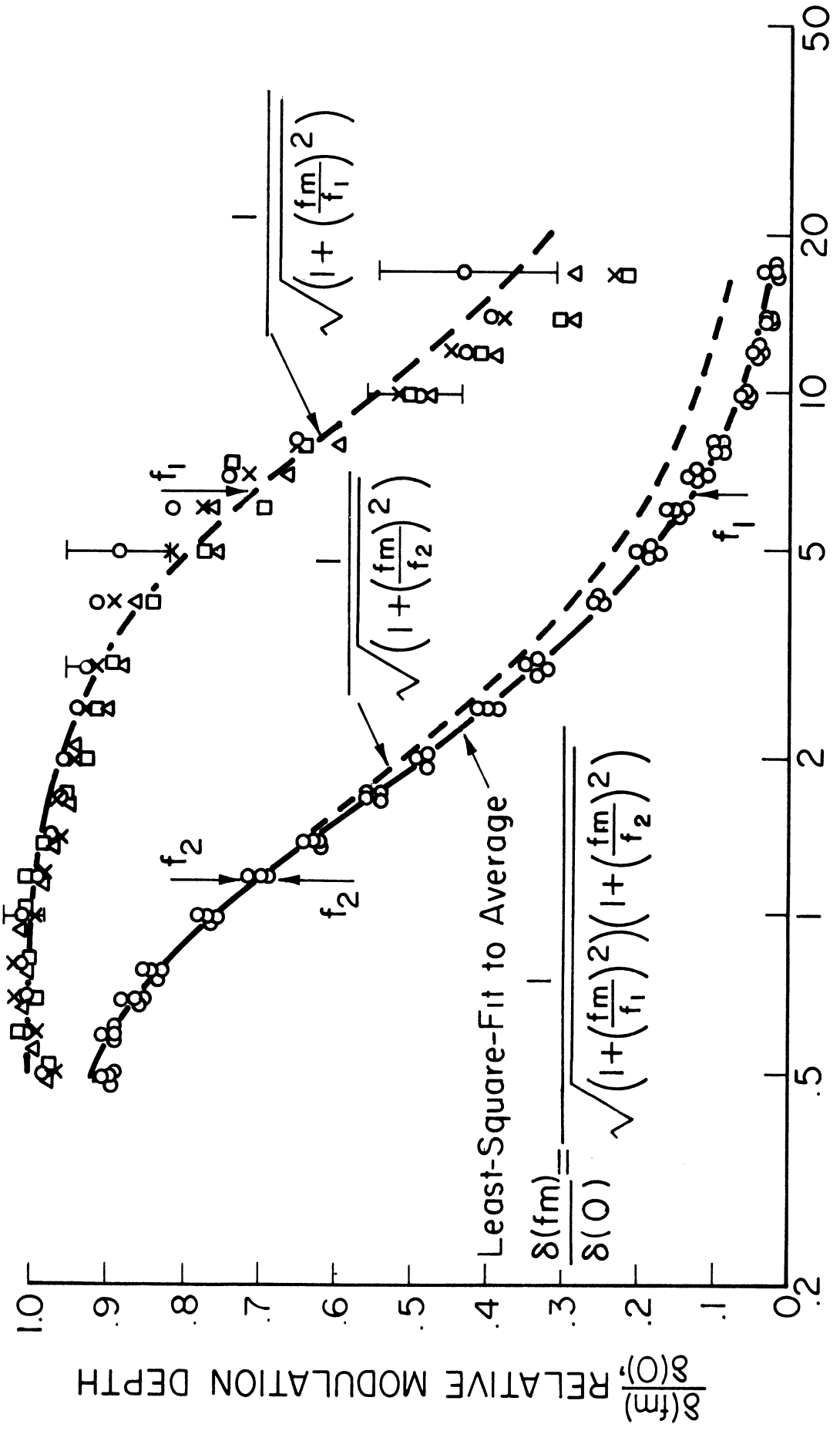

Fig. 4.10. Four sets of normalized cross-modulation data with computer solution.

$$\frac{1}{\sqrt{1 + (f_m/f_2)^2}} \qquad (4.7)$$

have been plotted in Fig. 4.10. The data points surrounding the upper curve were simply the original data divided by the corresponding values of Eq. (4.7), and therefore they represent the "information" in the original data which determines the break frequency f_1. Similar reasoning applies to the other curve, although the data were not plotted in this case. A few of the individual error bars have been indicated on the upper curve. The individual values for f_1 determined by the four sets of data ranged from 5.8 to 7.2 K Hz. This indicates the reproducibility of the measuring and analyzing technique. The fractional standard deviation of the mean value between the data and the matching transfer function,[28] Eq. (4.5), for this example was about ± 2% (standard deviation for <u>one</u> more data point was about ± 10%).

Over a six week period, 107 sets of data were taken and analyzed in the preceding manner. These data are tabulated in Appendix E along with other information on each measurement. Although the data appear to vary over a broad range of values for the break frequencies, no correlation was found during the extent of the experiment between the variations and the average plasma properties or microwave circuitry alignment. Therefore, the sets of data were treated collectively by finding their average and root-mean-square deviation. As an illustration of this interpretation the number of break frequency measure-

ments for f_1 and f_2 occurring in a fixed frequency interval vs. the frequencies are plotted in Fig. 4.11. The distribution plots are compared with the normal-distribution function based on the averages and root-mean-square deviations indicated abcve. The area under the normal-distribution curve and the bar graphs are equal for each of the two plots. The results of this analysis were

$$\bar{f}_1 = 6.34 \pm 3\% \text{ K Hz} \tag{4.8}$$

$$\bar{f}_2 = 1.65 \pm 3\% \text{ K Hz} \tag{4.9}$$

with the average plasma conditions of

$$\bar{I}_{DC} = 170 \pm 8\% \text{ mA} \tag{4.10}$$

$$\bar{V}_{DC} = 965 \pm 8\% \text{ V} \tag{4.11}$$

$$P_o = .378 \pm 3\% \text{ Torr} \tag{4.12}$$

The indicated uncertainties are the standard deviations of the mean values for $\bar{f}_1$ and $\bar{f}_2$, the spread in the values of $\bar{I}_{DC}$ and $\bar{V}_{DC}$, and the reproducibility of P_o.

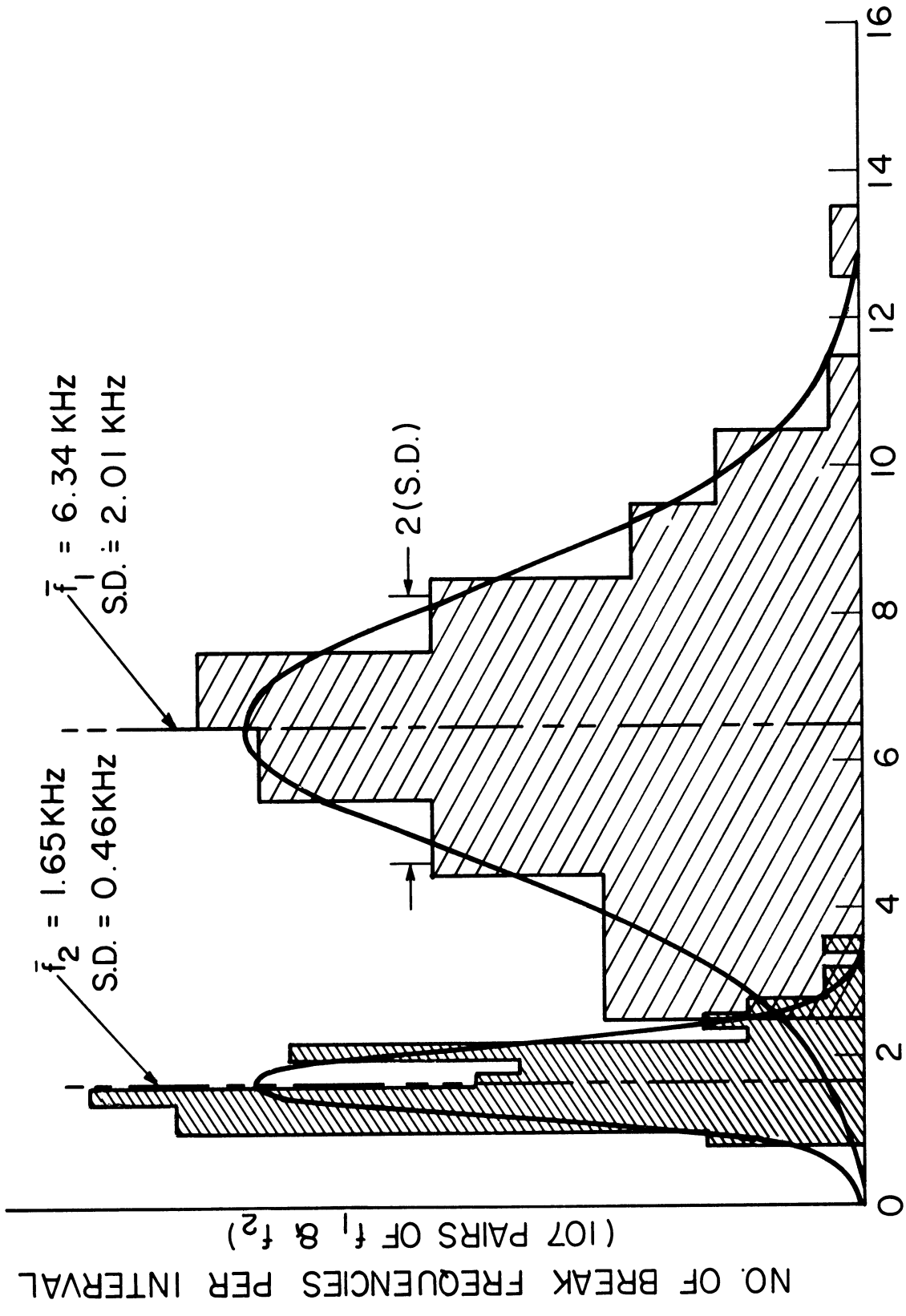

Fig. 4.11. "Frequency distribution" plots of the measured break frequencies.

V. RESULTS AND DISCUSSION

The results of the theory for cross-modulation from Chapter II showed that the normalized variation in the detector output voltage, in response to the received sensing microwave signal, is given by* Eq. (2.21),

$$\delta v = \delta(f_m) \cos(2\pi f_m t - \Phi) \tag{5.1}$$

In this experiment only the normalized cross-modulation depth, $\delta(f_m)/\delta(0)$, was measured. From Eq. (2.25) it is given by

$$\frac{\delta(f_m)}{\delta(0)} = \sqrt{\frac{1 + (f_m/f_3)^2}{(1+(f_m/f_1)^2)(1+(f_m/f_2)^2)}} \tag{5.2}$$

where f_1 and f_2 are

$$f_{1,2} = \frac{f_a + f_b}{2} \pm \frac{1}{2}\sqrt{(f_a - f_b)^2 - 4 f_c f_d} \tag{5.3}$$

and

*In this chapter all frequencies are in Hertz, cps, instead of rad/sec, i.e., let $f = \omega/2\pi$.

$$f_3 = f_b + \frac{b}{a} f_d \tag{5.4}$$

The restoring rate for the electron temperature variations, f_a from Eq. (2.84), is

$$f_a = \frac{1}{2\pi}\left(\frac{2m}{M}\right)\left\{\nu_{en}\left[\left(\frac{3}{2}-\rho_\theta\right) - \left(\frac{1}{2}-\rho_\theta\right)\frac{\theta_o^n}{\theta_o^e}\right]\right.$$

$$\left. - \nu_{ei}\left[\left(\frac{1}{2}+\rho_\theta\right) - \left(\frac{3}{2}+\rho_\theta\right)\frac{\theta_o^n}{\theta_o^e}\right]\right\} \tag{5.5}$$

The restoring rate for the electron density variations, f_b from Eq. (2.96), is

$$f_b = \frac{\alpha_o n_o^e}{2\pi}\left(\frac{5}{4} + \frac{\rho_\theta}{2}\right) \tag{5.6}$$

The coupling frequencies between the electron temperature and density variations, Eqs. (2.87) and (2.98), are

$$f_c = \frac{1}{2\pi}\left(\frac{2m}{M}\right)\nu_{en}\left(1-\frac{\theta_o^n}{\theta_o^e}\right)\frac{1}{2}\left[y^2 + (1 + y^2/2)\left(\frac{1}{2}+\rho_\theta\right)\right] \tag{5.7}$$

and

$$f_d = \frac{\alpha_o n_o^e}{2\pi}\left(\rho_\theta + \frac{3}{2}\right) + \frac{D_o \nabla^2 n_o^e}{2\pi n_o^e} \tag{5.8}$$

neglecting terms in the ionization coefficient β_o and the gradient of the diffusion coefficient D_o. The following functions of the electron temperature, θ_o^e, electron density, n_o^e, and the cross-section for electron-neutral atom collisions, q_{en}, were defined. The effective electron-neutral atom collision frequency is

$$\nu_{en} = \frac{4}{3} N q_{en} \sqrt{\frac{8\theta_o^e}{\pi m}} \tag{5.9}$$

The effective electron-ion collision frequency is

$$\nu_{ei} = \frac{4}{3} \frac{n_o^e e^4 \sqrt{2\pi}}{\sqrt{m}(\theta_o^e)^{3/2}} \ln\left(\frac{3}{2}\frac{\theta_o^e}{e^3}\sqrt{\frac{\theta_o^e}{\pi n_o^e}}\right) \tag{5.10}$$

The electron diffusion coefficient is

$$D = \frac{32\,\theta_o^e}{9\pi m \nu_{en}}\left[1 - y^2 g(y)\right] \tag{5.11}$$

where the bracketed term is plotted in Appendix B vs. the variable $y = (2\nu_{ei}/\nu_{en})^{1/2}$. The factor ρ_θ is the logarithmic derivative of the dc conductivity with respect to the electron temperature, and has been evaluated and plotted in Appendix B as a function of y. α_o is the electron-ion recombination coefficient.

The method of least-squares, as discussed in Chapter IV, Section B, and Appendix D, was used to fit the function in Eq. (5.2) to the measured transferred modulation depth (arbitrarily normalized). For all the data analyzed, the term $(1 + f_m^2/f_3^2)^{1/2}$ was found to be close to unity. That is, the experiment showed that the cross-modulation depth varied as $1/f_m^2$ for the largest f_m. Using calculations for f_b and f_d, we find that this response requires that the ratio (b/a) in Eq. (5.4) be greater than 20. Furthermore, from Eq. (2.13) we can conclude that the cross-modulation measurement is primarily due to the electron density variations. Since this result may be surprising in contrast to the results and assumptions of other cross-modulation experiments, we have presented in Chapter II, Section E, a qualitative discussion of the parameters (a) and (b). A large value of (b/a) appears reasonable for a sensing microwave signal which is primarily reflected by the plasma[29] and this was apparently the case in this experiment. As an experimental result, therefore, the cross-modulation depth is given by

$$\frac{\delta(f_m)}{\delta(0)} = \frac{1}{\sqrt{\left(1 + (f_m/f_1)^2\right)\left(1 + (f_m/f_2)^2\right)}} \qquad (5.12)$$

In Chapter IV, we discussed the techniques used to measure $\delta(f_m)/\delta(0)$ and to obtain the experimental values for the two break frequencies, f_1 and f_2. 107 sets of data were measured and analyzed for the pair of break frequencies with a fairly constant helium plasma (I_{DC} = 170 mA with an 8% spread and P_o = .378 Torr with a 3% uncertainty). The average values are

$$\bar{f}_1 = 6.34 \pm .19 \text{ K Hz} \tag{5.13}$$

and

$$\bar{f}_2 = 1.65 \pm .04 \text{ K Hz} \tag{5.14}$$

where the uncertainties are the standard deviations of the mean values.[28*]

We now relate the measured values of the break frequencies to the functions defined in Eq. (5.3) as

$$\bar{f}_1 = f_1\left(\theta_o^e, n_o^e, q_{en}, \alpha_o, \frac{\nabla^2 n_o^e}{n_o^e}\right) \tag{5.15}$$

and

*The standard error is defined for a normal distribution by

$$S.E. = \left(\frac{1}{n(n-1)}\sum_{i=1}^{n}(x_i - \bar{x})^2\right)^{1/2}$$

$$\bar{f}_2 = f_2\left(\theta_o^e,\ n_o^e,\ q_{en},\ \alpha_o,\ \frac{\nabla^2 n_o^e}{n_o^e}\right) \tag{5.16}$$

In order to solve Eqs. (5.15) and (5.16) for the electron-neutral atom collision cross-section and the electron-ion recombination coefficient, the electron temperature, the electron density, and the plasma "buckling" $\nabla^2 n_o^e / n_o^e$ were required. In particular, we needed these variables at the point $(\underline{x}_p)$ of cross-modulation. As discussed in Chapter II, Section E, cross-modulation was expected to occur for ω_p^2/ω_s^2 close to 1, where the plasma frequency is defined by

$$\omega_p^2 = 4\pi \frac{n^e e^2}{m} \tag{5.17}$$

and ω_s is the sensing microwave carrier frequency. For the conditions in our plasma this ratio was approximately one at the center of the discharge (9-1/2 in. above the anode) and decreased along the radius. Therefore, the interaction was greatest in the inner region of the discharge. We consider points in a cylindrical volume 4 in. in height and 6 in. in diam, centered about the axial point 9-1/2 in. above the anode. The sensing microwave free-space wavelength is about 4 in.

From Fig. 4.6, we have

$$\frac{\nabla^2 n_o^e}{n_o^e} = (.0062 \pm 11\%)\ cm^{-2} \tag{5.18}$$

The set of equations [Eqs. (5.5), (5.6), (5.7), (5.8), (5.15), and (5.16)] can now be solved using iteration techniques for the values of q_{en} and α_o determined by the measurements of $\bar{f}_1(\underline{x}_p)$, $\bar{f}_2(\underline{x}_p)$, $\theta_o^e(\underline{x}_p)$, and $n_o^e(\underline{x}_p)$. This has been done for the four locations indicated in Table 5.1.

The electron temperature and density at x_1 corresponds to the average discharge current, I_{DC}, using Figs. 4.4 and 4.5. The other temperatures and densities have been scaled to the values of x_1 using the variations in Figs. 4.6 and 4.7. The uncertainties in θ_o^e and n_o^e are a measure of the absolute value and reproducibility of the probe measurements. The uncertainties for P_m and α_o are due to those in θ_o^e and n_o^e, assuming that these variables are independent. The total spread of P_m in this volume, about the central value, is only ±6% compared to the uncertainty of ±9% at each point. We consider the point x_1 to represent the most likely interacting region, however we combine the uncertainties to obtain as our experimental results

$$P_m = (18.7 \pm 11\%)\ cm^{-1}\ TORR^{-1}\ AT\ 0°C \tag{5.19}$$

and

$$\alpha_o = (3.6 \pm 61\%) \times 10^{-8}\ cm^3\ sec^{-1} \tag{5.20}$$

TABLE 5.1

EVALUATION OF THE PROBABILITY OF COLLISION FOR MOMENTUM TRANSFER, P_m(cm^{-1} $Torr^{-1}$ AT 0°C), AND THE ELECTRON-ION RECOMBINATION COEFFICIENT, α_o(cm^3 sec^{-1})

x_P	$x_1(9\frac{1}{2},0)$	$x_2(11\frac{1}{2},0)$	$x_3(9\frac{1}{2},3)$	$x_4(7\frac{1}{2},0)$
θ_o^e(eV) ± 15%	.052	.048	.055	.057
n_o^e(elec/cc)±22%	1.1×10^{11}	1.27×10^{11}	$.91\times10^{11}$	$.87\times10^{11}$
ν_{en}(sec^{-1})	1.28×10^{8}	1.28×10^{8}	1.19×10^{8}	1.18×10^{8}
ν_{ei}(sec^{-1})	1.71×10^{8}	2.23×10^{8}	1.32×10^{8}	1.25×10^{8}
$\bar{f}_a$(Hz) ± 6%	7140	7400	7000	6950
$\bar{f}_b$(Hz) ± 49%	860	750	1000	1040
$\bar{f}_c$(Hz)	6270	8100	4260	4100
$\bar{f}_d$(Hz)	690	640	790	800
P_m($cm^{-1}Torr^{-1}$)±9%	18.7	19.4	17.5	17.3
α_o(cm^3sec^{-1})±54%	3.6×10^{-8}	2.6×10^{-8}	5.1×10^{-8}	5.3×10^{-8}

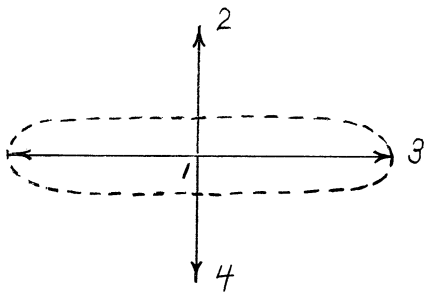

for

$$\theta_o^e = (.052 \pm 15\%)\ eV \tag{5.21}$$

The published values of P_m, the probability of collision for momentum transfer, for helium are given in Table 5.2 together with the value obtained in this experiment. A simple average of the values listed is 19.8 cm^{-1} $Torr^{-1}$.

TABLE 5.2

HELIUM COLLISION PROBABILITY

$P_m(cm^{-1}Torr^{-1})$	$\frac{3}{2}\theta_o^e(eV)$	Reference
19	.039	30--Phelps (1951)
18.3 ± 2%	0 to .75	31--Gould (1954)
24	.039	32--Anderson (1956)
21	≤ 2	33--Phelps (1960)
18.7	0 to .1	34--Pack (1961)
20 ± 5%	.039	35--Chen (1961)
18.5 ± 3%	~.1	36--Golden (1965)*
20 ± 11%	.038	37--Wald (1966)
18.7 ± 11%	.078	This experiment

The value for the electron-ion recombination is not as well known as P_m. The experimental values for this and other experiments are shown in Table 5.3.

*This is actually P_c, the total probability of collision, measured by the Ramsauer technique. We have estimated the value at 0.1 eV, which is probably accurate within the indicated error.

TABLE 5.3

HELIUM ELECTRON-ION RECOMBINATION COEFFICIENT

$\alpha_0 (cm^3 sec^{-1})$	Reference
1.7×10^{-8}	38--Biondi (1949)
1.0×10^{-8}	39--Johnson (1950)
8.9×10^{-9}	33--Chen (1961)
$(3.6 \pm 61\%) \times 10^{-8}$	This experiment

In conclusion, the experiment has shown that continuous cross-modulation of microwaves can be measured in a large steady state plasma. For a glow discharge with an electron collision frequency much less than the carrier wave frequency, the interaction is observable primarily for a reflected sensing microwave signal due to electron density variations. For this case, the cross-modulation depth depends on both the restoring rates for electron temperature and density variations. These rates or break frequencies were measured for a helium glow discharge and led to values for the probability of collision for electron momentum transfer and the electron-ion recombination coefficient. These quantities agree favorably with other published values.

APPENDIX A

THE HIGH FREQUENCY AND DC PLASMA CONDUCTIVITIES

We present the usual derivation for the complex high frequency conductivity including the effects due to both electron-neutral atom and electron-ion collisions, where the carrier frequency is much larger than the total collision frequency.[18] Then we present a less common solution for the dc conductivity including both collision processes.

The electron current density is defined in terms of the electron singlet distribution function as

$$\underline{J}(\underline{x},t) = -e\int d^3v\, \underline{v} f^e(\underline{x},\underline{v},t) \tag{A.1}$$

For the P_1-approximation, Eq. (2.31), this becomes

$$\underline{J}(\underline{x},t) = -e\int_0^\infty dv\, v^2\, \underline{J}(\underline{x},v,t) \tag{A.2}$$

in terms of the function $\underline{J}(\underline{x},v,t)$, which is related to the electric field by Eq. (2.37) and (2.38). Substituting $\underline{J}(\underline{x},v,t)$ from Eq. (2.37) into (A.2) and considering the contribution of electric field only, we get

$$\underline{J}(\underline{x},t) = -\frac{e^2}{3m}\int_0^\infty dv\, v^3 \frac{\partial f_o}{\partial v}\int_0^\infty du\, \underline{E}(\underline{x},t-u)\, e^{-g_m u} \tag{A.3}$$

As before, we are treating f_o and g_m as slowly varying functions of time and will not be concerned with this feature here.

1. THE HIGH FREQUENCY CONDUCTIVITY

We consider an electric field given by $E(x)e^{-i\omega_s t}$. For this case the electron current density becomes

$$\underline{j}(\underline{x},t) = -\frac{e^2}{3m}\underline{\underline{E}}(\underline{x})\, e^{-i\omega_s t}\int_0^\infty dv\, v^4 \frac{(g_m - i\omega_s)}{g_m^2 + \omega_s^2}\frac{\partial f_o}{\partial v} \tag{A.4}$$

From Eq. (A.4) the complex conductivity is defined as

$$\sigma_{AC} = -\frac{e^2}{3m}\int_0^\infty dv\, v^4 \frac{g_m - i\omega_s}{g_m^2 + \omega_s^2}\frac{\partial f_o}{\partial v} \tag{A.5}$$

The collision rate with neutral atoms and ions is given by

$$g_m = N q_{en} v + \frac{\Gamma_{ei} n^i}{v^3} \tag{A.6}$$

where

$$\Gamma_{ei} = 4\pi\left(\frac{Z e^2}{m}\right)^2 \ln\left(\frac{3\theta_o^e}{2e^3}\sqrt{\frac{\theta_o^e}{\pi n_o^e}}\right) \tag{A.7}$$

and N and n^i are the scattering centers.[19] We treat both q_{en} and Γ_{ei} as constants for a helium plasma. We assume that f_o is the Maxwellian distribution function

$$f_o(\underline{x}, v, t) = 4\pi n_o^e \left(\frac{m}{2\pi\theta^e}\right)^{3/2} \exp\left[-\frac{mv^2}{2\theta^e}\right] \tag{A.8}$$

We substitute Eqs. (A.6) and (A.8) into Eq. (A.5), which can be readily solved for the case when $\omega_s^2 \gg g_m^2$ considered here, and obtain

$$\sigma_{AC} = \frac{n^e e^2}{m\omega_s^2}(\nu_{en} + \nu_{ei}) - i\frac{n^e e^2}{m\omega_s} \tag{A.9}$$

where

$$\nu_{en} = \frac{4}{3} N q_{en} \sqrt{\frac{8\theta^e}{\pi m}} \tag{A.10}$$

and

$$\nu_{ei} = \frac{4}{3} n^i \frac{(Ze^2)^2 \sqrt{2\pi}}{\sqrt{m}\,(\theta^e)^{3/2}} \ln\left(\frac{3\theta^e}{2e^3}\sqrt{\frac{\theta^e}{\pi n^e}}\right) \tag{A.11}$$

2. THE DC CONDUCTIVITY

For a constant electric field the conductivity is defined from Eq. (A.3) as

$$\sigma_{DC} = -\frac{e^2}{3m}\int_0^\infty dv\ \frac{v^3}{g_m}\frac{\partial f_o}{\partial v} \tag{A.12}$$

Substituting Eqs. (A.6) and (A.8) for g_m and f_o, we want to solve

$$\sigma_{DC} = \frac{4\pi e^2 n^e}{3\theta^e}\int_0^\infty dv\ \frac{v^4\ e^{-\frac{mv^2}{2\theta^e}}}{Nq_{en}v + \frac{\Gamma_{ei}n^i}{v^3}} \tag{A.13}$$

Changing the variable of integration using

$$x^2 = \frac{Nq_{en}}{\Gamma_{ei}n^i}v^4 \tag{A.14}$$

we have

$$\sigma_{DC} = \frac{32\ e^2}{9\pi m \nu_{en}}\left[y^2\int_0^\infty dx\ \frac{x^3 e^{-yx}}{x^2+1}\right] \tag{A.15}$$

where

$$y^2 = \frac{2\nu_{ei}}{\nu_{en}} \tag{A.16}$$

using the definitions in Eqs. (A.10) and (A.11). Letting $x^3 = x(x^2 + 1) - x$, we express the bracketed term as

$$\left[1 - y^2 g(y) \right] \tag{A.17}$$

where g(y) is a tabulated auxiliary exponential integral function.[40]

APPENDIX B

NORMALIZED VARIATION OF THE DC CONDUCTIVITY WITH THE ELECTRON TEMPERATURE

During the analysis presented in Chapter II, it was found convenient to define the factor ρ_θ Eq. (2.83) which is

$$\rho_\theta = \left[\frac{\theta^e}{\sigma_{DC}} \frac{\partial \sigma_{DC}}{\partial \theta^e}\right]_{\theta^e = \theta_o^e}$$

$$= \frac{\left[-\frac{1}{2} - y^2\left(1 - \frac{5}{2} g(y)\right) + y^3 f(y)\right]}{\left[1 - y^2 g(y)\right]} \tag{B.1}$$

where

$$g(y) = \int_0^\infty \frac{x\, e^{-yx}}{x^2 + 1}\, dx \,, \quad (\mathrm{Re}\ y > 0) \tag{B.2}$$

$$f(y) = \int_0^\infty \frac{e^{-yx}}{x^2 + 1}\, dx \,, \quad (\mathrm{Re}\ y > 0) \tag{B.3}$$

and

$$y^2 = \frac{2\nu_{ei}}{\nu_{en}} = \text{CONSTANT} \times \frac{n^e}{(\theta^e)^2} \tag{B.4}$$

Since we did not find tabulations for the functions g(y) and f(y) directly, we defined them in terms of the available sine and cosine integrals as[40]

$$g(y) = -Ci(y)\,Cos(y) - \left(Si(y) - \frac{\pi}{2}\right) Sin(y) \tag{B.5}$$

and

$$f(y) = Ci(y)\,Sin(y) - \left(Si(y) - \frac{\pi}{2}\right) Cos(y) \tag{B.6}$$

where

$$Si(y) = \int_0^y \frac{Sin\,x}{x}\,dx \tag{B.7}$$

and

$$Ci(y) = \gamma + ln(y) + \int_0^y \frac{Cos\,x - 1}{x}\,dx \tag{B.8}$$

The factor γ is Euler's constant and equals 0.57721 56649 . . .

We have numerically evaluated ρ_θ over the range of y equal 0.1 to 10 and have plotted the results in Fig. B.1. For the electron temperature of .05 eV ($q_{en} = 5.66 \times 10^{-16}$ cm^2 and $P_o = .378$ Torr), this range corresponds to the density range from about 5×10^8 to 10^{12} elec/cc. We have labeled the value corresponding to $\theta_o^e = .052$ eV and $n_o^e = 1.1 \times 10^{11}$ elec/cc which was used for the majority of our analysis in Chapter V.

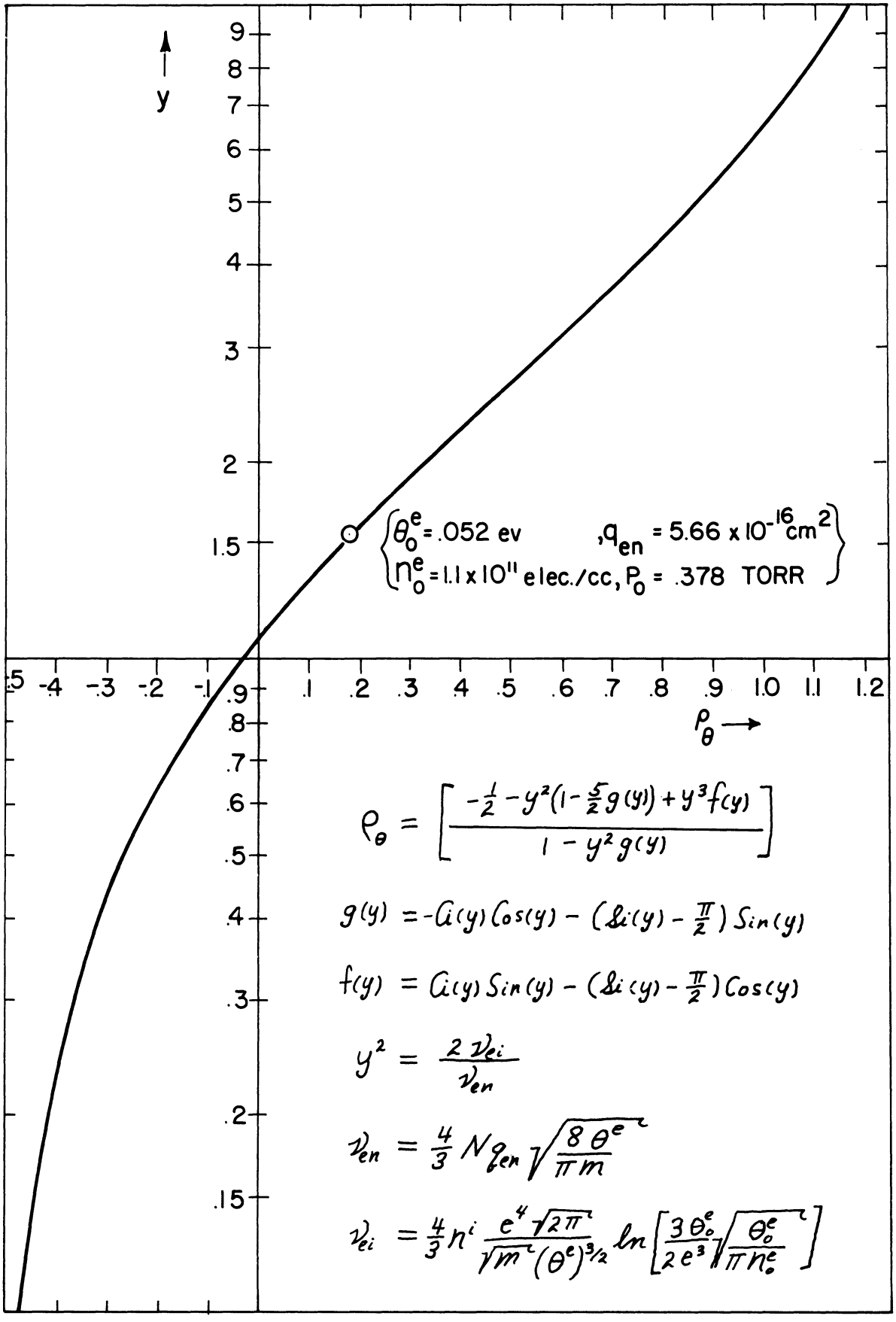

Fig. B.1. Variation of $\rho_\theta(y)$.

We have also plotted, in Fig. B.2, the variation of $(1 - y^2 g(y))$ as a function of y. From Chapter II Eq. (2.69) or Appendix A Eq. (A.17), this is the factor which determines the importance of the electron-ion collision frequency in dc conductivity. For large y it varies like $(6/y^2)$ or $(3\nu_{en}/\nu_{ei})$.

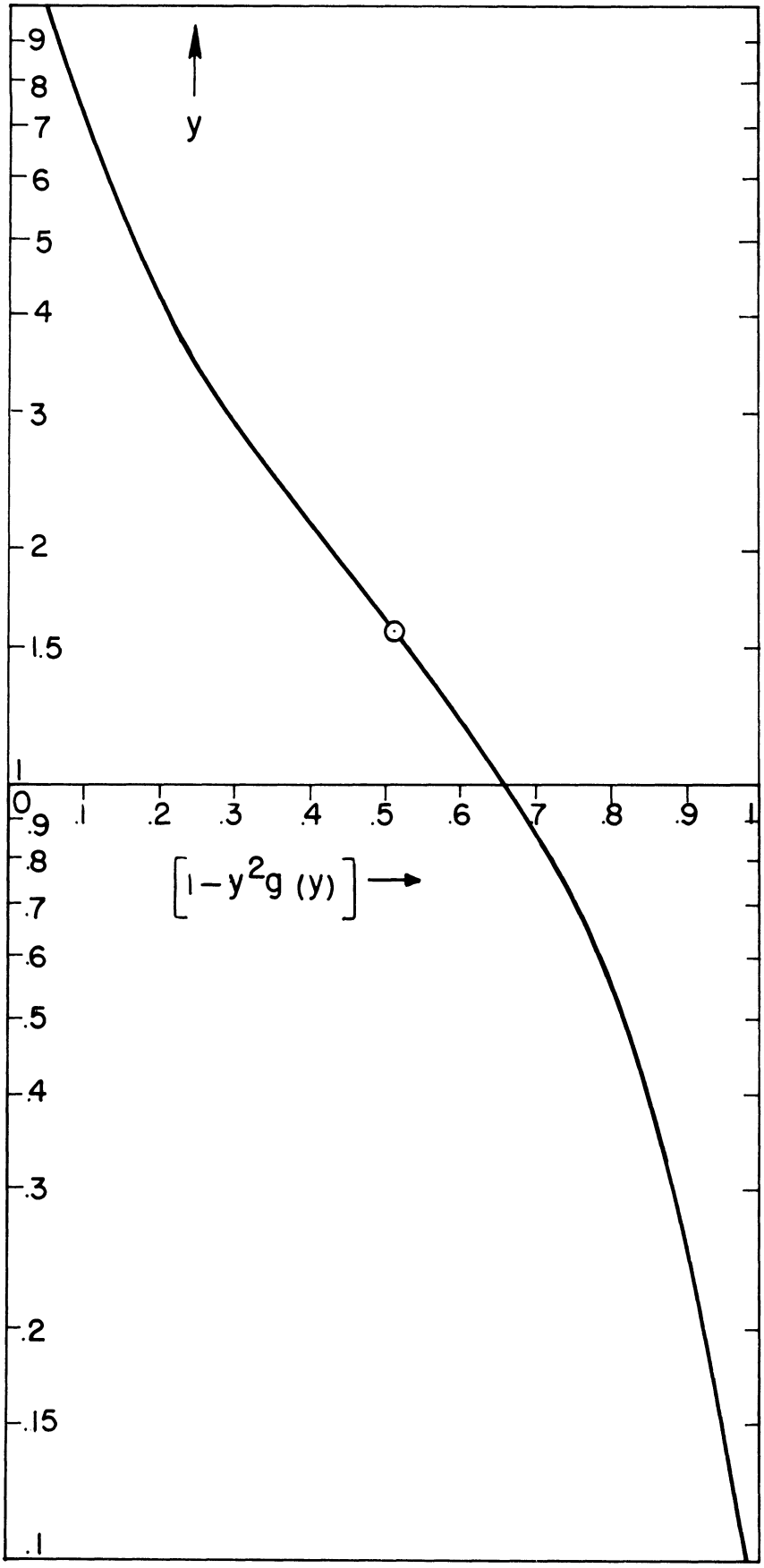

Fig. B.2. Variation of $[1-y^2g(y)]$ with y.

APPENDIX C

PRINCIPLES OF REFLECTED PLANE WAVE INTERACTION WITH SEMI-INFINITE TIME VARYING PLASMA

Consider a plane electromagnetic wave, $E_t e^{-i(\omega_s t - k_o x)}$, propagating in the x direction in vacuum with the angular frequency ω_s and propagation constant k_o, reflected at the plane boundary of a semi-infinite plasma at the point x_p. The amplitude of the reflected signal seen by an antenna located at x_r, in terms of the reflection coefficient, R, is given by

$$\underline{E}(x_r) = R(x_p)\,\underline{E}_t(x_p) \tag{C.1}$$

If the plasma properties are slowly changing, then the change in the received signal is given by

$$\delta\underline{E}(x_r) = \delta R(x_p)\,\underline{E}_t(x_p) \tag{C.2}$$

Therefore, the normalized detector voltage output is expressed by

$$\delta v(t) = \epsilon\, \mathcal{R}e\left(\frac{\delta R(t)}{R_o}\right) \tag{C.3}$$

where ϵ is the power law of the detecting circuit.

In terms of the normalized variations in the electron temperature and density we obtain

$$\delta v(t) = a \frac{\delta \theta^e}{\theta_o^e} + b \frac{\delta n^e}{n_o^e} \tag{C.4}$$

where

$$a = \mathcal{R}_e \left[\frac{\epsilon \theta_o^e}{R} \frac{\partial R}{\partial \theta^e} \right]_o \tag{C.5}$$

and

$$b = \mathcal{R}_e \left[\frac{\epsilon n_o^e}{R} \frac{\partial R}{\partial n^e} \right]_o \tag{C.6}$$

The reflection coefficient for this case is given by[41]

$$R = \frac{k_o - k}{k_o + k} \tag{C.7}$$

where

$$k = \alpha - i\beta \tag{C.8}$$

is given in Eq. (2.2) in terms of the complex conductivity. We can express the phase and attenuation constants, α and β, in terms of the real and imaginary parts of the conductivity, $\sigma = \sigma_R - i\sigma_I$, as

$$\alpha = \frac{k_o}{\sqrt{2}} \left\{ \left[\left(1 - \frac{4\pi}{\omega_s}\sigma_I\right)^2 + \left(\frac{4\pi}{\omega_s}\sigma_R\right)^2 \right]^{1/2} + \left(1 - \frac{4\pi}{\omega_s}\sigma_I\right) \right\}^{1/2} \tag{C.9}$$

and

$$\beta = \frac{k_o}{\sqrt{2}} \left\{ \left[\left(1 - \frac{4\pi}{\omega_s}\sigma_I\right)^2 + \left(\frac{4\pi}{\omega_s}\sigma_R\right)^2 \right]^{1/2} - \left(1 - \frac{4\pi}{\omega_s}\sigma_I\right) \right\}^{1/2} \tag{C.10}$$

where $k_o = \omega_s/c$. We approximate α and β for the condition when $\sigma_I \gg \sigma_R$. This corresponds to the approximation in Appendix A of $\nu \ll \omega_s$ which led to

$$\sigma = \frac{e^2 n^e}{m\omega_s^2}(\nu_{en} + \nu_{ei}) - i\frac{e^2 n^e}{m\omega_s} \tag{C.11}$$

We obtain

$$\alpha \approx k_o \sqrt{1 - \frac{4\pi}{\omega_s}\sigma_I} \tag{C.12}$$

and

$$\beta \approx \frac{k_o 4\pi \sigma_R}{2\omega_s \sqrt{1 - \frac{4\pi}{\omega_s}\sigma_I}} \tag{C.13}$$

Notice that for this approximation the phase constant α is independent of the electron temperature.

We are now in a position to evaluate the ratio (a/b). We want

$$\frac{a}{b} = \frac{\theta_o^e}{n_o^e} \frac{(\partial |R|^2/\partial \theta^e)_o}{(\partial |R|^2/\partial n^e)_o} \tag{C.14}$$

Using Eq. (C.7) and neglecting the partial derivative of α with θ^e we obtain

$$\frac{a}{b} = \frac{\theta_o^e (\partial |R|^2/\partial \theta^e)_o}{n_o^e (\partial |R|^2/\partial n^e)_o} \left\{ 1 - \frac{(k_o^2 + |k|^2)_o (\partial \alpha/\partial n^e)_o}{\alpha (\partial |k|^2/\partial n^e)_o} \right\}^{-1} \tag{C.15}$$

We define normalized variables as $\eta = (\omega_p/\omega_s)^2$ and $d = \nu/\omega_s$. Now (a/b) is written in terms of η and d, using Eqs. (C.12) and (C.13), as

$$\frac{a}{b} = \frac{\theta_o^e (\partial \sigma_R/\partial \theta^e)_o}{n_o^e (\partial \sigma_R/\partial n^e)_o} \left\{ \left[1 - \frac{(1-\eta)}{\eta d^2} \right] \left[1 - \frac{\eta(2-\eta)(1-\eta) + \eta^3 d^2/4}{2(1-\eta)[\eta(1-\eta)^2 - (1-\eta)\eta^2 d^2/2 - \eta^3 d^2/4]} \right] \right\}^{-1} \tag{C.16}$$

We now have the form which can be readily compared with the general case for (a/b) given in Eq. (5.13). Further discussion of Eq. (C.16) can be found in Chapter II, Section E.

APPENDIX D

COMPUTER PROGRAM

The computer program was designed to find the "best fit" $y(x,A,B)$ to the measured values of $y_i^{obs}(x_i)$ which had a first order fit of $y^o(x,A_o,B_o)$. The principle of Least-Squares indicates that if the deviations $d_i = y_i^{obs} - y_i$ are statistical in nature then y_i is the best fit when[6]

$$\sum_i d_i^2 = \text{minimum} \tag{D.1}$$

Therefore, we want to find a and b, of $A = A_o + a$ and $B = B_o + b$, such that $\sum_i d_i^2$ is a minimum, and then

$$y_i(x_i, A, B) = y_i^{obs} - d_i(x_i, A_o+a, B_o+b) \tag{D.2}$$

Treating a and b as small corrections to A_o and B_o, we attempt to find a solution to Eq. (D.1) by Taylor expanding $y(x,A,B)$ about $y^o(x,A_o,B_o)$ and keeping only the first correction terms. That is, take

$$y_i(x_i, A, B) \approx y_i^o(x_i, A_o, B_o) + a\left(\frac{\partial y_i}{\partial A}\right)_o + b\left(\frac{\partial y_i}{\partial B}\right)_o \tag{D.3}$$

Then d_i in (D.2) becomes

$$d_i \approx y_i^{obs}(x_i) - y_i^o(x_i, A_o, B_o) - a\left(\frac{\partial y_i}{\partial A}\right)_o - b\left(\frac{\partial y_i}{\partial B}\right)_o \tag{D.4}$$

We now perform the summation of $\sum_i d_i^2$ and minimize the sum by setting

$$\frac{\partial}{\partial A} \sum_i d_i^2 = 0 \tag{D.5}$$

and

$$\frac{\partial}{\partial B} \sum_i d_i^2 = 0 \tag{D.6}$$

This yields two equations for a and b which can be written as

$$a \sum_i \left(\frac{\partial y_i}{\partial A} \right)_o^2 + b \sum_i \left(\frac{\partial y_i}{\partial B} \frac{\partial y_i}{\partial A} \right)_o = \sum_i \left(y_i^{obs} + y_i^o \right) \left(\frac{\partial y_i}{\partial A} \right)_o \tag{D.7}$$

and

$$a \sum_i \left(\frac{\partial y_i}{\partial B} \frac{\partial y_i}{\partial A} \right)_o + b \sum_i \left(\frac{\partial y_i}{\partial B} \right)^2 = \sum_i \left(y_i^{obs} + y_i^o \right) \left(\frac{\partial y_i}{\partial B} \right)_o \tag{D.8}$$

Solving these equations simultaneously for a and b gives the desired results. Usually the resulting A and B will not satisfy the condition of Eq. (D.1) exactly, unless Eq. (D.3) is an exact expansion, and one must iterate the solution by replacing A_o by $A_o + a$ and B_o by $B_o + b$. If the iterations converge, one can obtain the values for A and B to within the accuracy justified by the measured values of y_i^{obs} and x_i.

The method can readily be extended for n number of independent parameters. This would result in n equations like Eq. (D.7) and Eq. (D.8) with n variables.

With the program described below we were interested in fitting the function

$$y(x, T, A, B, C) = \frac{T\sqrt{1 + Ax}}{\sqrt{(1+Bx)(1+Cx)}} \tag{D.9}$$

to the measurements of y_i^{obs} and $x_i (= f_m^2)$. For this experiment $A = f_3^{-2}$, $B = f_1^{-2}$, $C = f_2^{-2}$. An earlier used program, with A = 0, was based on a three parameter (T, B, and C) fit, but would not converge for the cases in which B and C were nearly equal. This appeared to be due to the finite accuracy of the computer such that the coefficients in the "normal equations" (Eqs. (D.7) and (D.8)) became nearly identical and the solution indeterminate. That is, once the values of B and C became nearly equal the computation was approximately a two parameter solution with three equations. If the denominator was treated as (1 + Bx) instead of $((1+Bx)(1+Cx))^{1/2}$ the program converged. For this reason, the program was set up as only a two parameter fit during any given iteration cycle. During the first iteration the solution was for $T_1 = T_o + t$ and $B_1 = B_o + b$ with C_o, and then during the next iteration $T_2 = T_1 + t$ and $C_2 = C_o + c$ with B_1. This approach converged for all cases tested, and was actually fastest for the cases when B was approximately equal to C. When A was allowed to be non-zero, it was iterated with B (or C) with T held constant.

The program below was written in the BASIC computer language and was used with an on-line teletype contact with a GE-235 computer.

```
100 DIM F(25), T(25), X(25), G(25), V(25)
110 READ D,M,N,E,T,W1,W2
120 FOR R = 1 TO N
130 READ F(R), T(R)
140 NEXT R
150 LET B = 1/W1↑2
160 LET C = 1/W2↑2
170       PRINT "DATA FILE NO."D;",DO YOU WANT IT?";
180       INPUT E1
190       IF E1 = 0 THEN 100
200       LET V4 = 0
210       LET A5 = 10
220       LET A6 = 10
230 LET U = 0
240       IF E1 = 2 THEN 890
250 PRINT "A =";
260 INPUT A
270       PRINT "INPUT VALUES OF T="T;"B="B;"C="C
280       LET V5 = 0
290 FOR J = 1 TO M
300 FOR K = 1 TO 10
310 LET S(K) = 0
320 NEXT K
330 FOR I = 1 TO N
340 LET X(I) = F(I)↑2
350 LET Z5 = 1 + X(I)*B
360 LET Z6 = 1 + X(I)*C
370 LET Z7 = 1 + X(I)*A
380 LET Z1 = SQR(Z7)/SQR(Z5*Z6)
390 LET Z2 = -T*Z1*X(I)/(2*Z5)
400 LET Z4 = T*Z1 - T(I)
410 LET S(9) = S(9) + Z4*Z4/((T*Z1)*(T*Z1))
420       LET V6 = V4 + V5
430       IF V6 < > 444 THEN 450
440       LET Z1 = T*Z1*X(I)/(2*Z7)
450 LET S(1) = S(1) + Z1↑2
460 LET S(2) = S(2) + Z1*Z4
470 LET S(3) = S(3) + Z1*Z2
480 LET S(4) = S(4) + Z2*Z2
490 LET S(5) = S(5) + Z2*Z4
500 NEXT I
510 LET P4 = S(3)*S(3) - S(4)*S(1)
520       IF P4 < > 0 THEN 550
530       PRINT "P4 IS ZERO"
540       GO TO 860
550 LET D2 = -(S(2)*S(3) - S(5)*S(1))/P4
560 LET D1 = -(D2*S(3) + S(2))/S(1)
```

```
 570 LET D5 = S(8)/SQR(N*(N-1))
 580 LET D6 = SQR(S(9)/(N*(N-1)))
 590 LET U = U + 1
 600       IF V6 < > 444 THEN 660
 610       LET A = A + D1*1.2
 620       LET A5 = D1/A
 630       IF A >= 0 THEN 680
 640       LET A = .0001
 650       GO TO 680
 660 LET T = T + D1*1.2
 670 LET A5 = D1/T
 680 LET G = 1.5
 690 LET B = B + D2*G
 700 IF B >= 0 THEN 720
 710 LET B = .0001
 720 LET A6 = D2/B
 730 LET C1 = B
 740 LET B = C
 750 LET C = C1
 760       IF J < 4 THEN 820
 770       IF ABS(A6) + ABS(A5) > E/100 THEN 810
 780       PRINT ABS(A6) + ABS(A5)
 790       IF J > = M-2 THEN 820
 800       LET J = M-2
 810       IF J < M-2 THEN 830
 820       PRINT U; T; A; B; C; D6*100; J
 830 NEXT J
 840 PRINT
 850 PRINT "W3 =" 1/SQR(A + 1E-6)
 860 PRINT "AFTER J ="U;"T ="T;"W1 ="SQR(1/B);"W2 ="SQR(1/C)
 870 PRINT
 880 PRINT
 890       INPUT V
 900       IF V < > 303 THEN 940
 910       PRINT "FOR T(CAL) LET C =";
 920       INPUT C1
 930       GO TO 1080
 940       IF V < > 0 THEN 990
 950       PRINT "M,E"
 960       INPUT M,E
 970       IF V > 400 THEN 250
 980       GO TO 290
 990       IF V < > 444 THEN 1020
1000       LET V4 = V
1010       GO TO 950
1020       IF V < > 441 THEN 1050
1030       LET V4 = 0
```

```
1040      GO TO 950
1050      IF V = 333 THEN 1080
1060 PRINT "NEXT SET OF DATA - PLEASE."
1070 GO TO 100
1080 PRINT "DATA FILE NO."D;"NORMALIZED BY ";
1090 INPUT V1
1100 PRINT
1110 PRINT "F(KHZ)     T(DATA)     T(CAL)     RATIO"
1120 PRINT
1130 FOR K = 1 TO N
1140 LET G(K) = T*SQR(1+A*X(K))/SQR((1+B*X(K))*(1+C1*X(K)))
1150 PRINT F(K),T(K)/V1,G(K)/V1,T(K)*T/(G(K)*V1)
1160 NEXT K
1170 PRINT
1180 GO TO 890
```

A feature of the on-line teletypewriter computer application is that it allows the operator to observe the progress of the program and make decisions at any pre-determined point. The program above makes use of this important feature. After giving the program a set of data and permission to proceed, the operator must give a value for A, usually letting A = 0 initially. The program then makes from six to M iterations with T and alternately B and C. The statements 760 to 820 control the printing. Only six sets of results are printed, the first and last three. If the error condition in 770 is not satisfied then only two more iterations will be made. Using statement 890 one can either: (1) continue with a new M and E; (2) continue with T held constant and allowing A to vary; (3) read in the next set of data; (4) print input data, T_i^{obs} and f_{m_i}, along with the calculated $T_i(f_{m_i},T,A,B,C)$ and the ratio of the T_i^{obs} to T_i; or (5) by using statement 910 and 920 with C1 = 0 the T_i becomes a calculation based only on $T_i(f_{m_i},T,A,B)$ and the ratio of T_i^{obs} to this T_i is effectively the fraction of the data which was used to predict C (see Fig. 4.10), of course C1 can be either B or C.

Below is the data taken from the sample trace in Fig. 4.9 as it is supplied to the program. Then the computer solution is presented along with tabulated data and calculation of the function $T(f_m,T,A,B,C)$ and the ratio T^{obs}/T. This result is plotted in Fig. 4.10; in the upper curve it is represented by the symbol "o".

```
1200 DATA 414.406,20,20,.01,2.3,2,7
1201 DATA .5,2.31,.6,2.28,.7,2.21,.8,2.14,1,1.96,1.2,1.77
1202 DATA 1.4,1.58,1.7,1.39,2,1.22,2.5,1.01,3,.853,4,.65
1203 DATA 5,.51,6,.39,7,.31,8,.239,10,.145,12,.104.14,.083,17,.074
2000 END
RUN
DATA FILE No. 414.406 , DO YOU WANT IT? 1
A = ? 0
INPUT VALUES OF T = 2.3   B = .25   C = 2.04082 E-2
1    2.46902   0  2.04082 E-2   .622071   5.98698   1
2    2.50822   0  .622071     3.12037 E-2 1.78691   2
3    2.54496   0  3.12037 E-2   .682793   1.75484   3
18   2.57422   0  .748957     1.89057 E-2 1.64799   18
5.28146 E-5
19   2.57435   0  1.89057 E-2   .748969   1.64017   19
20   2.57424   0  .748969     1.88545 E-2 1.64032   20

W3 = 1000
AFTER J = 20  T = 2.57424 W1 = 1.1555  W2 = 7.2827
? 333
DATA FILE NO. 414.406 NORMALIZED BY ? 2.57424
```

F(KHZ)	T(DATA)	T(CAL)	RATIO
.5	.897352	.915608	.980062
.6	.885698	.88449	1.00137
.7	.858506	.851373	1.00838
.8	.831313	.793173	1.04808
1	.76139	.749124	1.01637
1.2	.687582	.684396	1.00465
1.4	.613773	.625101	.981878
1.7	.539965	.547427	.986369
2	.473926	.482399	.982436
2.5	.392349	.396823	.988725
3	.33136	.332335	.997068
4	.252502	.243251	1.03803

F(KHZ)	T(DATA)	T(CAL)	RATIO
5	.198117	.185627	1.06728
6	.151501	.145954	1.038
7	.120424	.117421	1.02557
8	9.28429 E-2	9.62334 E-2	.964768
10	5.63273 E-2	6.75745 E-2	.833558
12	4.04003 E-2	4.97282 E-2	.812423
14	3.22425 E-2	3.79601 E-2	.849379
17	2.87463 E-2	.026704	1.07648

APPENDIX E

TABULATION OF THE DATA

Below is a complete table of the data and plasma conditions which were used in the distribution plot of Fig. 4.11. They were taken over a four month period (January 23, to April 17, 1967). The 107 sets of data represent 93% of the data analyzed during this period and about 25% of the traces (see Fig. 4.9) recorded.

In the table there is some special notation. The data designation, D in the program of Appendix D, is best described by an example: 223.135 means that the data was taken on the 23rd day of February with a helium glow discharge which had been on (P_o = .378 Torr, V_{DC} = 888 V, and I_{DC} = 182 mA) for 1 hr and 35 min after the evacuated condition. All the data below was taken at a helium pressure (room temperature) of .378 Torr. The other plasma conditions of voltage and current are in the table. The rest of the columns are: the discharge total run time (hr); the signal to noise ratio; and from the computer analysis: the "standard error" $(100[\sum_{i=1}^{N}((y_i^{obs} - y_i)/y_i)^2/N(N-1)]^{1/2}\%)$,[28] and the two break frequencies f_2 and f_1 (K Hz).

TABLE E.1

DATA

D	V_{DC}	I_{DC}	Time	SNR	SE	f_2	f_1
223.135	888	182	1.6	2.4	3.1	1.15	9.24
223.154	935	200	1.9	3.2	3.0	1.32	9.74
223.440	902	183	4.7	2.0	2.5	1.09	8.08
223.453	888	192	4.9	2.2	2.8	1.04	7.32
223.545	950	210	5.8	2.4	2.4	1.60	8.08
223.713	936	204	7.2	0.9	1.5	2.71	2.80
227.131	1030	175	1.5	1.0	2.8	2.68	2.97
227.137	990	170	1.6	0.8	4.9	1.90	2.97
227.037	1010	170	0.5	1.7	3.4	2.18	6.91
228.515	960	170	5.2	2.4	3.9	2.02	7.05
300.311	968	182	3.2	2.1	3.3	1.70	7.19
301.111	972	168	1.2	3.6	4.5	1.83	11.00
301.117	965	170	1.3	3.3	4.1	1.94	10.09
301.243	962	168	2.7	1.8	4.9	1.60	7.07
301.306	1020	180	3.1	1.6	4.3	2.01	6.69
302.057	978	172	0.9	1.7	4.2	2.41	5.81
302.101	978	172	1.0	1.7	3.4	2.07	7.81
302.105	968	172	1.1	2.0	3.7	1.98	8.25
302.109	976	174	1.2	2.0	3.1	1.87	7.84
305.111	935	155	1.2	1.2	2.0	1.49	6.69
305.115	928	152	1.3	1.3	1.9	1.40	7.12
305.123	928	152	1.5	1.0	2.9	1.44	5.41
305.215	928	152	2.3	1.2	3.0	1.50	5.43
305.222	928	152	2.4	0.9	2.6	1.49	5.17
305.415	980	170	4.3	1.4	2.7	2.02	5.95
305.424	978	172	4.4	1.1	2.5	1.87	6.34
305.431	970	170	4.5	1.1	1.6	2.16	5.27
305.451	968	172	4.9	0.8	3.9	2.09	5.24
305.501	981	174	5.0	0.9	2.3	2.07	6.69
305.505	968	172	5.1	0.9	2.6	1.82	6.39
306.321	925	155	3.4	0.8	2.6	1.19	6.03
306.336	928	157	3.6	1.0	3.2	1.30	6.48
306.421	925	160	4.4	0.8	4.0	1.18	6.90
307.704	940	160	7.1	0.9	4.1	1.24	6.17
309.331	918	177	3.5	2.5	3.8	0.99	9.47
309.335	917	178	3.6	1.9	3.8	1.04	8.46
309.345	917	178	3.7	1.6	3.6	0.89	6.96
309.358	932	188	3.9	1.7	2.9	1.00	8.38
309.359	932	188	4.0	1.7	2.3	1.12	7.08
309.409	935	185	4.1	2.1	3.1	1.06	8.40

TABLE E.1 (Continued)

D	V_{DC}	I_{DC}	Time	SNR	SE	f_2	f_1	
309.411	935	185	4.2	2.1	3.1	1.06	8.40	
309.435	930	190	3.7	1.9	2.3	1.10	8.15	
309.437	930	190	3.7	1.0	1.5	1.24	5.84	
320.230	1160	240	2.5	1.4	2.9	3.54	3.55	
320.241	1194	246	2.7	1.7	2.8	3.00	4.37	
320.243	1194	246	2.7	3.6	2.8	2.22	9.12	
320.245	1194	246	2.8	1.3	2.7	2.39	5.02	
320.249	1194	246	2.8	3.8	3.7	2.14	8.76	
322.124	1072	183	1.4	1.0	1.7	2.06	4.72	
322.126	1072	183	1.5	1.6	2.4	1.54	6.63	
322.128	1072	183	1.5	1.0	2.2	2.05	4.46	
322.131	1072	183	1.5	1.0	6.6	1.14	13.12	
322.133	1072	183	1.5	1.2	3.1	1.26	6.96	
411.306	923	172	3.0	2.0	3.2	1.22	10.08	
412.132	928	172	1.5	1.6	2.5	1.27	7.96	
412.137	928	172	1.5	1.9	3.1	1.04	7.88	
412.156	915	170	1.9	2.2	3.1	1.39	8.01	
412.158	915	170	2.0	2.3	4.5	1.49	7.36	
412.211	915	170	2.1	2.3	3.3	1.11	7.78	
412.214	915	170	2.2	2.5	3.9	1.08	7.98	
412.238	920	170	2.6	2.0	2.3	1.44	7.90	
412.242	920	170	2.8	2.7	2.2	1.12	8.88	
414.337	940	170	3.6	0.7	4.7	1.09	8.47	
414.347	937	168	3.8	1.6	2.2	1.20	6.76	Used in Fig. 4.10
414.406	937	168	4.1	1.6	1.6	1.16	7.28	
414.432	965	170	4.5	1.0	1.8	1.18	5.91	
414.437	965	170	4.6	1.0	2.4	1.22	5.93	
415.242	900	150	2.7	1.1	5.0	1.00	6.32	
415.253	934	166	2.9	2.3	3.4	1.13	8.97	
415.408	945	170	4.1	2.1	2.3	1.23	7.99	
415.1025	980	170	10.4	0.9	1.7	1.27	6.94	
415.1028	980	170	10.6	0.9	0.8	1.39	5.80	
415.1031	980	170	10.6	0.8	3.4	1.52	4.06	
415.1039	979	171	10.7	4.0	2.0	1.34	5.93	
415.1052	860	125	10.9	1.1	4.7	1.58	5.77	
415.1111	1031	189	11.2	1.1	2.7	1.62	6.06	
415.1113	1031	189	11.2	0.8	0.9	1.52	7.33	
415.1122	1026	179	11.4	2.2	3.7	2.02	3.64	
415.1128	1025	175	11.5	0.5	1.7	1.43	4.50	
415.1144	1020	175	11.7	0.6	3.8	1.61	3.11	
416.1918	903	142	19.3	0.5	6.0	2.51	2.51	
416.1923	905	140	19.4	1.7	4.5	1.64	6.50	

TABLE E.1 (Concluded)

D	V_{DC}	I_{DC}	Time	SNR	SE	f_2	f_1
416.1925	905	140	19.4	1.1	2.8	1.59	5.88
416.1928	905	140	19.5	1.4	5.3	1.56	5.79
416.2031	913	142	20.5	1.1	2.6	1.58	5.19
416.2036	913	142	20.6	0.9	2.7	1.45	5.13
416.2048	905	140	20.8	0.8	1.7	2.15	3.55
416.2053	905	140	20.9	0.9	4.1	2.93	2.97
416.2055	915	146	20.9	1.1	1.2	2.09	5.48
416.2100	914	146	21.0	1.4	0.8	1.80	6.86
416.2106	924	146	21.1	1.5	2.3	2.35	4.83
416.2142	1029	161	21.7	1.0	3.5	1.71	4.49
416.2154	1029	161	21.9	1.0	4.5	1.96	3.60
416.2200	1034	161	22.0	0.8	1.9	2.07	2.85
416.2207	1035	162	22.1	0.8	1.6	1.75	4.28
416.2225	1052	168	22.4	0.9	2.2	2.65	3.24
416.2241	1076	174	22.7	1.0	2.6	2.44	3.86
416.2311	960	150	23.2	1.0	3.2	1.50	4.61
416.2325	965	145	23.4	0.9	2.4	1.34	5.38
416.2330	963	147	23.5	1.4	2.4	1.51	4.47
416.2335	963	147	23.6	1.5	2.6	1.27	7.31
416.2355	999	151	23.9	0.7	1.2	1.60	3.93
417.3402	970	120	34.0	1.3	2.9	2.54	2.56
417.3425	993	157	34.4	1.3	1.9	1.61	4.76
417.3426	1000	160	34.4	1.2	1.0	1.54	5.47
417.3428	997	153	34.5	1.6	1.1	1.90	5.55
417.3430	997	153	34.5	1.5	1.9	1.65	7.08

REFERENCES

1. B. D. Tellegen, Nature 131, 840 (1933).

2. V. A. Bailey and D. F. Martyn, Phil. Mag. 18, 369 (1934); and V. A. Bailey, Phil. Mag. 18, 516 (1934); 23, 774 (1937); 23, 929 (1937); 26, 425 (1938).

3. L. G. H. Huxley and J. A. Ratcliffe, Proc. of I.E.E. 96, 433 (1949).

4. L. Goldstein, J. M. Anderson, and G. L. Clark, Phys. Rev. 90, 151, 486 (1953); L. Goldstein and T. Sekiguchi, Phys. Rev. 109, 625 (1958); J. M. Anderson and L. Goldstein, Phys. Rev. 100, 1037 (1955); 102, 933 (1956); A. A. Dougal and L. Goldstein, Phys. Rev. 109, 615 (1958); K. V. Narasinga, J. T. Verdeyen, and L. Goldstein, Proc. of I.R.E. 49, 1877 (1961); P. D. Goldan and L. Goldstein, Phys. Rev. 138, A39 (1965).

5. J. A. Stratton, Electromagnetic Theory, McGraw-Hill, New York (1941) page 268.

6. H. Margenau and G. M. Murphy, The Mathematics of Physics and Chemistry, D. Van Nostrand Company, Inc., New York (1961) page 534.

7. H. Margenau, Phys. Rev. 69, 508 (1946); 109, 6 (1958); H. Margenau and D. Stillinger, J.A.P. 30, 1385 (1959); V. E. Golant, Soviet Physics-Technical Physics 5, 1197 (1961). M. Epstein, Phys. of Fluids 3, 6 (1960); 5, 492 (1962).

8. E. Langberg and R. C. Siegel, Technical Report AFAL-TR-66-81 (1966).

9. E. H. Kennard, Kinetic Theory of Gases, McGraw-Hill Book Company, Inc., New York (1938) p. 89; L. Spitzer, Jr., Physics of Fully Ionized Gases, Interscience Publishers, Inc., New York (1956); R. K. Osborn, Fusion and Plasma Physics, Bound notes, Nuclear Engineering Department, University of Michigan, Ann Arbor (1963).

10. H. A. Lorentz, Theory of Electrons (Stechert) p. 267, New York (1923).

11. P. M. Morse, W. P. Allis, and E. S. Lamar, Phys. Rev. 48, 412 (1935).

12. S. Chapman and T. G. Cowling, The Mathematical Theory of Non-Uniform Gases, Cambridge University Press, Cambridge (1952); originally published in 1939.

13. H. Dreicer, Phys. Rev. 117, 343 (1960).

REFERENCES (Continued)

14. E. A. Desloge and S. W. Matthysse, Am. Jor. of Phys. 28, 1 (1960); E. A. Desloge, Phys. of Fluids 5, 1223 (1962).

15. J. C. Bowe, Am. Jor. of Phys. 31, 905 (1963).

16. D. Barbiere, Phys. Rev. 84, 653 (1951).

17. J. H. Cahn, Phys. Rev. 75, 293, 838 (1949).

18. H. Margenau, Phys. Rev. 73, 297 (1948); H. Margenau and L. M. Hartman, Phys. Rev. 73, 309 (1948); L. M. Hartman, Phys. Rev. 73, 316 (1948); H. Margenau, Phys. Rev. 73, 326 (1948).

19. D. J. Rose and M. Clark, Jr., Plasmas and Controlled Fusion, MIT Press and John Wiley & Sons, Inc., New York (1961) pg. 163.

20. S. C. Bloch, Phys. Rev. 144, 181 (1966).

21. H. Dreicer, Phys. Rev. 115, 238 (1959).

22. J. L. Delcroix, Introduction to the Theory of Ionized Gases, Interscience Publishers, Inc., New York (1960).

23. J. M. Anderson, Phys. Rev. 108, 898 (1958).

24. For examples: R. F. Whitmer, Microwave Jor., Part I pg. 18, Part II pg. 47 (1959); H. Hodara, H. R. Raemer, and G. I. Cohn, "A New Approach to Space Communications During Re-entry," XI International Astronautical Congress, Stockholm, Sweden, 1960.

25. J. D. Cobine, Gaseous Conductors, Dover Publication, Inc., New York, 1958.

26. I. Langmuir and H. Mott-Smith, Jr., Gen. Elec. Rev. 27, 449, 538, 616, 762, 810 (1924); Phys. Rev. 28, 727 (1926). For reference listing see, L. B. Loeb, Basic Processes of Gaseous Electronics, University of California Press, Berkeley and Los Angeles (1960) pg. 372.

27. F. W. Crawford and R. S. Harp, Rev. of Scientific Instruments 33, 1387 (1962).

28. R. D. Evans, The Atomic Nucleus, McGraw-Hill Book Company, Inc., New York, 1955.

REFERENCES (Concluded)

29. F. A. Albini and R. G. Jahn, "Reflection and Transmission of Electromagnetic Waves at Electron Density Gradients," Technical Note No. 3, Daniel and Florence Guggenheim Jet Propulsion Center, California Institute of Technology, Pasadena, California (1960).

30. A. V. Phelps, O. T. Fundingsland, and S. C. Brown, Phys. Rev. 84, 559 (1951).

31. L. Gould and S. C. Brown, Phys. Rev. 95, 897 (1954).

32. J. M. Anderson and L. Goldstein, Phys. Rev. 102, 933 (1956).

33. A. V. Phelps, J. L. Pack, and L. S. Frost, Phys. Rev. 117, 470 (1960).

34. J. L. Pack and A. V. Phelps, Phys. Rev. 121, 798 (1961).

35. C. L. Chen, C. C. Leiby, and L. Goldstein, Phys. Rev. 121, 1391 (1961).

36. D. E. Golden and H. W. Bandel, Phys. Rev. 138, A14 (1965).

37. L. H. Wald, "The Absorption of Microwave Radiation in a Slightly-Ionized Gas," Doctoral Thesis, The University of Michigan, 1966.

38. M. A. Biondi and S. C. Brown, Phys. Rev. 76, 1697 (1949).

39. R. A. Johnson, B. T. McClure, and R. B. Holt, Phys. Rev. 80, 376 (1950).

40. M. Abramowitz and I. A. Stegun, Editors, Handbook of Mathematical Functions, Dover Publications, Inc., New York, 1965.

41. S. Takeda and T. Tsukishima, "Microwave Reflection Techniques for Dense Plasma Diagnostics," NBS Technical Note 256 (1965).